

Gas Transport in Proton Exchange Membranes for Use in Fuel Cell Applications

By

Charles William James Jr

Dissertation submitted to the Faculty of the Virginia Polytechnic Institute and State University in partial fulfillment of the requirements for the degree of

DOCTOR OF PHILOSOPHY

In

Chemical Engineering

Dr. Eva Marand, Chair

Dr. James McGrath

Dr. Richey Davis

Dr. Don Baird

Dr. Chris Cornelius

November 19, 2007

Blacksburg, VA

Keywords: Poly(arylene ether sulfone), Diels Alder Poly(phenylene), Nafion, Fuel Cells, Relative Humidity, Gas Permeation, Gas Sorption

Gas Transport in Proton Exchange Membranes for use in Fuel Cell Applications

Charles William James Jr

(Abstract)

The objectives of this research were to study the gas transport properties of proton exchange membranes (PEM), namely disulfonated poly(arylene ether sulfone) (BPSH-35), post sulfonated diels-alder poly(phenylene) (SDAPP), and poly(perfluoro sulfonic acid) (Nafion). The O₂ gas permeabilities were found to be lower in BPSH and SDAPP as compared to poly(perfluoro sulfonic acid) because of difference in T_g (T_gBSPH= 250 °C, T_gSDAPP= 330 °C versus T_gNafion=150 °C). Higher T_g polymers have a more rigid, inflexible polymer segments causing a reduction in gas permeability. In comparison to SDAPP, BPSH has a lower O₂ gas permeability because of the bulky side groups in the SDAPP backbone.

O₂ sorption measurements were carried out both under non-humidified and humidified conditions as a function of relative humidity and temperature at a normal PEM operating pressure of 1 atm. Under non-humidified conditions, BPSH, SDAPP, and Nafion 112 exhibited Henry's Law sorption, consistent with dilute dissolution of O₂ into the polymer matrix. The enthalpies of sorption were calculated to determine the interaction of O₂ with each membrane. The sorption enthalpies in BPSH and SDAPP increased with increasing pressure indicating the formation of more O₂-O₂ interactions. The enthalpies in Nafion 112 were relatively constant with increasing pressure. In the presence of moisture, the sorption behavior changed from Henry's Law to Type IV sorption behavior, which is common in hydrophilic polymers. The SDAPP membrane was found to have the highest percent wet O₂ mass uptake because of a higher number of sulfonic acid groups interacting with the water/O₂ system.

Finally the O₂ sorption for various porous catalyst powders, consisting of platinum supported on carbon was measured in the non-humidified and humidified state. The catalysts were found to have Knudsen diffusion in the non-humidified state with 20 wt% Pt-C having the largest O₂ sorption. In the humidified state, the highest O₂ mass uptake was achieved with 40 wt% Pt-C. These results are explained in terms of the trade-off between catalyst dispersion and catalyst size. Furthermore, O₂ sorption measurements were utilized for membrane electrode assemblies containing 40 wt% Pt-C and hot pressed at 210 °C for BPSH-35 (25 and 80K) and Nafion 112 membranes. The same sorption behavior occurred in the MEAs as in the neat membrane, but at a lower capacity. This is because the electrode introduces a more tortuous path to the gas molecules permeating across the membrane.

*Mom and Dad,
Hope you are looking down together with big
smiles and lots of joy.*

Will

Acknowledgements

First and foremost, this work is dedicated to my mother and father who have both passed away this year. They gave me every opportunity to succeed and motivated me to finish what I start. They are no longer here physically, but they will be looking down smiling from above.

There are so many people I wish to thank; I just hope I don't forget anyone. I would like to express many thanks to my advisor, Dr. Eva Marand. Thank you for your guidance, understanding, and the ability to perform research in an area I enjoy greatly. To Dr. James McGrath and Dr. Chris Cornelius words cannot express the gratitude for providing me with the materials, funding, and guidance. The rest of my committee, Dr. Baird and Dr. Davis, your help has also been extremely appreciated.

I would also like to extend thanks to Steve McCartney (microscopy) for helping me with some AFM work even though the material didn't exactly work out. I would like to thank the rest of the VT Chemical Engineering faculty and staff for their help and assistance. I would like to extend my appreciation to people who have helped me in various aspects of my research: Abhishek Roy and Kent Wiles in Dr. McGrath's group and Cy Fujimoto, Chad Staiger, and Michael Hibbs at Sandia National Laboratories.

There are so many fellow grad students and friends I wish to acknowledge.

First, there were my fellow classmates that I have become such great friends with: Tom Muscenti, Tregei Starr, Kylie Gaskins, and Brian Mather. I know I am the last one to finish, but we were saving the best for last.

Then there are my current and former lab mates: Todd Pechar, Ben Vaughan, Sangil Kim, and Jose Herrera-Alonso, thank you for your help and insight. There are my fellow grad students whom I have come to call friends: Matt and Mary McKee, Matthew Cashion, Erika Borgerding, Rebecca Huyck, Leslie Adamczyk, Melissa Pendergast, Sukit Leekumjorn, Rich Oldland, Anthony Gaglione, Eric Mullins, Brian Wolfe, and Chris McGrady.

Next, there are the VCOMers (Ed Jones, Quincy, Kyle, Mike, JT, Minh, Danielle) who added excitement in my life with their crazy outings and parties. It is kind of scary that one day you all will be doctors. (just kidding)

There are my friends that I grew up showing horses with: Jay and Kristy, Shane and Holt, Kyle Hughes, Kevin, and Laura who gave me a break from school to keep me updated on what is happening in AQHA.

Thanks also goes out to the Gamecock and local SC crew: Dave, Dr. Rob, Alex, Ed Stehmeyer, Tim, Deena, Natasha, Kyle Peterson, D.J., Dana, Kelly, Kelvin, and Maurice. Can't wait for the next great tailgate and SEC game...GO GAMECOCKS!!!!

Last but not least, a huge thank you goes to my sister and her husband Stan. I know we might not be close in age, but that gap is filled with much love. To the rest of my family, you have given me the support to help me succeed, thank you.

Table of Contents

Abstract.....	ii
Dedication.....	iii
Acknowledgements.....	iv
List of Figures, Tables, & Schemes.....	ix
Chapter 1 Introduction.....	1
1.1 Motivation.....	1
1.2 Outline of Chapters.....	4
1.3 References.....	5
Chapter 2 Literature Review.....	6
2.1 Introduction.....	6
2.2 General Full Cell Concepts and History.....	6
2.3 Polymer Electrolyte Membranes in Fuel Cells.....	9
2.4 Components of PEMFCs.....	10
2.4.1 Hydrogen and Other Fuels.....	10
2.4.2 Membrane Electrode Assembly.....	12
2.4.3 Future of Fuel Cells.....	14
2.5 Proton Exchange Membranes (Commercial and New Membranes).....	14
2.5.1 Commercially Available Nafion.....	15
2.5.2 Poly(arylene ether sulfone)/Poly(arylene ether disulfonated sulfone) copolymer.....	16
2.5.3 Post-Sulfonated Diels Alder Poly(phenylene).....	26
2.6 States of Water.....	28
2.7 Gas Permeation.....	30
2.7.1 General Concepts.....	30
2.7.2 Permeability Coefficient (P).....	31
2.7.3 Diffusion Coefficient (D).....	31
2.7.4 Solubility Coefficient (S).....	35
2.7.5 Gas Transport Through a Rubbery Polymer.....	38
2.7.6 Gas Transport Through a Glassy Polymer.....	39
2.7.7 Time Lag Method.....	40
2.8 Gas Sorption.....	44
2.8.1 General Concepts.....	45
2.8.1.1 Henry's Law Sorption.....	46

2.8.1.2	Langmuir-type Sorption.....	46
2.8.1.3	Dual-mode Sorption.....	46
2.8.1.4	Flory-Huggins Sorption.....	47
2.8.1.5	Type IV Sorption.....	48
2.8.2	Adsorption Background.....	48
2.8.3	Water Sorption.....	49
2.9	References.....	55

Chapter 3 Determination of the Effect of Temperature and Humidity on the O₂ Sorption in Sulfonated Poly(arylene ether sulfone) membranes versus Nafion 112.....58

3.1	Introduction.....	58
3.2	Experimental.....	59
3.2.1	Materials.....	59
3.2.2	Membrane Preparation.....	59
3.2.3	Gas Permeation Characterization.....	60
3.2.4	Gas Sorption Characterization.....	60
3.3	Results.....	61
3.3.1	Gas Permeability Measurements.....	64
3.3.2	Gas Sorption Measurements.....	65
3.4	Conclusions.....	73
3.5	References.....	74

Chapter 4 Determination of the Effect of Temperature and Humidity on the O₂ sorption in Post Sulfonated Diels Alder Polyphenylene versus Nafion 112.....76

4.1	Introduction.....	76
4.2	Experimental.....	78
4.2.1	Materials.....	78
4.2.2	Membrane Preparation.....	78
4.2.3	Gas Permeation Characterization.....	78
4.2.4	Gas Sorption Characterization.....	79
4.3	Results.....	80
4.3.1	Gas Permeability Measurements.....	80
4.3.2	Gas Sorption Measurements.....	81
4.4	Conclusions.....	90
4.5	References.....	91

Chapter 5	Determination of the Effect of Temperature and Humidity on the O₂ sorption in Platinum supported on Carbon Black and Membrane Electrode Assemblies used in PEM Fuel Cells.....	93
5.1	Introduction.....	93
5.2	Experimental.....	96
5.2.1	Materials.....	96
5.2.2	MEA Preparation.....	96
5.2.3	Gas Permeation Characterization.....	96
5.2.4	Gas Sorption Characterization.....	97
5.3	Results.....	98
5.3.1	Catalyst Powders.....	98
5.3.2	Membrane Electrode Assembly Characterization.....	106
5.4	Conclusions.....	114
5.5	References.....	115
Chapter 6	Conclusions and Future Work.....	117
Vita	121

List of Figures

Chapter 2

Figure 2-1: Single Fuel Cell Design.....	7
Figure 2-2: Stacked PEM Fuel Cells for higher power applications.....	8
Figure 2-3: Effect of temperature and acidification method on proton conductivity for a) BPSH-30 and BPSH-40 and b) Nafion 1135 systems.....	19
Figure 2-4: Influence of amount of disulfonation on a) proton conductivity and b) water up-take at 80 °C for BPSH.....	20
Figure 2-5: Influence of Relative humidity on the (a) proton conductivity and (b) equilibrium water sorption.....	21
Figure 2-6: Effect of aging temperature on the proton conductivity of fully hydrated membrane at (a) 80 °C, (b) 100 °C, & (c) 120 °C.....	23
Figure 2-7: DSC curves showing the effect of water uptake on the Tg and the appearance of loosely and freely bound water for BPSH-40.....	24
Figure 2-8: DSC cooling curve of water sorbed for polyhydroxystyrene: Curve A = 7.8%; Curve B = 9.2%; Curve C = 10.7%; and Curve D = 26.3% and Curve E = pure (bulk) water....	29
Figure 2-9: Indicates the difference between a penetrant molecule's ability to diffusion through a membrane based on a series of jumps when a gap is available.....	33
Figure 2-10: Exponential relationship between the fractional free volume (FFV) and diffusivity (D).....	34
Figure 2-11: Effect of polar groups on the solubility for various polymers.....	36
Figure 2-12: Effect of temperature on solubility coefficient for Nafion 117 and BPSH-40.....	37
Figure 2-13: Effect of pressure on the solubility coefficient for polysulfone cast membranes in CO ₂	38
Figure 2-14: Typical permeation experiment data analyzed using Time Lag Method.....	41
Figure 2-15: Typical types of sorption behavior: (a) Henry's Law, (b) Langmuir, (c) Flory-Huggins, (d) dual mode, (e) Type IV, BET.....	45
Figure 2-16: Pulsed field gradient spin-echo (PGSE) sequence.....	49

Figure 2-17: Water Sorption curve for Nafion 117 at T = 30 °C.....	51
Figure 2-18: Water sorption curves for ● H ⁺ ; ○ Li ⁺ ; ▲ N(CH ₃) ₄ ⁺ ; Δ Cs ⁺ ionic forms of Nafion 117 at 25 °C.....	52
Figure 2-19: Relative humidity effect on amount of free water in cellulose.....	53
Figure 2-20: Sorption curve for cellulose.....	54

Chapter 3

Figure 3-1: Proton Conductivity Measurements for (a) BPSH-35 and (b) Nafion 117.....	63
Figure 3-2: Pressure O ₂ sorption isotherms for (a) BPSH-35 (25K) and (b) Nafion 112 over a temperature range of 25-75 °C.....	67
Figure 3-3: O ₂ sorption isotherm for Nafion 112.....	70
Figure 3-4: O ₂ sorption isotherm for BPSH-35 25K.....	71
Figure 3-5: O ₂ sorption isotherm for BPSH-35 80K.....	72

Chapter 4

Figure 4-1: Non-humidified pressure O ₂ sorption isotherms for (a) SDAPP 1.6, (b) SDAPP 2.2, and (c) Nafion 112 over a temperature range of 25-75 °C.....	84
Figure 4-2: O ₂ sorption isotherm for SDAPP 1.6.....	87
Figure 4-3: O ₂ sorption isotherm for SDAPP 2.2.....	88
Figure 4-4: O ₂ sorption isotherm for Nafion 112.....	89

Chapter 5

Figure 5-1: Simple structure make-up of the catalyst layer of a PEMFC.....	94
Figure 5-2: O ₂ sorption isotherms for various Pt-C powders as a function of pressure and temperature in the non-humidified state over a temperature range of 25-75 °C.....	102

Figure 5-3: % Wet O₂ mass uptake as a function of temperature and vapor pressure of water for various Pt-C catalyst powders in the humidified state.....105

Figure 5-4: Simple schematic of turnover frequency as a function of particle size.....106

Figure 5-5: Membrane electrode assembly schematic.....107

Figure 5-6: O₂ sorption isotherms for MEAs hotpressed at 210 oC in the non-humidified state: (a) Nafion 112, (b) BPSH-35 (25K), and (c) BPSH-35 (80K).....110

Figure 5-7: O₂ sorption isotherm for MEAs hotpressed at 210 °C for the humidified state: (a) Nafion 112, (b) BPSH-35 (25K), (c) BPSH-35 (80K).....113

Chapter 6

Figure 6-1: Isopiestic graph of % wet O₂ mass uptake as a function of proton conductivity for Nafion 112 and BPSH -35.....118

Figure 6-1: Compilation of the effect of O₂ sorption in the (a) non-humidified state and (b) humidified state for Nafion 112, 25K BPSH-35, 40 wt% Pt-C, and the respective MEAs.....120

List of Tables

Chapter 2

Table 2-1: Various Types of Fuel Cells.....	9
Table 2-2: Effect of disulfonation on the states of water.....	25
Table 2-3: Influence of ion exchange capacity for SDAPP samples on water uptake and proton conductivity.....	28
Table 2-4: Kinetic diameters of penetrant gas molecules.....	32

Chapter 3

Table 3-1: Membrane water dependence for BPSH-35 series and Nafion 112.....	61
Table 3-2: % Water Uptake for Nafion 112 and BPSH-35 over a temperature range of 25-75 °C.....	62
Table 3-3 (a): Gas permeability in Barrers for the respective polyelectrolyte membranes under fully hydrated conditions.....	64
Table 3-3 (b): Pure oxygen solubility in BPSH-35 and Nafion under fully hydrated conditions.....	65
Table 3-4: Enthalpy results for BPSH-35 (25K) and Nafion 112 membranes at 0% relative humidity.....	68

Chapter 4

Table 4-1: Membrane water dependence for SDAPP 1.6, SDAPP 2.2, and Nafion 112.....	80
Table 4-2 (a): Gas permeability in Barrers for the respective polyelectrolyte membranes under fully hydrated conditions 25-75 °C.....	81
Table 4-2 (b): Pure oxygen solubility in SDAPP series and Nafion under fully hydrated conditions.....	81

Table 4-3: Enthalpy results for SDAPP 1.6, SDAPP 2.2, and Nafion 112 membranes at 0% relative humidity85

Chapter 5

Table 5-1: Particle Size and surface areas for various Pt-C powders and unsupported Pt black.....98

Table 5-2: Permeability values for various MEAs hot pressed at 210 °C and 40 wt% Pt-C.....108

List of Schemes

Chapter 2

Scheme 2-1.....16

Scheme 2-2.....18

Scheme 2-3.....27

1.1 Motivation

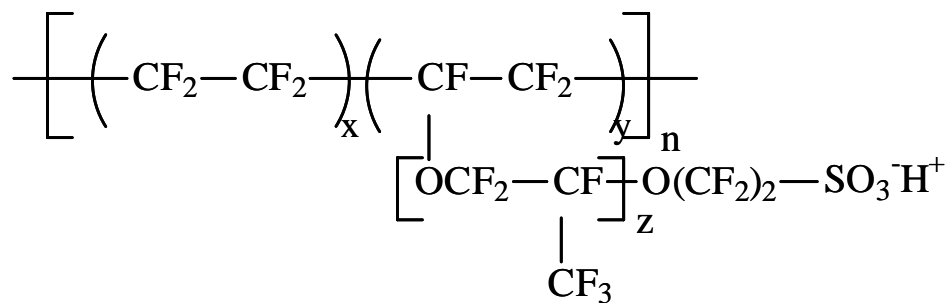
Proton-exchange membrane fuel cells (PEMFC) have been considered in recent years as an alternative form of energy for such portable and stationary applications as automobiles and computers, respectively. One of the most desirable goals for PEMFC is elevated temperature operation (e.g. $> 100^{\circ}\text{C}$) because of the decrease in carbon monoxide poisoning of the platinum anode catalyst and higher current densities due to higher hydrogen oxidation and oxygen reduction at the anode and cathode respectively. However there are drawbacks, maintaining an optimal hydration level for the proton exchange membrane is one of the major concerns in fuel operation at elevated temperatures and motivation for this work.

Proton exchange membranes are designed to have low oxygen and hydrogen permeability, while maintaining high proton transport. The objectives of this study are to determine the gas transport mechanism as a function of molecular structure and water content. This will be accomplished by comparing the oxygen and hydrogen transport in Nafion 112, a fluoropolymer with a low T_g , with a hydrocarbon based disulfonated poly(arylene ether sulfone) and post-sulfonated diels alder polyphenylene with intermediate and high T_g s, respectively. Our hypothesis is that the plasticization caused by tightly bound water as well as the presence of free water facilitates the gas transport over a limited range of hydration, which is determined by the state of water in the system. Furthermore, this range should vary with the architecture of the hydrophilic and hydrophobic domains.

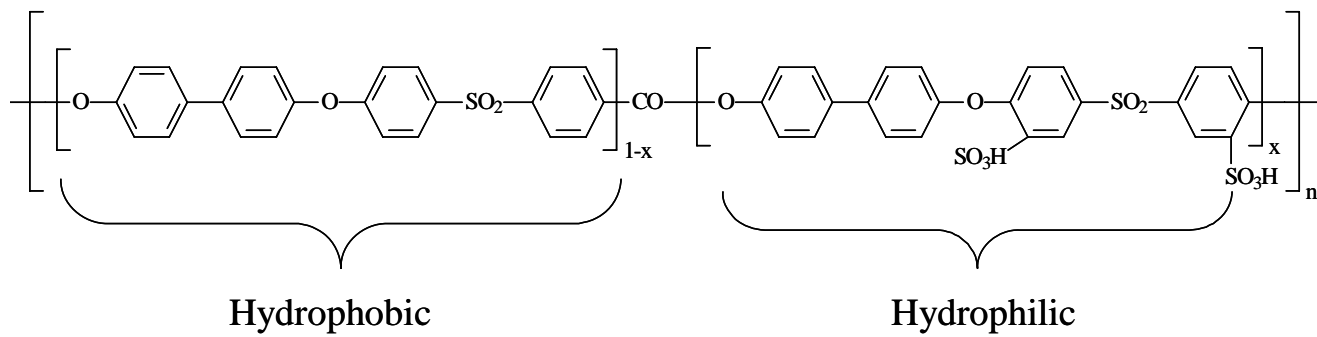
In a proton exchange fuel cell (PEMFC), a thin organic proton conducting membrane is used as an electrolyte and gas separator. Nafion is a perfluorosulfonated polymer that has been used as an industry standard for many years. However, with the high cost of production coupled with low fuel cell performance at temperatures above 80°C and high fuel permeability (crossover) has caused an increase in the need to find alternative fuel cell membranes. Current research has shifted from fluorinated systems to hydrocarbon based polymers such as polysulfone and polyphenylene polymers, which have a lower cost of manufacturing, equal potential, and enhanced performance. Much research has been devoted to understanding how

varying parameters such as relative humidity and temperature affect properties such as proton conductivity, water-uptake, and open circuit voltage (OCV). It is critical to link structure and architecture to observations seen in fuel cells in order to improve and advance this area of science.

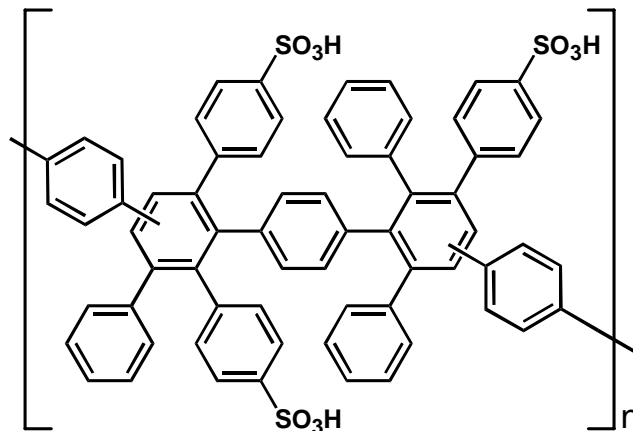
When examining the viability of a polymer for use as a fuel cell membrane, the chemical make-up of each system can provide distinct properties. Nafion, Structure 1-1, is a well studied polymer, composed of a highly hydrophobic polytetrafluoroethylene (PTFE) with pendant side-chains consisting of $\text{SO}_3^- \text{M}^+$. In the case of fuel cell membranes $\text{M}^+ = \text{H}^+$, and the $T_g = 150^\circ\text{C}$. The disulfonated poly(arylene ether sulfone) copolymer, BPSH, Structure 1-2, developed by Dr. James McGrath's group at Virginia Tech, contains a rigid, wholly aromatic backbone with a $T_g = 250^\circ\text{C}$. The post-sulfonated diels-alder poly(phenylene), SDAPP, Structure 1-3, $T_g = 388^\circ\text{C}$, is a highly rigid, rod-like aromatic backbone with large aromatic side chains containing acidic sulfonate groups, which will further decrease the gas transport inside the polymer. The polymer was developed by a group at Sandia National Lab in Albuquerque, NM headed by Dr. Chris Cornelius. The newly developed membranes will allow the opportunity to contrast flexibilities and transport in Nafion versus BPSH and SDAPP.



Structure 1-1



Structure 1-2



Structure 1-3

Oxygen permeability in Nafion has been found to increase with both temperature and relative humidity. Oxygen has a kinetic diameter of 0.346 nm compared to 0.289 nm for hydrogen. The permeability of oxygen is half that of hydrogen, because the molecular size of O_2 is larger than H_2 .¹ It is important when discussing permeability to look at how the diffusion and solubility change with temperature and relative humidity as these are important operating parameters. In Nafion, three distinct regions have been found to affect the gas permeability, the rigid hydrophobic backbone, flexible perfluorocarbon side chain, and hydrated ionic cluster region. In comparison to PTFE (Nafion's parent polymer with no $-SO_3H$ groups), Nafion has significantly higher water up-take correlating to an increase in diffusion, whereas the solubility is slightly lower.^{1,2} The large increase in diffusion gives an indication that the gas mainly permeates through the hydrated hydrophilic ionic clusters.

In the presence of varying relative humidity, water containing ionic clusters could enhance permeability. Initial water uptake introduces tightly bound water into the system that acts as a plasticizer in the polymer matrix causing an increase in the diffusion coefficient. When free water is introduced, swelling occurs causing an increase in the size of ionic clusters, but leads to dimensional changes in the polymer. This theory does not eliminate the possibility of gas transport through hydrophobic regions. For Nafion, permeability has been shown to increase with temperature at constant RH, but with a decrease in water-uptake due to a phase change in the water from liquid to vapor.¹ The highest permeability occurs at the lowest water content.

This can be explained by the amorphous hydrophobic region, thus gas transport may involve transport through both the hydrophilic and hydrophobic regions.

1.2 Outline of Chapters

The following is a brief description for each chapter in this dissertation:

Chapter 2 is a literature review containing background information about fuel cells, proton exchange membrane used in fuel cells, the three states of water in an ionomer system, gas permeability, and gas sorption concepts.

Chapter 3 is a comparison study of how relative humidity affects the O₂ gas sorption for disulfonated poly(arylene ether sulfone) and Nafion 112. This study compares two different polymer structure architecture with two distinct T_g's, 250 °C and 150 °C for the BPSH and Nafion 112 respectively. We will further determine the effect molecular weight has on the O₂ gas sorption using 25K and 80K samples. Gas permeability measurements will be utilized as a base experiment when no moisture is present. We will use gas transport correlations to determine such important parameters as the solubility or concentration and enthalpy of solution for both the non-humidified and humidified state at a normal fuel cell operating pressure of 1 atm over a temperature range of 25 to 75 °C.

Chapter 4 is a comparison study of how relative humidity affects the O₂ gas sorption for post-sulfonated diels-alder polyphenylene, developed at Sandia National Laboratories in Albuquerque, New Mexico, and Nafion 112. This is a continuation of Chapter 3, but for a much broader T_g range. The SDAPP T_g is near 388 °C for SDAPP as compared to the previously reported 150 °C for Nafion 112. We will examine two different SDAPP polymers with different ion exchange capacities and determine the effect that IEC has on gas permeability and gas sorption as a function of relative humidity. Furthermore, we will use gas transport correlations to determine such important parameters as the solubility or concentration and enthalpy of solution for both the non-humidified and humidified state at a normal fuel cell operating pressure of 1 atm over a temperature range of 25 to 75 °C.

Chapter 5 is a study of a series of platinum supported on carbon catalyst used in the production of membrane electrode assemblies (MEAs) as well as prepared MEAs, which contain the platinum supported on carbon and ionomer. We will examine the O₂ sorption on pure platinum and 20, 40, 60, and 80 wt% Pt-C as function of pressure, temperature, and relative humidity. Membrane electrode assemblies have been made by the “decal method” using the BPSH-35 series membrane with both the 25K and 80K molecular weight and Nafion 112 membrane using Nafion as the ionomer. Gas permeability measurements are also utilized for the case of the MEAs.

Chapter 6 contains the conclusions from this research and future recommendations.

1.3 References

- [1] K. Broka and P. Ekdunge, Oxygen and hydrogen permeation properties and water uptake of Nafion(R) 117 membrane and recast film for PEM fuel cell, *J. Appl. Electrochem.*, 27 (1997) 117.
- [2] T. Sakai, H. Takenaka and E. Torikai, Gas-Diffusion in the Dried and Hydrated Nafions, *J. Electrochem. Soc.*, 133 (1986) 88.

2.1 Introduction

The focus of this work is to investigate the gas transport mechanism of two novel proton exchange membranes, a poly(arylene ether sulfone) copolymer and a post sulfonated diels-alder poly(phenylene). More specifically, the objective is to understand the gas transport mechanism utilizing permeation and sorption experiments by varying factors such as humidity and temperature. These properties have a dramatic effect on the performance of a proton exchange membrane fuel cell (PEMFC). The results of the proposed work will lead to optimizing fuel efficiency and performance. This chapter begins with the brief history and concept of fuel cells. It then discusses PEMFC materials and concludes with the definition permeation and sorption.

2.2 General Fuel Cell Concepts and History

The history of fuel cells can be traced back to 1839 when a lawyer and scientist named Sir William Grove developed a system, which allowed water to be electrolyzed into hydrogen and oxygen when an electrical current is passed through it. Some 100 years later, Sir Francis Bacon developed what could be described as the first operational fuel cell, utilizing a hydrogen-oxygen cell that included nickel electrodes and alkaline electrolytes. Then by the late 1950s, NASA began developing a compact electricity generator for space missions.¹ Today, fuel cells have become the most desirable alternative energy source. Research in this area has been significantly funded by the Department of Energy (DOE).

Fuel cells are electrochemical energy conversion devices that produce not only electricity, but water and heat using fuel and oxygen from the air. In principle, they can be two to three times more efficient than an internal combustion engine converting fuel to power. The biggest advantage of a fuel cell is the elimination of emissions of dangerous pollutants to the environment, the only by-product of a hydrogen fuel system being water. In comparison to

batteries, fuel cells have access to an abundant external fuel source, whereas batteries either have to be recharged or discarded due to an internal fuel source. The amount of electricity produced by fuel cells is several times greater than battery operated systems.

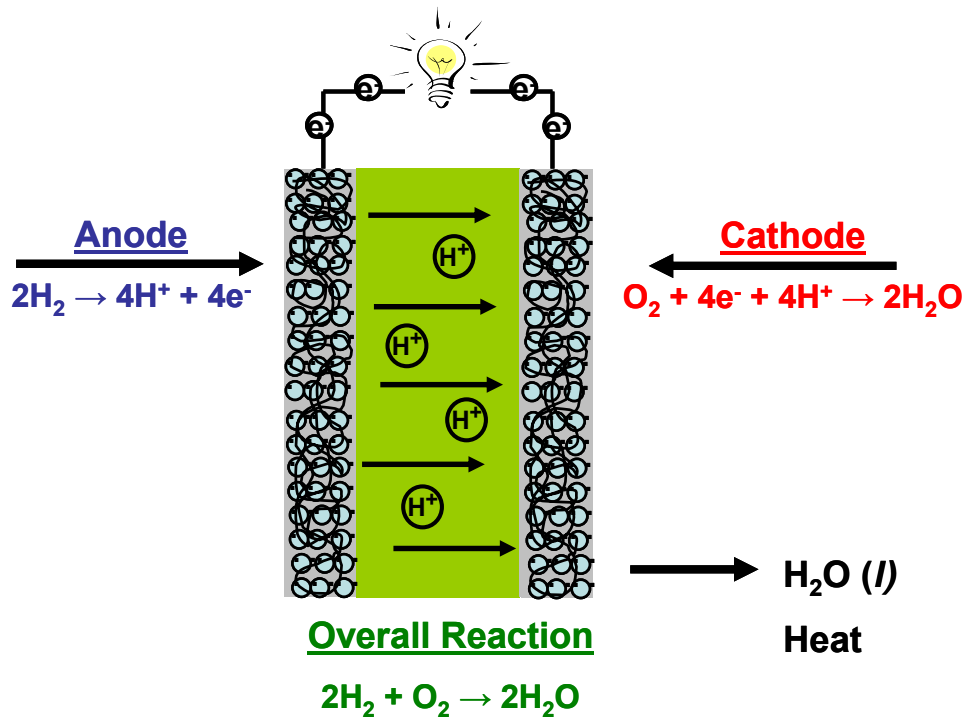


Figure 2-1: Single Fuel Cell Design.

A typical voltage for a single fuel cell is 0.7 volts with 55 % efficiency, which is just about enough to power a light bulb. To power automobiles, the cells must be stacked in series, where the operating voltage of 0.7 volts is multiplied by the number of stacks. Some typical stack targets include 65 kW of power and a voltage output of 300 V for applications such as boats and automobiles. A single and stacked fuel cell is shown in Figure 2-1 and Figure 2-2, respectively.

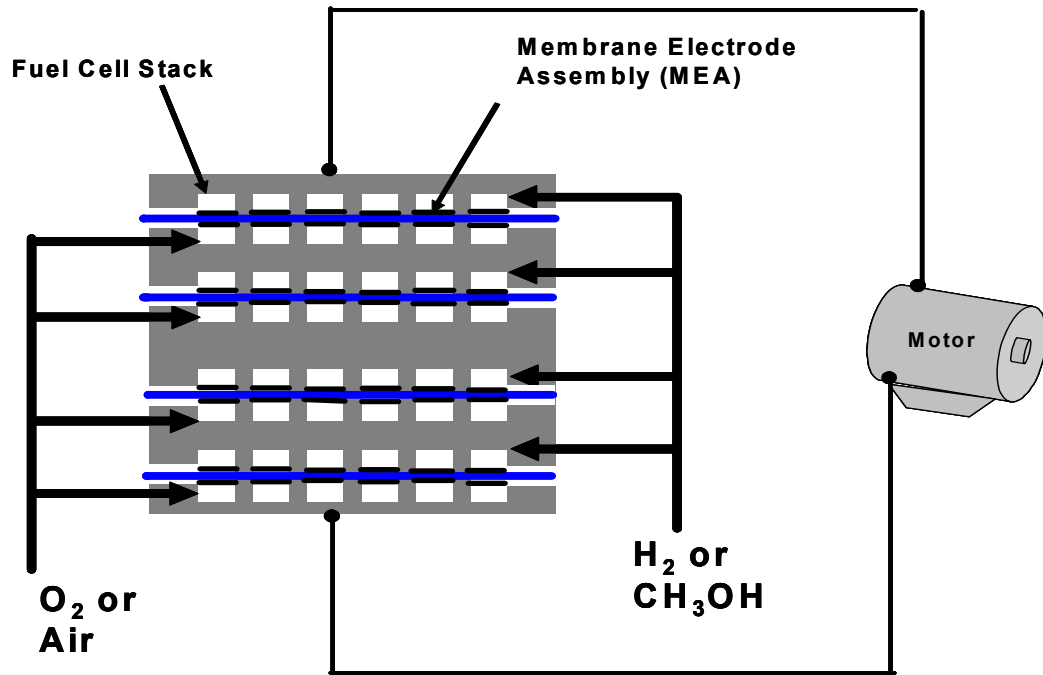


Figure 2-2: Stacked PEM Fuel Cells for higher power applications

The basic operation of fuel cells is based on a series of half reactions involving protons generated at the anode and transported through the membrane, reacting with oxygen/air at the cathode. Electrons produced at the anode flow around the membrane because they cannot pass through the membrane. An external source containing a motor or another electrical load is attached to store the electricity produced by the electrons. Table 2-1 contains several types of fuel cells based on hydrogen gas as fuel at the anode. The lower temperature fuel cells have applications related to cell phones, automobiles, computers, portable generators. Higher temperature fuel cells such as MCFC and SOFC are designed for large stationary power applications.

²Table 2-1: Various Types of Fuel Cells

Fuel Cell	Electrolyte	Operating Temperature (°C)	Electrochemical Reaction
Polymer Electrolyte Membrane (PEMFC)	Solid Organic Polymer	60 – 100	Anode: $H_2 \rightarrow 2H^+ + 2e^-$ Cathode: $\frac{1}{2}O_2 + 2H^+ + 2e^- \rightarrow H_2O$ Cell: $H_2 + \frac{1}{2}O_2 \rightarrow H_2O$
Alkaline (AFC)	Aqueous solution of potassium hydroxide soaked in a matrix	90 – 100	Anode: $H_2 + 2(OH^-) \rightarrow 2H_2O + 2e^-$ Cathode: $\frac{1}{2}O_2 + H_2O + 2e^- \rightarrow 2(OH^-)$ Cell: $H_2 + \frac{1}{2}O_2 \rightarrow H_2O$
Phosphoric Acid (PAFC)	Liquid phosphoric acid soaked in a matrix	175 – 200	Anode: $H_2 \rightarrow 2H^+ + 2e^-$ Cathode: $\frac{1}{2}O_2 + 2H^+ + 2e^- \rightarrow H_2O$ Cell: $H_2 + \frac{1}{2}O_2 \rightarrow H_2O$
Molten Carbonate (MCFC)	Liquid solution of lithium, sodium, and/or potassium carbonates, soaked in a matrix	600 -1000	Anode: $H_2 + CO_3^{2-} \rightarrow H_2O + CO_2 + 2e^-$ Cathode: $\frac{1}{2}O_2 + CO_2 + 2e^- \rightarrow CO_3^{2-}$ Cell: $H_2 + \frac{1}{2}O_2 + CO_2 \rightarrow H_2O + CO_2$ (CO ₂ is consumed at cathode and produced at anode)
Solid Oxide (SOFC)	Solid zirconium oxide to which a small amount of yttria is added	600 – 1000	Anode: $H_2 + O^{2-} \rightarrow H_2O + 2e^-$ Cathode: $\frac{1}{2}O_2 + 2e^- \rightarrow O^{2-}$ Cell: $H_2 + \frac{1}{2}O_2 \rightarrow H_2O$

2.3 Polymer Electrolyte Membranes in Fuel Cells

This section provides a general overview of polymer electrolyte membranes. The polymer electrolyte must be an ion conducting membrane to which a porous catalyst electrode is hot-pressed or bonded to each side. Ideally, in the case of PEMFCs, thinner membranes allow for better gas transport, leading to an increase in fuel cell performance. The advantages of electrolyte membranes are a fast device start due to low temperature operation, compact cell design, and non-hazardous materials.

The main problem facing electrolyte membranes involves water management that directly affects proton transport. Materials employed as fuel cell membranes are typically highly hydrophobic, have good mechanical properties, and high chemical resistance. Hydrophilic domains are modulated by either sulfonating the monomer or post-sulfonation of the polymer.

The amount of sulfonation can vary. The hydrophobicity of the material allows the water to be transported through the electrode and the hydrophilic domains allow the adsorption of water, which is necessary for the transport of H^+ ions. Since sulfonic acid is highly hydrophilic, water drawing clusters are formed causing a micro-phase separated polymer-water morphology. The more hydrophilic domains that a membrane has the more water up-take will occur. An optimal balance between degree of sulfonation and water-uptake will maximize the movement for the H^+ ions.

2.4 Components of PEMFCs

This section describes the key components that contribute to the function of PEMFCs. This includes systems that use hydrogen and oxygen/air for operation as well as the reformate systems which employ alternative gases as fuel. Membrane electrode assemblies consist of the catalyst layer, diffusion layer, and a polymer membrane. Finally, as fuel cells gain more and more exposure, the DOE has set some stringent standards that should be met in the near future for automobiles, etc. These standards are in this section, and include high temperature operation (80 to 100°C), low relative humidity (25 % at 80°C and 50% at 100°C) and a 300 mile range of travel for automobiles.

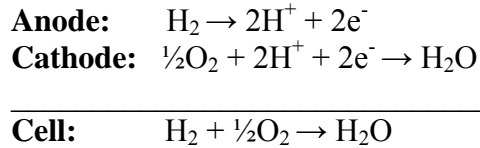
2.4.1 Hydrogen and Other Fuels

Hydrogen

Hydrogen powered fuel cells are the most environmentally friendly fuel cells, because water is the only by-product. Hydrogen fuel cells are designed for high power and high performance applications. Another advantage of using hydrogen as the fuel is the ease of the reactions occurring at the catalyst layer under mild conditions.

At the anode, hydrogen is oxidized generating two electrons and two protons. The electrons move through an electricity generating external path. The protons permeate through the catalyst layers and the proton exchange membrane to the cathode. At the cathode, oxygen or

air is reduced. This process gives an overall reaction with water and heat being the only by-products.



The disadvantage of hydrogen power systems is the water management. For every four hydrogen protons that are produced at the anode and permeate to the anode, one molecule of oxygen is present to react. At the cathode, the reaction producing water is slow, causing the need for an external water source to prevent dehydration of the membrane. The relative humidity of the membranes can be varied based on the operating temperature maintaining ideal hydration for extended periods of time. When a fuel cell is not operated at proper relative humidity there is possibility of flooding (too much water produced) and/or “drying out” (to little water). In each case, the performance of the fuel cell decreases dramatically.

Others concerns include hydrogen infrastructure and scale-up on global basis. There are storage and distribution issues under normal conditions as well gas purity problems. These challenges as well as the requirement of low temperature operation and membrane cost will have major impact on the success of fuel cells in the future.

Reformate

Reformate systems have been experimentally examined as a possible alternative. A reformate system usually consist of 40% nitrogen, 20% carbon dioxide, and 40% hydrogen with trace amounts of carbon monoxide. The problem with this system is the need to overcome the dilution of hydrogen as well as the effect of carbon monoxide poisoning on platinum based catalysts. These types of systems could be a possible alternative for pure hydrogen systems because of easier distribution and storage within a fuel cell.

2.4.2 Membrane Electrode Assembly

Catalysts along with the membrane comprise the most important part of a fuel cell called the membrane electrode assembly (MEA). The membrane electrode assembly consists of two platinum supported mixtures that are both ionically and electrically conductive, i.e. that facilitate transport of the electrons and protons throughout the fuel cell. For the PEMFC, the platinum mixture usually contains 20-30 wt% platinum supported on a carbon black surface and ionomer of the polymer/copolymer used as the proton exchange membrane, and a bonding agent such as glycerol or water. The platinum catalysts can either be supported (PEMFC) or unsupported (Direct Methanol Fuel Cell) on a carbon black surface.

Ideally, the catalyst layer should be thin and have low mass transport resistances, high platinum surface area, and high electrical and ionic conductivities. The thickness of the catalyst layer determines the rate of oxygen transport through the layer to utilize the platinum. The layer should be thin to allow access to all of the platinum and to reduce the paths that the electrons, protons, and reactant gases travel. Low mass transport resistances are necessary to achieve the maximum current and voltage. To reduce the mass transport resistance, the catalyst layer should contain high porosity to allow accessibility to the reaction sites and aid in the removal of water. At the same time, the porosity should not decrease the paths available for protons and ions to travel. Achieving high ionic and electrical conductivities means having sufficient amounts of platinum and carbon so that the pores are not blocked. High platinum surface area maximizes the reaction and fuel cell performance. Proper dispersion of the platinum is critical so that two platinum particles do not touch and reduce the surface area available for reaction. Overall, when optimizing the catalyst layer, the presence of platinum is kept at a minimum due to cost.

Some of the problems involved with the platinum supported catalysts include cost and low CO tolerance. There are two ways to reduce the cost: reduction of the catalyst loading and improve the catalyst utilization. Catalyst utilization is those catalyst particles that are in contact with the membrane and reactant gas.³ All other catalyst particles are inactive. Earlier catalyst work used unsupported platinum at loadings of ~ 4 mg Pt/cm² corresponding to a cost of $\sim \$400/\text{kW}$ at 500 mA/cm².⁴ To lower the platinum content and increase utilization, Taylor et al. discusses increasing platinum size (120 Å) and the inaccessibility of the reactants to the platinum. Therefore, an approach for preparing smaller platinum particles supported on a high

surface area material such as carbon was examined.⁴ This technology had been used for phosphoric acid fuel cell technology. Further research determined that incorporating ionomer (Nafion) into the electrode at low platinum loadings (0.35 to 0.4 mg Pt/cm²) allowed similar performance to that of high platinum loadings. By implementing Nafion into the electrode, the active surface area of the platinum covered by Nafion and the gas diffusion in decreases because the Nafion is in the pores of the catalysts. This prevents the gas from escaping and to have more gas present to react.⁵⁻⁸

There are currently several methodologies being used that are historically based on battery technology to apply a MEA to the membrane. In each case, both methods utilize dilute polymer solution and lead to the same result, but differ in the approach of preparation and application. The first method involves “inking” or painting the mixture directly onto the surface of the membrane. The “inking” takes place at a temperature above room temperature (> 60 °C). Once completed, the membrane is dried and can be inserted into a fuel cell, where further testing can be completed. This method is usually performed for direct methanol fuel cells.

The second method involves hot pressing a decal onto the membrane.⁹ The decal is made by the first method; however, it is not inked directly to the membrane. The decal is dried and then hot pressed at an elevated temperature (150-200 °C) and pressure (3000 psi) to the membrane to form the MEA. The condition for this step is dependent on the decal’s adhesion to the surface of the membrane. This method is preferred for proton exchange membrane fuel cells.

2.4.3 Future of Fuel Cells

Because companies like DuPont, W.L. Gore & Associates, 3M, Solvay, Arkema, and Asahi Glass are working on fluoropolymers and Polyfuel (spin-off from SRI International) and Pemeas (former Celanese unit) are developing nonfluoropolymer membranes, it is no doubt that fuel cells have become real and present. The Department of Energy has set a goal for fuel cell demonstration vehicles by 2009 capable of 300-mile range, 2,000-hour lifetime, and \$125 per kW cost for power. In addition, laboratory fuel cells should achieve a 5,000-hour lifetime and \$45 per kW cost at the same time. It has been projected by Polyfuel that to meet the DOE's goals, the membranes will have to cost at most \$150 per m². Most companies are speculating the ideal cost for membranes would be \$35 per m². A typical fuel cell automobile will have approximately 10 m² of membrane. Also, ideal temperature range of operation would occur in the range of 95 to 100 °C with a relative humidity of around 50% (25% at 80°C), which is higher than the current mark of 80 °C and 80% RH. Often issues such as problems of hydrogen infrastructure, hydrogen storage, and membranes have to be solved in the overall task of commercializing fuel cells. There are many companies and individuals working to solve these problems daily making this concept realistically viable by 2009.¹⁰

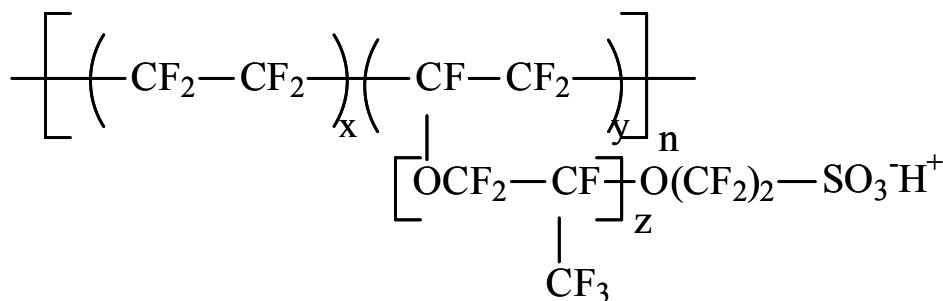
2.5 Proton Exchange Membranes (Commercial and New Membranes)

As mentioned previously, PEMFCs are designed to produce electricity by a series of half-reactions. In general, at the anode, hydrogen gas is ionized, releasing H⁺ protons and electrons. This reaction releases energy and at the anode, oxygen reacts with the protons and electrons from the anode to form water.

One of the most desirable objectives in PEMFC development is operation at elevated temperatures (e.g. > 100°C). High temperatures decrease carbon monoxide poisoning of the platinum anode catalyst and induce higher current densities due to greater hydrogen oxidation and oxygen reduction at the anode and cathode, respectively. However, the problem at elevated temperatures is maintaining membrane hydration, which is critical for proton transport.

2.5.1 Commercially Available Nafion

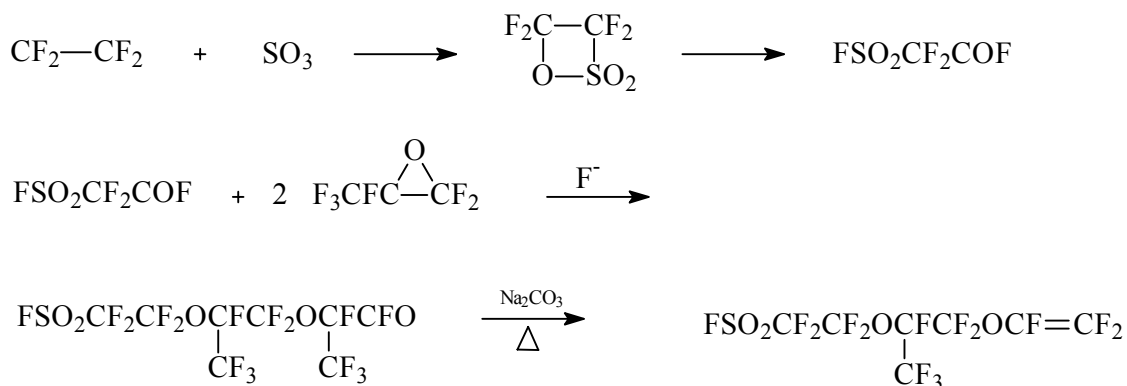
The polyelectrolyte membrane that is commercially available is Nafion[®], Structure 2-1, a poly(perfluoro sulfonic acid), supplied by DuPont. Nafion was first manufactured in the 1960's for use in the NASA space program. The membrane provides excellent properties for a fuel cell such as protonic conductivity (0.08-0.10 S/cm), mechanical and chemical resistance, long term stability, and the ability to stay hydrated by storing large quantities of water. However, maintaining these properties above a temperature of 80 °C is difficult and the cost of producing the electrolyte has made researchers seek alternatives.



Structure 2-1

Even today, after investigating alternative fuel cell membranes such as polyketones, polyimides, polysulfones, and poly(phenylene sulfides), fluorinated ionomers (i.e.-Nafion) has still passed the test as the best material. This perfluorinated membrane is synthesized by free radical copolymerization of tetrafluoroethylene and the sulfonated comonomer, Scheme 2-1, form. Approximately 13 mole% vinyl ether containing pendant sulfonyl fluoride is added to assure the proper equivalent weight (milli-equivalents of sulfonic acid/gram polymer).¹¹ In the case of fuel cell applications, 1100 meq/gram suffices. Nafion comes in a variety of thickness. The “00” in 1100 meg/gram is replaced with the appropriate thickness (mil). For example Nafion 117, consists of a sheet of 1100 meg/gram membrane that is 7 mils thick. Some other common membrane thicknesses include Nafion 112, Nafion 1135, and Nafion 115. As mentioned earlier, Nafion is still not the ideal fuel cell membrane material. There is ongoing research aimed at

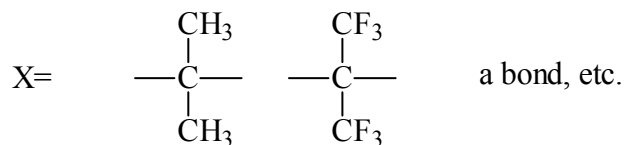
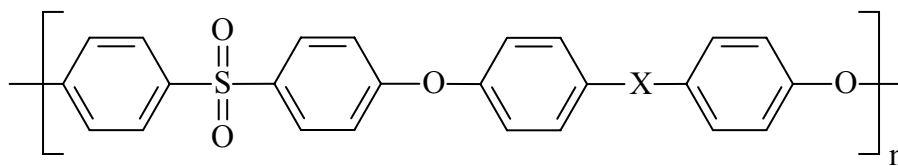
understanding structure-property relationships including conductivity, electro-osmosis, and transport in alternate membrane materials.



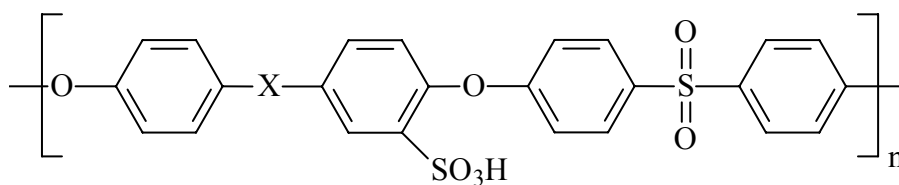
Scheme 2-1

2.5.2 Poly(arylene ether sulfone)/Poly(arylene ether disulfonated sulfone) Copolymer

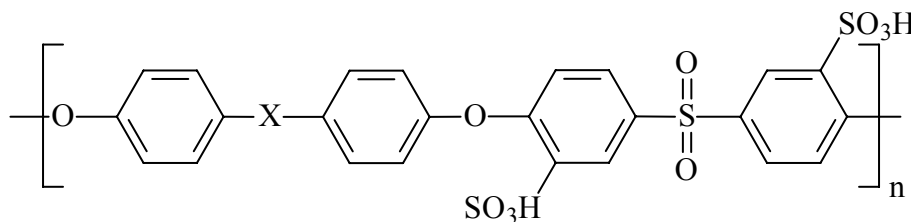
Poly(arylene ether sulfone)s, Structure 2-2, are engineering thermoplastics with excellent thermal and mechanical properties, especially when there is a presence of aliphatic units. These polymers maintain resistance to oxidation and acid catalyzed hydrolysis. One area of particular importance is modifying the structure without sacrificing properties. Post-sulfonated poly(arylene ether sulfone)s have been investigated using a variety of sulfonation agents such as chlorosulfonic acid and a sulfur trioxide-triethyl phosphate complex. It was determined that the sulfonic acid group was restricted to the activated position *ortho* to the aromatic ether bond shown in Structure 2-3 (top). Problems with this method include precise control over the location of sulfonation and in the case of bisphenol-A-based systems, the achievement of a maximum of one sulfonate group per repeat unit.



Structure 2-2



Activated Ring

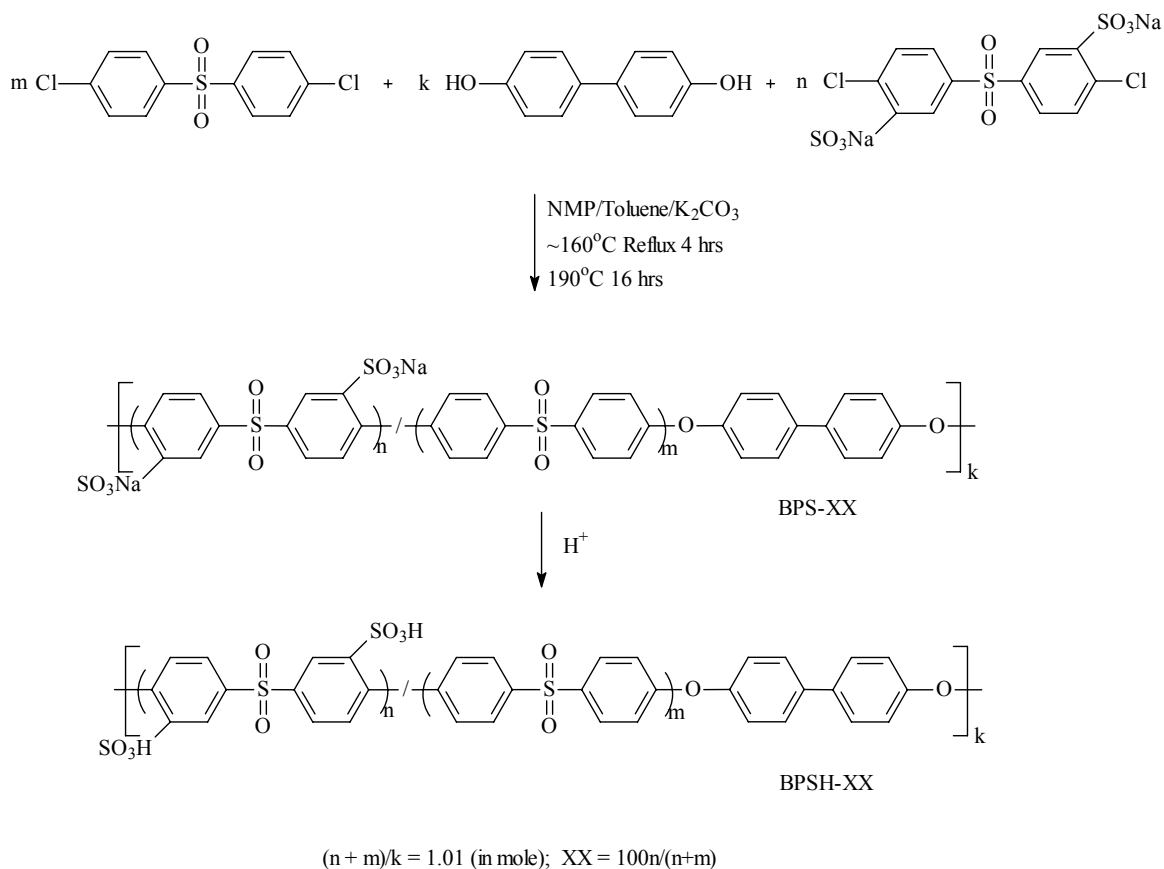


Deactivated Ring

Structure 2-3

An alternate effort was aimed at investigating the effect of sulfonating the deactivated sites of the repeat unit, Structure 2-3 (bottom). It was expected that enhanced stability and higher acidity could be achieved due to strong electron-withdrawing action by the sulfone group. This was shown to be true earlier by Robeson and Matzner¹² in a patent about flame retardant additives and later by Ueda et al.¹³ A modified procedure has allowed a wholly aromatic, highly

sulfonated poly(arylene ether sulfone) copolymers via direct polymerization to be produced. A simple outline of the copolymer synthesis is shown in Scheme 2-2 and can be found in more detail in references.¹⁴⁻¹⁷

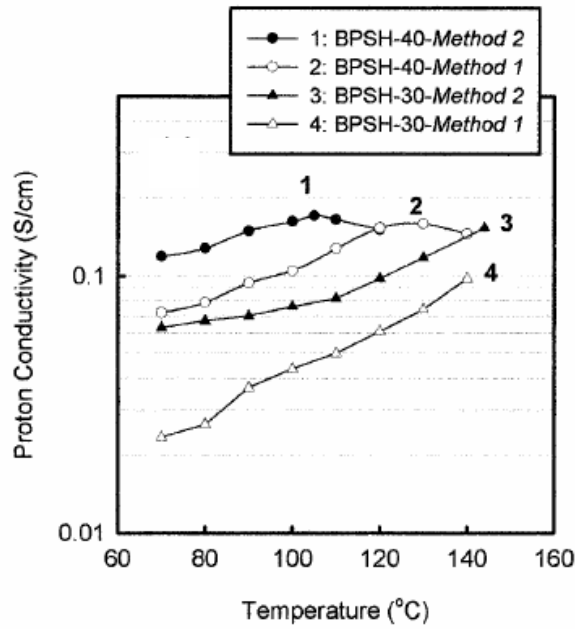


Scheme 2-2

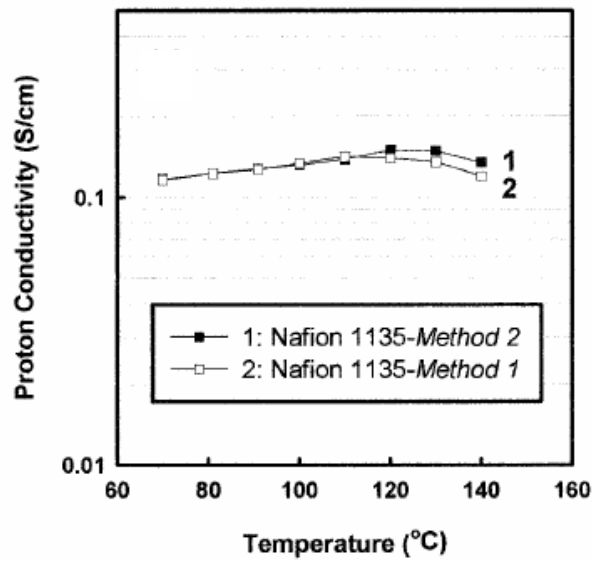
It has been shown that the method of acidifying a proton exchange membrane can affect the proton conductivity in the poly(arylene ether sulfone)s.¹⁸ Two acidifying methods were compared. The first method (Method 1) involved immersing the membranes in 1.5 M H₂SO₄ at 30 °C for 24 hrs followed by immersion in a deionized water bath at 30 °C for 24 hrs. The second method (Method 2) involved a boiling 0.5 M H₂SO₄ bath at 80 °C for 2 hrs followed by a boiling deionized water bath at 80 °C for 2 hrs. For Nafion 1135, BPSH-30, and BPSH-40, it was concluded that preparation of these films, Method 1 versus Method 2, effects the proton conductivity over a variety of temperature ranges, Figure 2-3.¹⁸ The proton conductivity for

Nafion 1135 was independent of acidification method; whereas, BPSH-30 and BPSH-40 showed an increase in proton conductivity utilizing Method 2 as compared to Method 1.

a)

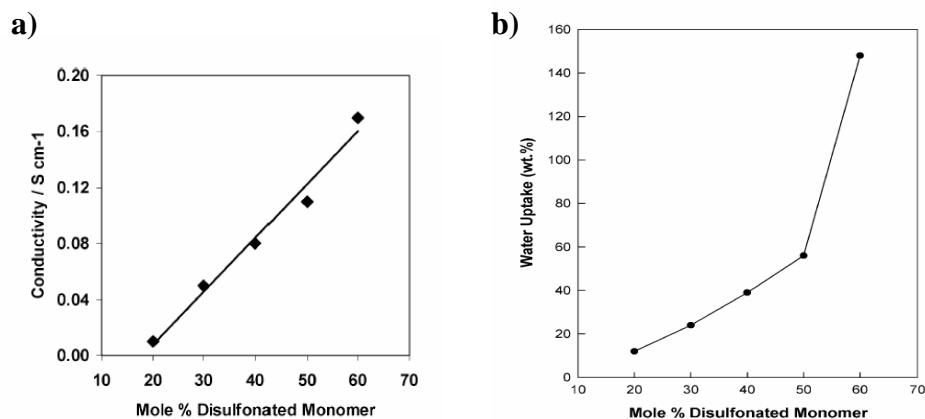


b)



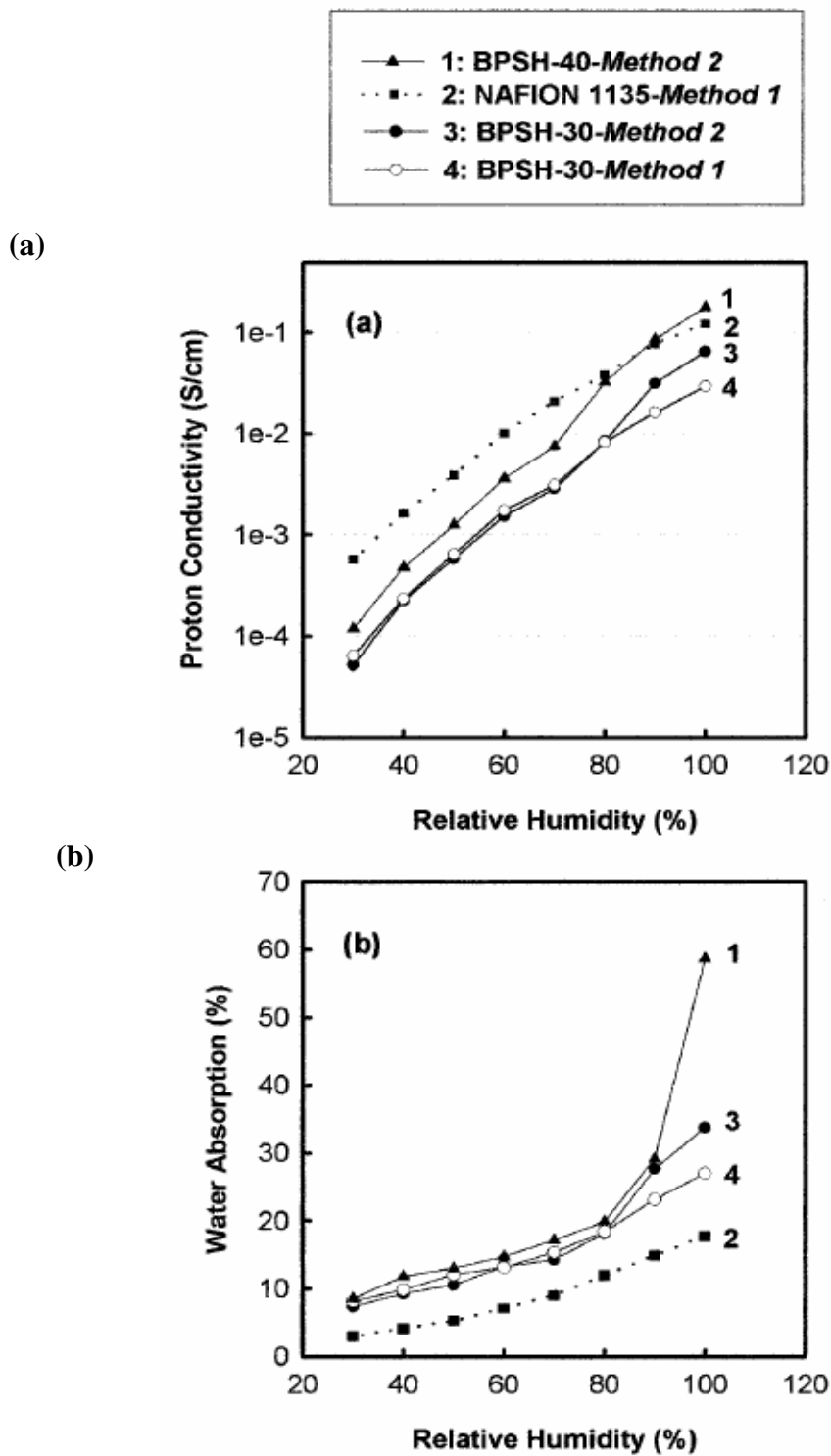
¹⁸Figure 2-3: Effect of temperature and acidification method on proton conductivity for a) BPSH-30 and BPSH-40 and b) Nafion 1135 systems.

As stated earlier, poly(arylene ether sulfone) are known thermoplastics that display excellent thermal and mechanical properties and are resistant to acid catalyzed hydrolysis as well as oxidation. The McGrath group at VT has shown that sulfonating this polymer does not sacrifice its excellent properties. In comparison to Nafion 117, the conductivity of BPSH is comparable when the degree of sulfonation approaches 30 % or higher at 30 °C. It would be reasonable to speculate that the higher the degree of sulfonation, the better the proton conductivity and performance. However, as the degree of sulfonation is increased above 50 %, the water uptake and swelling increases at a more rapid rate. Thus, to maintain good performance, the hydration rate for the membrane will have to be increased. This is not viable at this time with current PEM systems. A range of sulfonation between 30 to 45 % gives the best indication for a good PEMFC membrane. Figure 2-4 indicates the effect of the degree of sulfonation on proton conductivity as well as water uptake and graphically provides indication of the above-mentioned trend.¹⁵



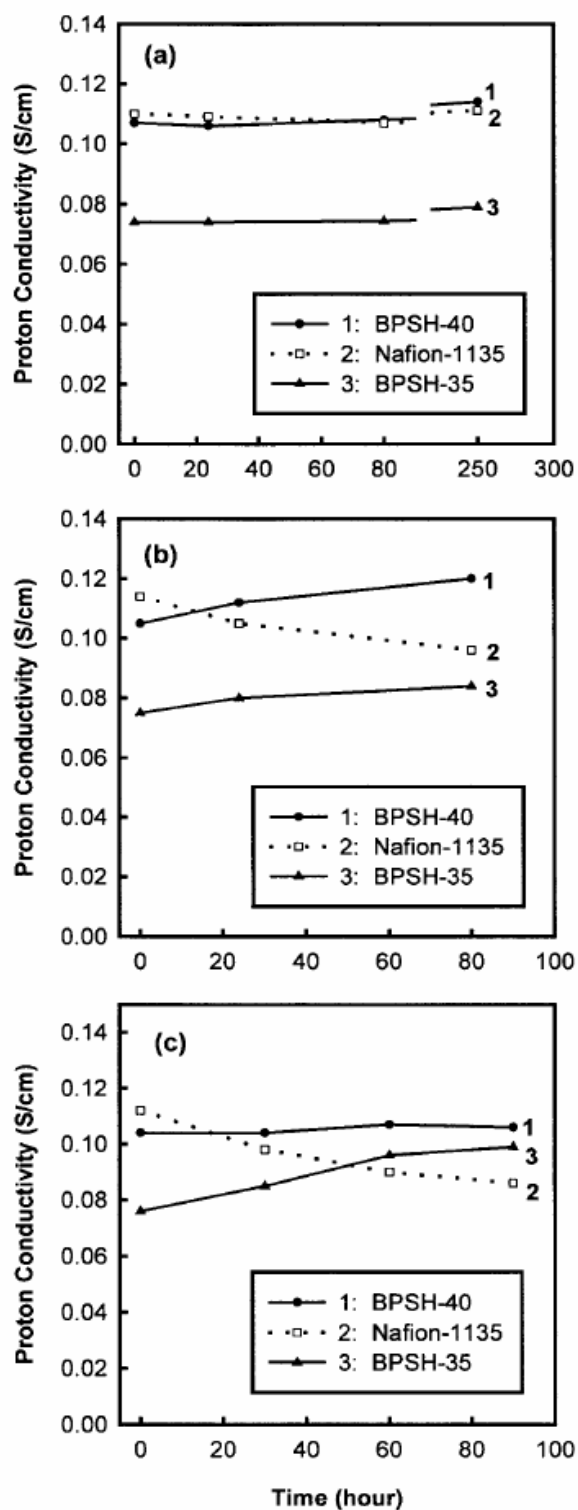
¹⁵Figure 2-4: Influence of amount of disulfonation on a) proton conductivity and b) water up-take at 80 °C for BPSH.

A further investigation of the proton conductivity shows that it is significantly affected by the relative humidity at elevated temperatures and aging temperature. Figure 2-5 displays the proton conductivity of Nafion 1135 and BPSH systems over a relative humidity range of 0 to 100%. The acidity of Nafion ($pK_a \approx -5$) and BPSH ($pK_a \approx -1.2$) explains the trend of increasing conductivity with increasing RH, even though for Nafion the equilibrium water sorption is lower.¹⁸



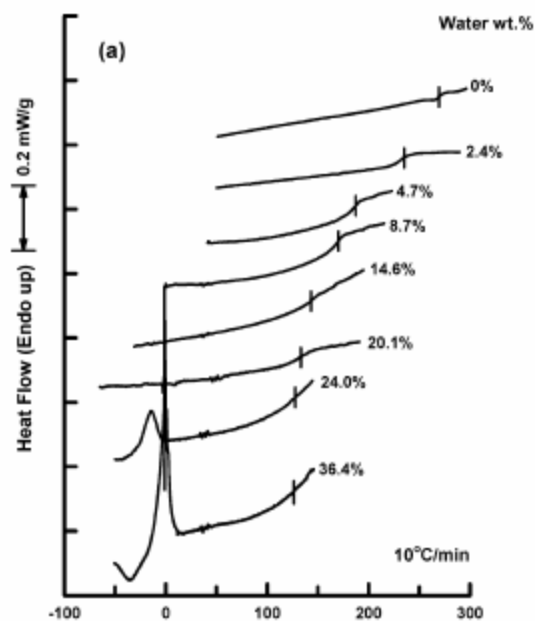
¹⁸Figure 2-5: Influence of Relative humidity on the (a) proton conductivity and (b) equilibrium water sorption.

Aging temperature plays a huge role in the longevity of a material. It has been shown in Figure 2-6 that high operating temperatures (80, 100, & 120 °C) can change the proton conductivity of a fully hydrated membrane. These experiments were conducted by exposing the samples at the desired temperature for a controlled time and then cooled to 30 °C. The samples were then acidified using acid treatment Method 1 and the proton conductivity was measured at 30 °C in liquid water. At 80 °C, the conductivity is constant because the membrane is not undergoing polymer chain rearrangement. However, at 100 °C, the hydrothermal energy is sufficient to cause the polymer's morphology to change. An increase in conductivity occurs for the BPSH system, whereas the conductivity of Nafion declines with time, which is caused by destruction of the ionic domains. This same trend continues at 120 °C with a larger difference in proton conductivities between Nafion and BPSH. The aging temperature of BPSH correlates to a longer operating and better performing fuel cell system over time than with Nafion.¹⁸



¹⁸Figure 2-6: Effect of aging temperature on the proton conductivity of fully hydrated membrane at (a) 80 °C, (b) 100 °C, & (c) 120 °C.

Finally, it has been shown that proton conductivity and water transport are dependent on the hydration level. The hydration level is attributed to the solvation of the acid group and the amount of water bound to the polymer chains and in the bulk within a pore. It has been determined that the water resides in the hydrophilic domains and maintains three states: *Nonfreezing water*, *Freezable bound water*, and *Free water*. Nonfreezing water is strongly associated with the polymer and shows no thermal transition either by DSC or TGA, but depresses the T_g . Freezing water is related to either the polymer or bound nonfreezing water and displays a broad melting behavior around 0 °C. Free water provides a sharp melting peak at 0 °C. This phenomenon is demonstrated in Figure 2-7, which shows how the water uptake depresses the glass transition temperature. Once the percolation temperature, T_p , is reached, the non-freezing water and free water appear in the form of a melting peak at approximately 0 °C.¹⁹



¹⁹Figure 2-7: DSC curves showing the effect of water uptake on the T_g and the appearance of loosely and freely bound water for BPSH-40.

Table 2-2 indicates that the amount of Nonfreezing bound water is independent of the degree of disulfonation. However, as the degree of disulfonation is increased there is a rise in the amount of water adsorbed as well as the presence in loosely and freely bound water.

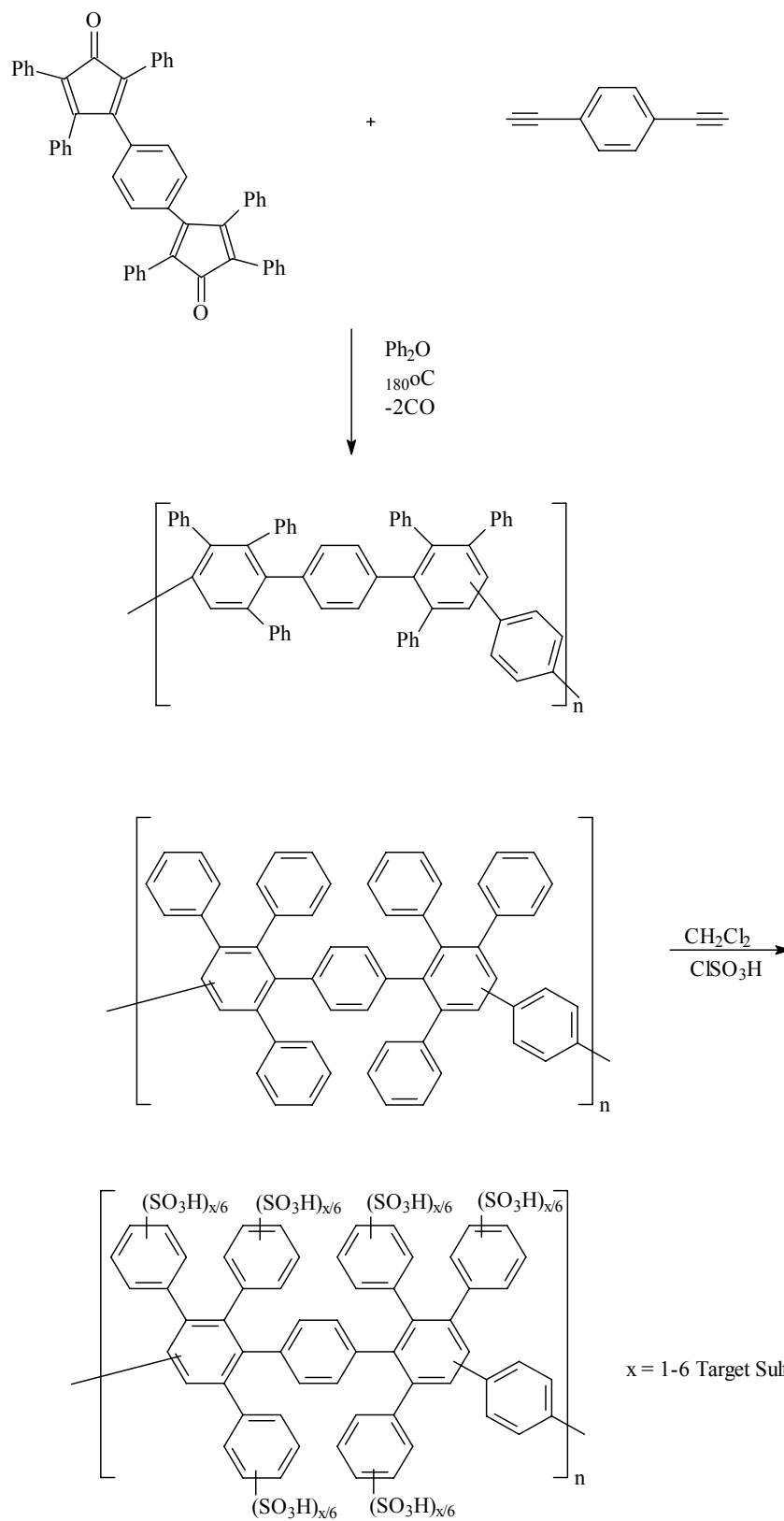
¹⁹Table 2-2: Effect of disulfonation on the states of water.

copolymer	IEC (mequiv/g)	no. of water per sulfonic acid group, λ					T_g of dried sample (°C)	T_g of fully hydrated sample (°C)
		water uptake (%)	total water	non- freezing water	loosely bound water	free water		
BPSH-0	0	0	0	0	0	0	223	
BPSH-10	0.5	7	8.1	3.2	4.9	0	232	
BPSH-20	0.9	18	10.8	3.6	7.2	0	246	
BPSH-30	1.3	29	12.0	4.1	7.9	0	257	136
BPSH-40	1.7	56	18.0	5.1	10.8	2.2	267	126
BPSH-50	2.0	124	33.1	4.9	24.5	3.7	272	98
Nafion-1135	0.9	33	20.2	2.2	13.1	4.9	160	99

Gas permeation and sorption measurements will be used to monitor the effect the states of water and changes in the material have on the gas transport mechanism of fuel cell membranes. The non-freezing water accounts for the T_g depression; however, it is the presence of bound and free water that determines the ability of the penetrant and water molecule to move throughout the membrane. Gas permeation experiments are transient measurements, which are easier to carry out for membranes in the dehydrated form. Gas sorption experiments incorporate the gravimetric balance method to allow monitoring of gas uptake as a function of humidity. This method will allow transport properties, such as solubility and enthalpy of solution to be calculated under non-humidified and humidified conditions.

2.5.3 Post-Sulfonated Diels Alder Poly(phenylene)

The aromatic nature of poly(phenylene)s can enhance the thermochemical stability of the PEM in comparison to commercially available materials. High molecular weight polymers are essential for chain entanglements to occur in order to produce physically robust films. The pendant group of the aryl halide monomer controls the achievable molecular weight and limits broad functionalization as well as the degree of sulfonation.²⁰ A robust film is a critical characteristic for films to perform well in a PEMFC environment. Thus far, the group at Sandia National Labs have produced a post sulfonated poly(phenylene) (SDAPP) with a relatively high proton conductivity (10^{-2} S/cm) and good PEM characteristics. The parent SDAPP polymerization is formed by reacting 1,4-bis(2,4,5-triphenylcyclopentadienone)-benzene with diethynylbenzene, Scheme 2-3. The resulting polymer is sulfonated (sodium form) using dichlorobenzene, which was diluted in chloroform. A film is formed by dissolving the salt form of SDAPP in dimethyl acetamide (DMAc) and casting the solution onto a glass plate. The film is removed from the glass plate and converted to the acid (proton) form by immersing the film in 2.0 M H_2SO_4 at 100 °C for 1 h, followed by a deionized water (18M Ω) at 100 °C for an additional hour to remove any excess acid. Further details of the synthesis of SDAPP are found in reference 13. The SDAPP series can be modified to have a wide range of ion exchange capacities which results in a variety of proton conductivities, water up-take, etc. shown in Table 2-3.



Scheme 2-3

Table 2-3: Influence of ion exchange capacity for SDAPP samples on water uptake and proton conductivity.

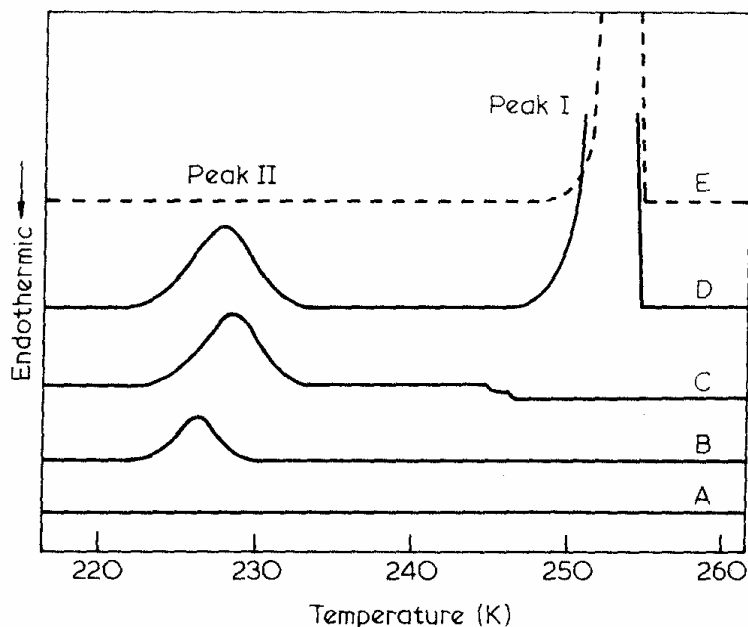
Sample	IEC (meq/g)	Water Uptake (weight %)	λ (H ₂ O/HSO ₃)	Conductivity (mS/cm)
SDAPP1	0.98	21	12	13
SDAPP2	1.4	36	14	49
SDAPP3	1.6	75	19	87
SDAPP4	2.2	137	30	123

2.6 States of Water

The three states of water in polyelectrolytes have been previously mentioned in Section 2.5.2. The three states of water include *Nonfreezing water* (tightly bound), *Freezable bound water* (loosely bound), and *Free water*. Nonfreezing water is strongly associated with the polymer and shows no thermal transition by either differential scanning calorimetry (DSC) or thermal gravimetric analysis (TGA), but depresses the T_g . Freezing water is related to either the polymer or bound nonfreezing water and displays a broad melting behavior around 0 °C. Free water provides a sharp melting peak at 0 °C. The term bound water has been defined as the summation of the nonfreezing and freezable bound water. There have been many methods used to measure the amount of bound water such as drying techniques, sorption and desorption isotherms, non-freezing water evaluated using calorimetric methods, and nuclear magnetic resonance (NMR) relaxation methods (discussed later).

The determination of bound water by DSC is one of the most useful techniques for this research. Nakamura and et al.²¹ examined the relationship between bound water and the effect hydrogen bonding in polyhydroxystyrene, which is a hydrophilic polymer unlike the hydrophobic polystyrene. Figure 2-8 displays the DSC cooling curve for polyhydroxystyrene. Curve A displays a curve for low water sorption and as the water sorption is increased to 9.2% (curve B), a broad, loosely bound water peak appears. Eventually, when high water sorption is achieved (26.3% water sorption, curve D), a narrow, free water peak appears. The free water

peak is easily identifiable due the similarity to the bulk water DSC curve (curve E). It is not clear in Figure 2-8, but the tightly bound water is always present and is represented as the plasticizer of the T_g . Nakamura et al defined a term called ‘critical water content’ as the calculated water content needed to depress the T_g of polyhydroxystyrene to that of polystyrene. It was determined through calculation of the enthalpy of crystallization that all the water does not crystallize and therefore the difference between the water added and observed from DSC can be accounted for by being tightly bounded to the sample. Also, as the mole fraction of the hydroxyl group is increased, the percentage of bound water and critical water content increases indicating a disruption in hydrogen bonding and the water molecules attaching to hydroxyl groups.



²¹Figure 2-8: DSC cooling curve of water sorbed for polyhydroxystyrene:
 Curve A = 7.8%; Curve B = 9.2%; Curve C = 10.7%; and
 Curve D = 26.3% and Curve E = pure (bulk) water

2.7 Gas Permeation

The rate of gas transport through a membrane is called permeation. Gas transport through polymeric membranes is described as a three-step solution diffusion mechanism. The model was first proposed by Sir Thomas Graham in 1866.²² Graham stated that a penetrant or gas molecule undergoes a three-step process that involved sorption, diffusion, and desorption. During the first step, sorption, the gas molecules dissolve into the membrane surface from high pressure (feed) side. The second step, diffusion, involves the transport of gas molecules or movement from the high pressure side to the low pressure side. At this point, the diffusion is the rate controlling step because it takes time for the polymer chains to make a gap for the penetrant to “jump” into. The penetrant goes through a series of these “jumps” until it reaches the low pressure face of the membrane. Now, the penetrant desorbs into the permeate stream during the third step, desorption.

2.7.1 General Concepts

There are three fundamental parameters used to describe gas transport in a polymeric membrane. The first is the permeability coefficient (P), or permeability which is the steady-state gas flux through a membrane. The permeability is normalized with respect to thickness and pressure gradient across the membrane. Secondly, the diffusion coefficient (D) describes the ease for a penetrate molecule to move across the membrane. The third parameter is the solubility coefficient (S) and it describes how the penetrant is held in the membrane through interactions at equilibrium. These three parameters are related through the simple equation shown below. Limitations as well as more detail descriptions are found in the proceeding sections.

$$P = D \cdot S \qquad \text{Eq. 2-1}$$

2.7.2 Permeability Coefficient (P)

The permeability coefficient (P), permeability for short, is a measure of the rate a penetrant moves through a membrane. The permeability of a pure gas i , P_i , with a membrane thickness of l can be defined as follows:

$$P_i = \frac{J_i}{(p_f - p_p)} \cdot l = \frac{J_i}{-\Delta p} \cdot l \quad \text{Eq. 2-2}$$

where J_i is the steady-state gas flux through the membrane, p_f and p_p are the upstream (high or feed) and downstream (low or permeate) pressures respectively, and Δp is defined as $p_f - p_p$. For gas mixtures, p_f and p_p are referred to as the partial pressures of component i on the high and low pressure side of the membranes. Penetrant transport across a membrane is driven by differences in the penetrant's chemical potential across the membrane. In the case of non-ideal gas mixtures, the pressures in Eq. 2-2 are replaced with fugacities, f_i . Permeability in polymers is typically measured in units called Barrers and can be defined as

$$1 \text{ Barrer} = 1 \times 10^{-10} \frac{\text{cm}^3(\text{STP}) \cdot \text{cm}}{\text{cm}^2 \cdot \text{sec} \cdot \text{cmHg}} \quad \text{Eq. 2-3}$$

2.7.3 Diffusion Coefficient (D)

The diffusion coefficient or diffusivity is a kinetic parameter which characterizes the ability of the penetrant molecule to be transported across the membrane. The easier the transport, the higher the diffusivity will be. Typically, diffusion coefficients are measured in units of cm^2/s .

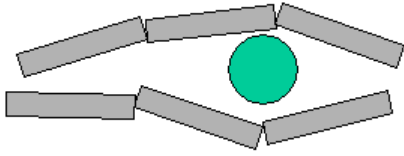
Diffusion depends on the penetrant size and shape, polymer morphology, polymer segmental dynamics, and temperature. Smaller penetrants tend to permeate faster across the

membrane causing an increase in the diffusion coefficient, such as that observed for helium in comparison to nitrogen. The penetrant size is characterized by van der Waals volume of the penetrant. Helium has a smaller kinetic diameter than nitrogen, 0.26 nm and 0.364 nm, respectively, indicating helium will diffuse faster than nitrogen. Also, linear or oblong penetrant molecules have less difficulty moving across the membrane than spherical molecules, thus having a higher diffusivity. For example, CO₂ (linear) will diffuse faster than CH₄ (spherical). Table 2-4 displays the kinetic diameters of various gases. In our research focus will be solely on hydrogen and oxygen.

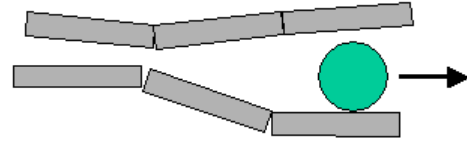
Table 2-4: Kinetic diameters of penetrant gas molecules.

Molecule	Kinetic Diameter (nm)
H ₂	0.289
He	0.26
CO ₂	0.33
O ₂	0.346
N ₂	0.364
CH ₄	0.38

The diffusion coefficient is also affected by a polymer's segmental dynamics or structure which controls the ability of the penetrant to make diffusive jumps. For a penetrant to move across the membrane, the chains must form a gap large enough for the molecule enter. These gaps develop from the polymer's chains intersegmental motion. Also, addition of more flexible linkages, such as -O- will allow the polymer to more easily make gaps for penetrant movement. More rigid groups such as aromatic groups reduce flexibility, which decreases the diffusion coefficient. Figure 2-9 is a conceptual representation of how the gaps form and allow diffusive jumps across the membrane.



No diffusive jump



Penetrant jump

Figure 2-9: Indicates the difference between a penetrant molecule's ability to diffusion through a membrane based on a series of jumps when a gap is available.

A polymer's morphology or free volume also affects the diffusion coefficient. Whether the polymer is in the rubbery or glassy phase, the gas diffusion will be distinctly different. Rubbery polymers tend to have diffusion coefficient that are significantly higher than glassy polymers. For example, rubbery, flexible, polymer like polybutadiene has a D_{O_2} value of $150 \times 10^{-8} \text{ cm}^2/\text{s}$ whereas; a less flexible, polymer such as polycarbonate has D_{O_2} value of $5 \times 10^{-8} \text{ cm}^2/\text{s}$.^{23,24} When discussing a polymer's chain mobility, an introduction of free volume or fractional free volume (FFV) is needed. A polymer's fractional free volume is defined as the total specific volume not occupied by polymer molecules and which can participate in penetrant molecule transport. Another way to think about free volume is the empty space in a polymer matrix. The fractional free volume is defined as

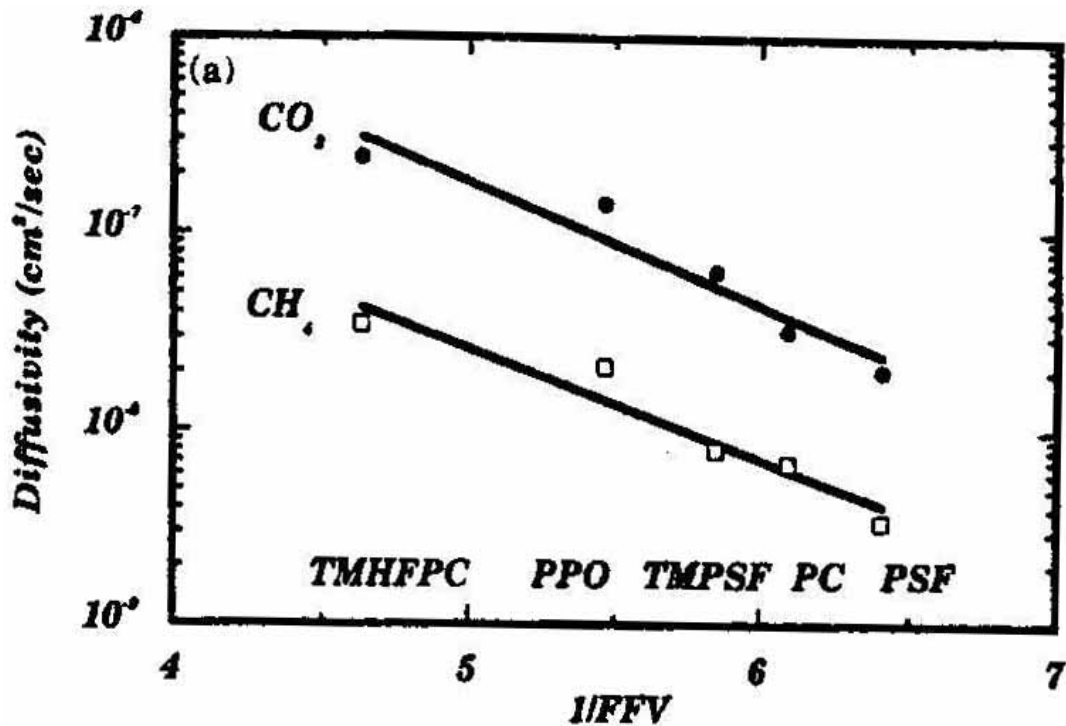
$$FFV = \frac{V - V_o}{V} \quad \text{Eq. 2-4}$$

where V is the polymer specific volume calculated from bulk polymer density values and V_o is the occupied volume. V_o is also defined as 1.3 times the van der Waals volume. The diffusion coefficient is related to the FFV through the Dolittle expression

$$D = D_0 \exp\left(\frac{-B}{FFV}\right) \quad \text{Eq. 2-5}$$

where D is the diffusion coefficient, FFV is the fractional free volume, and D_0 and B are constants characteristic of the polymer-penetrant system. From Eq. 2-5, it is shown that as the

FFV increases, the diffusion coefficient increases. The fact that the FFV and diffusion coefficient increases exponentially was shown by Ghosal and Freeman²⁴ and displayed in Figure 2-10. The last parameter affecting diffusivity is temperature. As the temperature is increased, the movement of polymer chains increases causing the diffusion of penetrants to increase.



²⁴Figure 2-10: Exponential relationship between the fractional free volume (FFV) and diffusivity (D).

Also, there is an increase in kinetic energy causing a faster diffusion by the penetrant molecules. Temperature is related to diffusion the Arrhenius-type equation below

$$D = D_o \exp\left(-\frac{E_d}{RT}\right) \quad \text{Eq. 2-6}$$

where E_d is the activation energy of diffusion, D_o is a constant, R is the ideal gas constant. In general, the diffusion coefficient is a stronger dependent of temperature than the solubility

coefficient unless the polymer undergoes crystallization. Crystals act as barriers to gas molecules and will decrease the diffusion as well as the permeability.

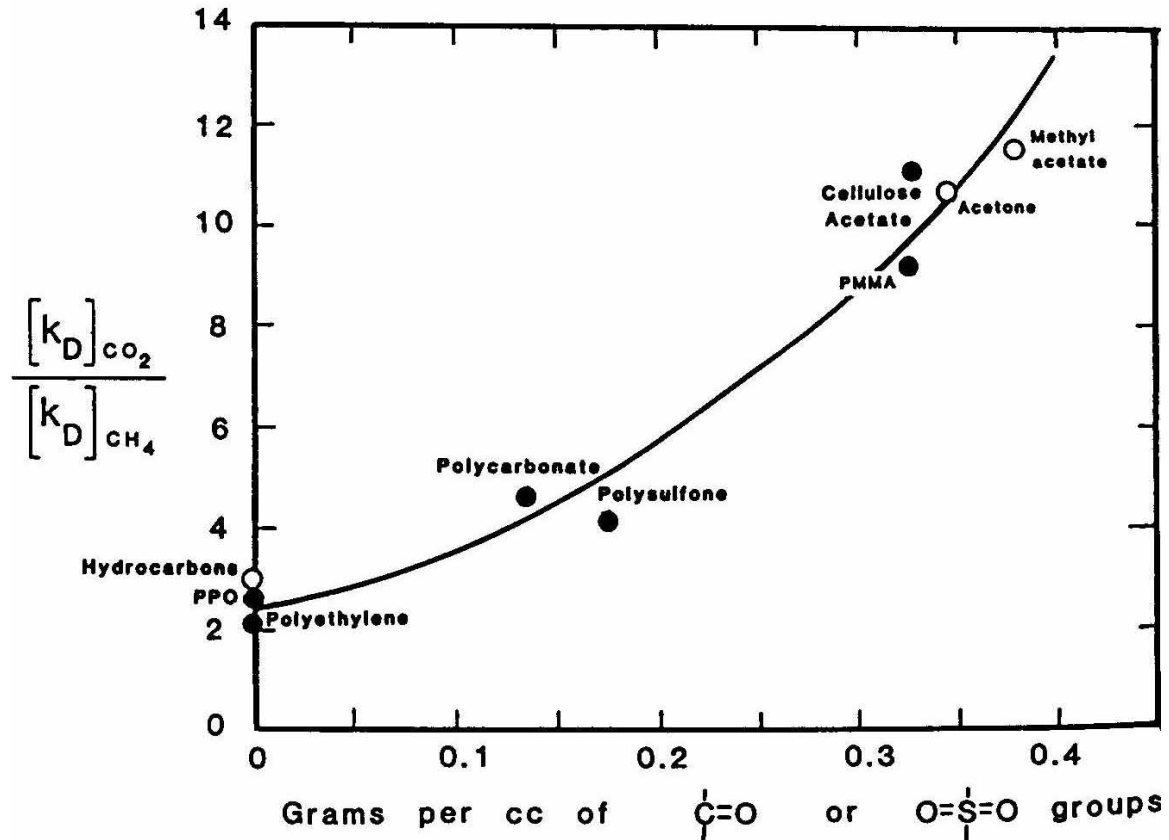
2.7.4 Solubility Coefficient (S)

The solubility coefficient (S) is defined as a membrane's maximum storage capacity thermodynamically at a given pressure. Solubility is defined as the concentration per pressure and is given in the equation below:

$$S_i = \frac{C_i}{P_i} \quad \text{Eq. 2-7}$$

where S_i is the solubility of component i , C_i is the concentration of i in the membranes ($\text{cm}^3_{\text{gas}}(\text{STP})/\text{cm}^3_{\text{polymer}} \text{cmHg}$), and P_i is the partial pressure of i in the feed stream.

The solubility coefficient is affected by not only the polymer's properties but a gas molecule's properties as well. Firstly, a gas molecule with a higher critical temperature (T_c) usually correlates to an increase in solubility because of an increase in the gas condensibility. This is also holds when comparing the normal boiling temperature (T_b) and the Lennard-Jones force constant. Next, the solubility coefficient is affected by the interactions between the membrane and gas molecule based on polarity. For example, carbon dioxide contains quadrupole moments which increase its solubility in polar polymers in comparison to nonpolar polymers. Freeman and Ghosal²⁴, Figure 2-11 showed an increase in solubility with increasing polar groups for polymers such as polyethylene, polysulfone, and poly(methyl methacrylate).



²⁴Figure 2-11: Effect of polar groups on the solubility for various polymers.

The solubility has been shown to be related to temperature through an Arrhenius relationship between the condensibility and polymer and is express in Eq. 2-8:

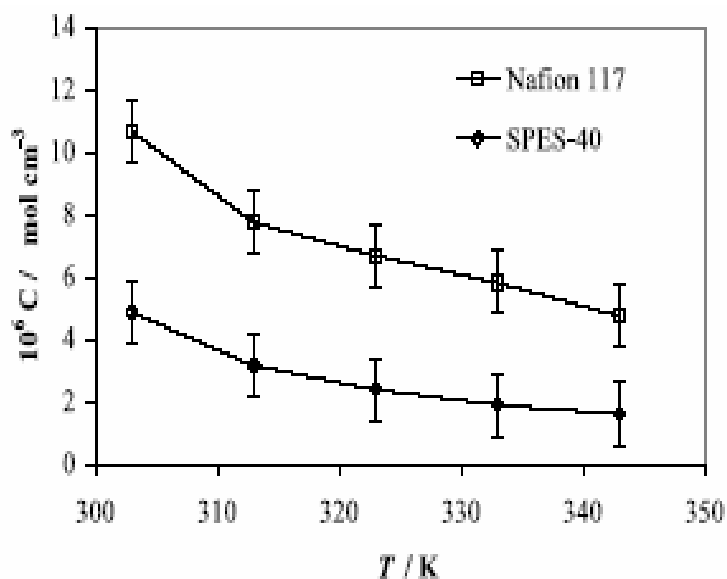
$$S = S_o \exp\left(\frac{-\Delta H_s}{RT}\right) \quad \text{Eq. 2-8}$$

where S_o is a constant, R is the ideal gas constant, T is temperature, and ΔH_s is the partial molar enthalpy of sorption. ΔH_s can be calculated using Eq. 2-9.

$$\Delta H_s = \Delta H_{cond} + \Delta H_{mix} \quad \text{Eq. 2-9}$$

where ΔH_{cond} is the change in enthalpy associated with a phase change from a gas penetrant to a condensed density and ΔH_{mix} is the enthalpy change associated with creating a gap for a gas

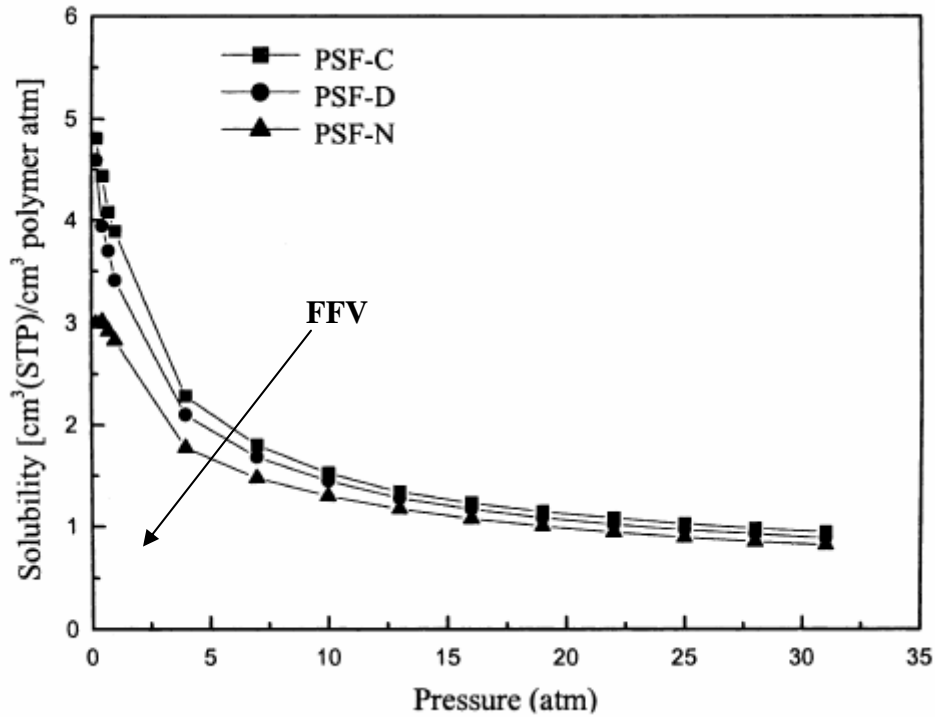
molecule to dissolve in the membrane. In the case of small molecules with low molecular weight and low T_c 's like H_2 or He, ΔH_{cond} is small causing the ΔH_{mix} term to dominate ΔH_s . When weak interactions between the polymer and gas occur, ΔH_{mix} is positive causing an increase in S with an increase in temperature. In the case of a condensable gas such as CO_2 , ΔH_{cond} could give a large, negative contribution to ΔH_s , which would cause S to decrease with increasing temperature. Zhang and et al.²⁵ have studied the effect of temperature for the disulfonated poly (arylene ether sulfone) and Nafion 117 systems in MEA form. The solubility coefficient as a function of temperature is shown in Figure 2-12 and was found to decrease with increasing temperature for Nafion 117 and theBPSH-40 system.



²⁵Figure 2-12: Effect of temperature on solubility coefficient for Nafion 117 and BPSH-40.

Finally, free volume not only affects the diffusion process, but the solubility coefficient as well. Sorption sites open due to excess volume formed from a polymer's inability to undergo conformational rearrangement fast enough to achieve equilibrium once the temperature falls below the glass transition temperature. As the pressure increases, these sites can become saturated resulting in no increases in concentration and lowering in the solubility coefficient without impacting the permeability. Hu and et al.²⁶ demonstrated the pressure and free volume

effect on solubility in polysulfone in CO₂. The only difference in each case was the solvent used to cast the polysulfone membrane. This is shown in Figure 2-13.



²⁶Figure 2-13: Effect of pressure on the solubility coefficient for polysulfone cast membranes in CO₂.

2.7.5 Gas Transport Through a Rubbery Polymer

The gas transport through rubbery polymers can be modeled easily using Henry's Law dependence on concentration, Eq. 2-10, when no strong interactions between the membrane and gas penetrant occur.

$$C = k_D P \quad \text{Eq. 2-10}$$

Here, C is the concentration of the penetrant in the membrane, k_D is the Henry's constant, and P is the pressure. By substituting Eq. 2-7 into Eq. 2-10, the solubility coefficient is equal to the Henry's constant, k_D . When no crystallization occurs, the diffusion of gas in a rubbery polymer follows Fick's law, shown below.

$$J = -D \frac{\partial C}{\partial x} \quad \text{Eq. 2-11}$$

Substituting Eq. 2-10 into Eq. 2-11 and replacing x with l (membrane thickness) and the new equation for permeability (P) is shown below and now model gas transport through a rubbery polymer.

$$P = k_D \cdot D \quad \text{Eq. 2-12}$$

Typically, the permeability through rubbery polymers is significantly higher than in glassy polymers. This is the result of the polymer backbone being more mobile due to the loss of restrictions on rotation and/or interactions between chains.

2.7.6 Gas Transport Through a Glassy Polymer

The introduction to excess volume causes the ability to model gas transport in glassy polymers to be more difficult than in rubbery polymers. Excess volume occurs when there is a loss in large scale movement in the polymer when the T_g is crossed. The chains are prohibited from rearranging fast enough to reach equilibrium. Once the T_g is crossed, the polymer undergoes long relaxation times causing the presence of excess volume. However, over time the polymer will approach equilibrium and reduce the amount of excess volume. This process is called physical aging. Various modes of gas sorption in polymer membranes, such as Langmuir isotherm and Dual Mode sorption will be discussed in section 2.8.

2.7.7 Time Lag Method

This section outlines the experimental method I used to determine the diffusion coefficient and the solubility coefficient for the membranes studied. The method is called the Time Lag Method.

The time lag is defined as the amount of time required for a gas or vapor to permeate through a membrane. It can be calculated using a two chambered closed volume-variable pressure. The upstream chamber simply contains the feed gas and a pressure transducer to record the feed gas pressure. This chamber is separated from the downstream chamber by a membrane, which is degassed before testing. At the beginning of the test, a feed gas is introduced into the system and the permeate pressure is recorded as a function of time. The Time Lag is defined where the pressure is zero on the time axis (x-axis), when a line is extrapolated to the time axis from the linear part of the response curve. The pressure data can be divided into two regions: unsteady state region and steady state region. The unsteady state region exists at shorter times, and includes portions where the permeate pressure is zero. The steady state region is the area of interest in the Time Lag Method, and consists of a linear relation between permeate pressure and time. Figure 2-14 shows the location of the Time Lag, θ , and the unsteady state and steady state regions for gas permeation.

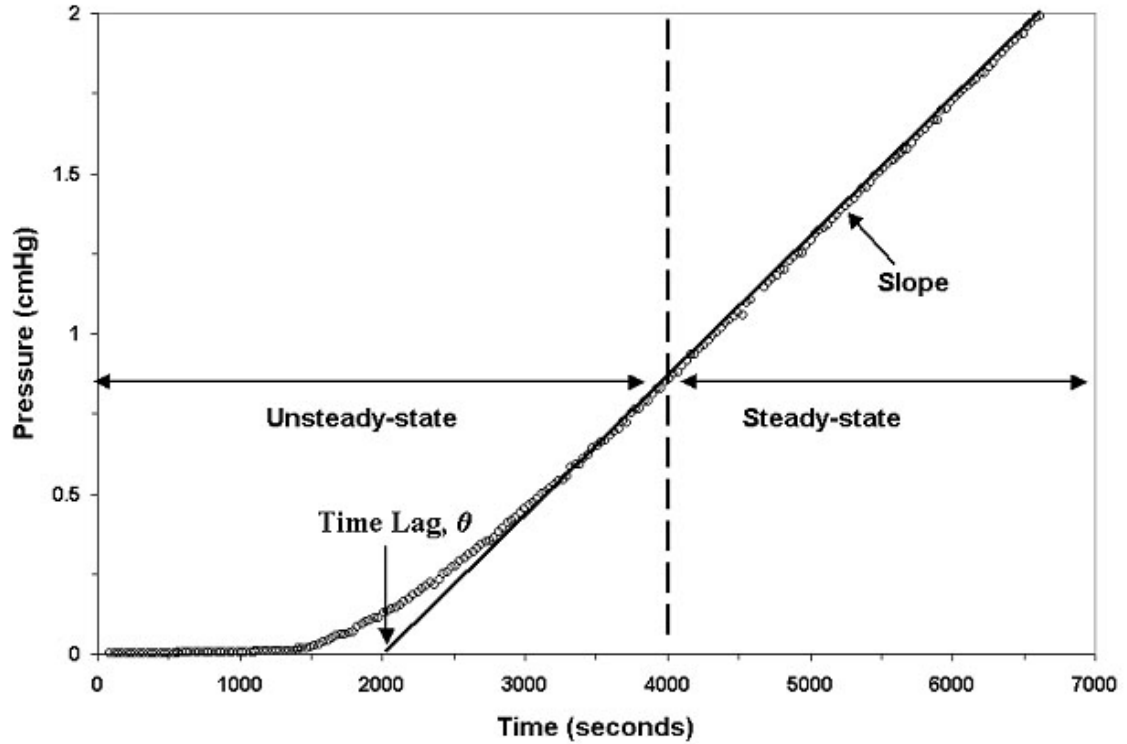


Figure 2-14: Typical permeation experiment data analyzed using Time Lag Method

To define the Time Lag method, one must recall Fick's second law of diffusion. This law can be used to model the permeation process, which is shown below.

$$\frac{\partial C}{\partial t} = D \frac{\partial^2 C}{\partial x^2} \quad \text{Eq. 2-13}$$

In order to solve for the Time Lag using the previous equation, the following boundary conditions are imposed.

$$\begin{array}{lll} t < 0 & 0 \leq x \leq l & C = 0 \\ t \geq 0 & x = 0 & C = C_{2,m} = S p_2 \\ t \geq 0 & x = l & C = \partial C / \partial x = 0 \end{array}$$

Applying these boundary conditions results in the numerical solution shown in Eq. 2-13. This solution is for one-dimensional flow through the membrane, with the assumption that the diffusion coefficient D is a constant. This statement implies that D is independent of temperature and concentration.

$$\frac{Q}{lC_2} = \frac{Dt}{l^2} - \frac{1}{6} - \frac{2}{\pi^2} \sum_{n=1}^{\infty} \frac{(-1)^n}{n^2} \exp\left(-\frac{Dn^2\pi^2 t}{l^2}\right) \quad \text{Eq. 2-14}$$

In Eq. 2-14, Q is the total permeant passing through the membrane, and l is the thickness of the film. The other variables in this equation are the concentration in the film at the feed side C_2 , the diffusion coefficient D , and the time t . It is possible to reduce Eq. 2-14 when time t is allowed to approach infinity. When t is allowed to approach infinity, the summation element goes to zero, and the following equation is obtained.

$$\frac{2}{\pi^2} \sum_{n=1}^{\infty} \frac{(-1)^n}{n^2} \exp\left(-\frac{Dn^2\pi^2 t}{l^2}\right) \Bigg|_{t \rightarrow \infty} = 0 \quad \text{Eq. 2-15}$$

The steady-state region of the pressure response curve, shown in (Figure 2-15), implies that t has gone to infinity. This steady-state region also signifies that $\partial C/\partial t = 0$. When Eq. 2-15 is substituted into Equation 2-14, then the reduced equation becomes

$$\frac{Q}{lC_2} = \frac{Dt}{l^2} - \frac{1}{6} \quad \text{Eq. 2-16}$$

Rearranging this in terms of Q reveals the Time Lag θ shown in Equation 2-17. Equation 2-17 indicates that the total gas passing through the membrane, Q , is zero until a time t has elapsed, which is greater than the Time Lag θ . Q is also commonly referred to as the accumulation term, since the gas permeate is trapped within a fixed volume.

$$Q = \frac{DC_2t}{l} - \frac{lC_2}{6} = \frac{DC_2}{l} \left(t - \frac{l^2}{6D} \right) = \frac{DC_2}{l} (t - \theta) \quad \text{Eq. 2-17}$$

$$\theta = \frac{l^2}{6D} \quad \text{Eq. 2-18}$$

Obtaining the Time Lag θ shown in equation 2-17 provides a direct route for calculating the diffusion coefficient D .

The permeability coefficient P is calculated from the slope found in (Figure 2-15) within the steady-state region. Solving for the flux J , is the starting point for the solution of the permeability coefficient P . The solution for the flux J , through the membrane is given by the following expression.

$$J = \frac{\text{Slope}}{RT} \cdot \frac{V}{A} \left(\frac{22414 \text{ cm}^3(\text{STP})}{\text{mol}} \right) \quad \text{Eq. 2-19}$$

The solution for the flux J is converted to *STP* conditions, and the slope is obtained during a permeation experiment, within the steady-state region shown in Figure 2-14. In Equation 2-19, V is the volume of the evacuated chamber into which gas permeates, and A is the cross-sectional area of the membrane. The temperature of the experiment is T , R is the ideal gas constant, and l is the membrane thickness. Because the downstream pressure p_1 is much smaller than the feed pressure p_2 , the pressure difference Δp can be replaced with p_2 , shown with Equation 2-20.

$$J = P \frac{\Delta p}{l} \cong P \frac{p_2}{l} \quad \text{Eq. 2-20}$$

This can be rearranged to give equation 2-21

$$P \cong J \frac{l}{p_2} \quad \text{Eq. 2-21}$$

Using the Time Lag and its relationship with the permeability coefficient P , the diffusion and solubility coefficients are then given by the following expressions.

$$D_{eff} = \frac{l^2}{6\theta} \quad \text{Eq. 2-22}$$

$$S_{eff} = \frac{P}{D} \quad \text{Eq. 2-23}$$

2.8 Gas Sorption

The concept of adsorption can be traced back more 220 years ago when the uptake of gases on charcoal was first explained by C.W. Scheele in 1773 and by Abbé F. Fontana in 1777. Fontana observed freshly calcined charcoal, cooled under mercury, could adsorb several times its own volume of various gases. Scheele, now in 1777, found “air” expelled from charcoal on heating is re-adsorbed on cooling. The first systematic approach to examine the adsorption of a variety of gases on several solids was developed by T. de Saussure in 1814. He discovered that the amount adsorbed is dependent on the exposed surface area and varies based on the type of gas. Later, in 1843, Mitscherlich emphasized the role of pores in charcoal and estimated their average diameter to be approximately $1/2400$ ".^{27,28} It is the work performed by these pioneers that surface area and porosity (or pore volume) are acknowledged as significant contributors to the gas or vapor adsorption onto a solids.

In this chapter, background information will be given on the gravimetric adsorption method, which has been employed to determine the effect of relative humidity (RH) has on the gas transport mechanism for the disulfonated poly(arylene ether sulfone) (BPSH) and post sulfonated diels-alder poly(phenylene) (SDAPP) series. The goal is to gain a better understanding that RH has on gas transport and ultimately, fuel cell performance.

2.8.1 General Concepts

Sorption is a general term used to describe the initial penetration and dispersal of permeant molecules into the polymer matrix. This includes adsorption, absorption, cluster formation, and possible incorporation in microvoids. As the permeant is being sorbed into the matrix, several modes of sorption could occur simultaneously. Furthermore, the permeant can be distributed in the matrix based on such parameters as concentration, temperature, and swelling as a function of time.

The amount and type/mode of sorption is dependent upon the activity of the permeant interaction with the polymer at equilibrium, i.e.- enthalpy and entropy between the permeant and polymer. The different sorption behaviors are based on the interactions/strengths between the permeant molecules and the polymer or the permeant molecules themselves. Figure 2-15, displays graphically the five most common modes of sorption.²⁹

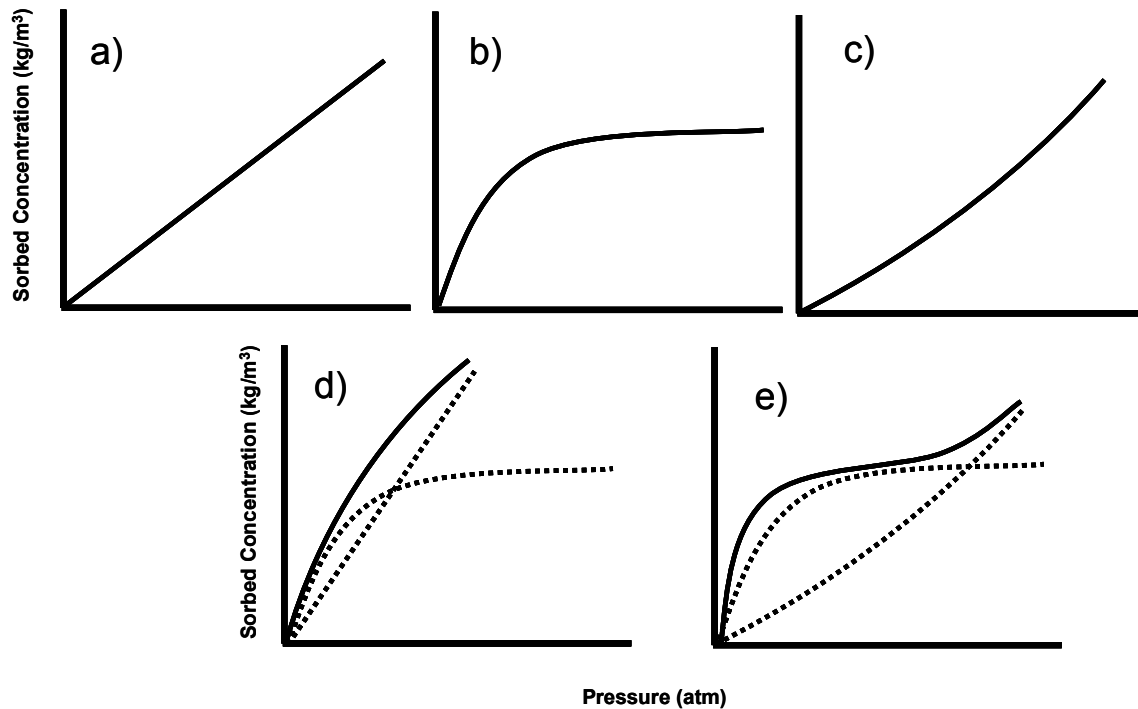


Figure 2-15: Typical types of sorption behavior: (a) Henry's Law, (b) Langmuir, (c) Flory-Huggins, (d) dual mode, (e) Type IV, BET.

2.8.1.1 Henry's Law Sorption

Henry's Law, Type I, sorption is the simplest type of sorption. Type I sorption occurs when the interaction between polymer/permeant and permeant/permeant is weak relative to polymer/polymer interaction, i.e.- Henry's Law is obeyed and ideally dilute solution behavior occurs. The solubility coefficient, S , is independent of the sorbed concentration at a given temperature and the sorption isotherm displays a linear relationship between concentration vs. pressure/vapor activity as shown by Equation 2-24. Commonly, type I sorption occurs when permeant gases are sorbed by rubbery polymers at low pressures ($<10^5$ Pa) and very low solubility ($<0.2\%$) of the permeant gas in the polymer.

$$C = Sp \quad \text{Eq. 2-24}$$

2.8.1.2 Langmuir-type Sorption

Langmuir sorption or Type II sorption occurs when large amounts of sorption takes place at low pressures. Type II sorption begins by sorption occurring at a specific site or microvoids immobilizes permeant molecules. When almost all the sites are occupied, a small amount of the permeant will dissolve into the polymer matrix. This type of sorption commonly occurs when dyes are absorbed by ionic polymers or polymers containing polar groups. Also, polymers containing dispersed porous particles with high surface area (i.e.- inorganic fillers like carbon black or silica gel) Equation 2-25 is used to describe this type of sorption, where C_H is the concentration of permeant sorbed by the sites, C_H is a site saturation constant, and b is a site affinity constant (ratio of ratio of rate constants for adsorption and desorption).

$$C_H = \frac{C_H b p}{1 + b p} \quad \text{Eq. 2-25}$$

2.8.1.3 Dual-mode Sorption

Dual-mode is a combination of Henry's and Langmuir sorption that is commonly used to describe the gas sorption in glassy polymers. Initially, it was speculated that gas molecules are present as a mobile population dissolved in bulk of the polymer, following Henry's Law, and are free to diffuse down a concentration gradient, while the remaining gas molecules are bound to a

fix number of adsorption sites/microvoids within the polymer. Therefore, the bound and mobile molecules are in equilibrium. The total concentration, C_{eq} , of sorbed molecules at low concentrations (Henry's Law dominates) is found using Equations 2-24 and 2-25

$$C_{eq} = Sp + \frac{C_H bp}{1 + bp} \quad \text{Eq. 2-26}$$

Dual-mode has been used to predict the permeation of such gases as CO_2 and $\text{C}_1\text{-C}_5$ hydrocarbon vapors through glassy polymers^{30,31} and vapors through rubbery polymers with adsorptive fillers.³² Equation 2-27 relates permeability to the dual-mode sorption where P is the mean permeability, S is the Henry's Law constant, D_D is the diffusivity of the mobile fraction of the sorbed molecules, $K = C_H b/S$ and the ratio characteristic of the relative amounts of gas sorbed in the two modes and R' is a measure of the degree of immobilization. For total immobilization, $R'=0$, and Equation 2-27 reduces to Equation 2-28. When complete mobility occurs, $R'=1$, and the permeability is strongly dependent on the pressure.

$$P = SD_D \left(1 + \frac{KR'}{1 + bp}\right) \quad \text{Eq. 2-27}$$

$$P = SD_D \quad \text{Eq. 2-28}$$

2.8.1.4 Flory-Huggins Sorption

Flory Huggins sorption describes a system where the interactions between permeant molecules are stronger than the permeant/polymer interactions. The solubility will increase as pressure increases and Equation 2-29 can be used to describe non-polar systems:

$$\ln \frac{P}{P^o} = \ln \phi_1 + (1 - \phi_1) + \chi(1 - \phi_1)^2 \quad \text{Eq. 2-29}$$

where P is the saturation vapor pressure, ϕ_1 is the volume fraction of permeant in the polymer and χ is the Flory-Huggins interaction parameter. In the case of simplest Flory-Huggins theory, χ is a measure of the heat of mixing of the sorbed molecules with the polymer. For non-polar systems, Equation 2-30 is used to estimate χ

$$\chi = \frac{V_1}{RT}(\delta_1 - \delta_2)^2 \quad \text{Eq. 2-30}$$

Where V_1 is the molar volume of the permeant and δ_1 and δ_2 are the solubility parameters of the permeant and polymer respectively. When $\delta_1 = \delta_2$, the permeant has achieved the highest solubility in the polymer. Finally, in terms of sorption, χ is a positive quantity and the extent of sorption decreases as χ increases.

2.8.1.5 Type IV Sorption

Type IV or Brunnauer, Emmett and Teller (BET) sorption isotherm is the sum of type II and type III sorption. Such sorption has been used to describe sorption of water by highly hydrophilic polymers such as poly(vinyl alcohol), poly(acrylic acid) or cellulosic materials.³³ Initially, strong sorption of water molecules occur onto specific sites (i.e. – these with polar groups) whereas, at higher pressures, either dissolution or clustering phenomena takes over.

2.8.2 Adsorption Background

There are two types of adsorption, physical adsorption and chemical adsorption or chemisorption. Physical adsorption or van der Waals adsorption describes weak interactions between the solid and gas penetrant, similar to condensation. Chemical or activated adsorption is due to strong interactions that occur between the solid and gas penetrant, similar to chemical reactions. In theory, there are many forces that can play a role, such as electrostatic, Coloumb, or van der Waals forces, etc. Each type of force can be most important based on the type of solid. For example, electrostatics forces are the most important forces in ionic crystals. However, in terms of adsorption, the forces inside of a body or solid are subject to equal forces in all directions; whereas, the forces on plane or surface contain unbalanced forces, the inward pull being greater than the outward forces. Once a gas molecule is adsorbed by the solid, whether physical or chemical, the unbalanced forces become saturated causing spontaneous adsorption and a decrease in the free energy of the system.

The free energy of the adsorption process is given by $\Delta G = \Delta H - T\Delta S$, where the ΔG and ΔS are negative causing a decrease in heat content, ΔH . This makes all adsorption processes

exothermic whether the measurement is made directly or indirectly. The decrease in the heat content is called the heat of adsorption. In terms of physical adsorption, the heat of adsorption is of the same magnitude as the heats of condensation of gases where chemical adsorption can be at magnitude higher. For example, the van der Waals adsorption of nitrogen on an iron catalyst is about 2-3,000 calories per mole, the heat of liquidification of nitrogen gas is 1360 calories per mole. For chemisorption of nitrogen on the same solid, adsorption was found to be approximately 35,000 calories per mole.²⁷ In the case of van der Waals adsorption, gas can be adsorbed either in a single layer, unimolecular, or more than one layers, multimolecular, onto the surface of the solid. Gas adsorption is an important phenomenon in areas such as gas purification, gas separation and recovery, and catalysis.

2.8.3 Water Sorption

It is important to understand the effect of water in membranes. This section will be devoted to water sorption as a function of relative humidity or water activity and some of the techniques used.

NMR T_2 relaxation studies have been used to determine the sorption and diffusion coefficient as a function of water activity.³⁴⁻³⁷ More specifically, the technique used is called the pulse gradient spin echo (PGSE) technique. The NMR sends pulses through the sample to allow the calculation of the intradiffusion coefficient for species bearing the detectable nucleus using diffusional dephasing of a gradient-encoded magnetization. The key is to have a pair of field gradient pulses space symmetrically onto a normal spin echo. Figure 2-16 illustrates this concept.^{37,38}

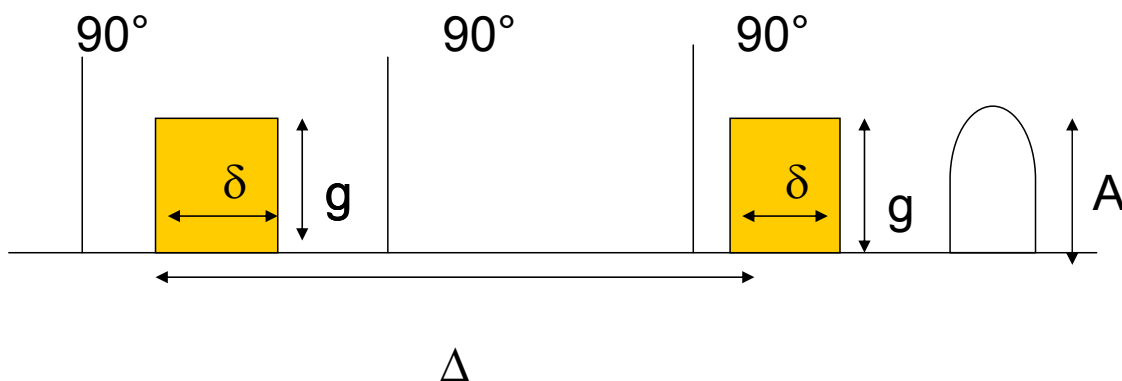


Figure 2-16: Pulsed field gradient spin-echo (PGSE) sequence.

To determine the intradiffusion coefficient, D, Eq. 2-31 is used.

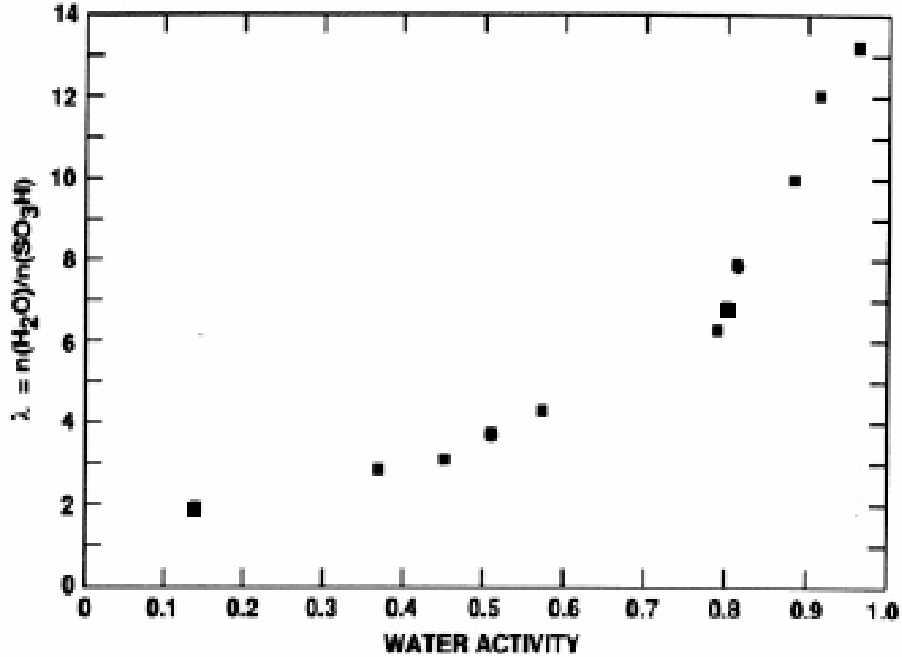
$$A(g) = A(o) \exp[-\gamma^2 D g^2 \delta^2 (\Delta - \frac{\delta}{3})] \quad \text{Eq. 2-31}$$

Where A is NMR signal intensity as a function of gradient strength, γ is gyromagnetic ratio (26752 radG⁻¹s⁻¹ for protons), δ is length of the gradient pulse, and Δ is the Time between gradient pulse, which is proportional to diffusive length. The diffusion coefficient can be determined fitting a triexponential decay function diffusion coefficient versus effective diffusion time, $(\Delta - \delta/3)$.³⁸

$$D_{tb} e^{(-\frac{t}{\lambda_{tb}})} + D_{lb} e^{(-\frac{t}{\lambda_{lb}})} + D_f e^{(-\frac{t}{\lambda_f})} \quad \text{Eq. 2-32}$$

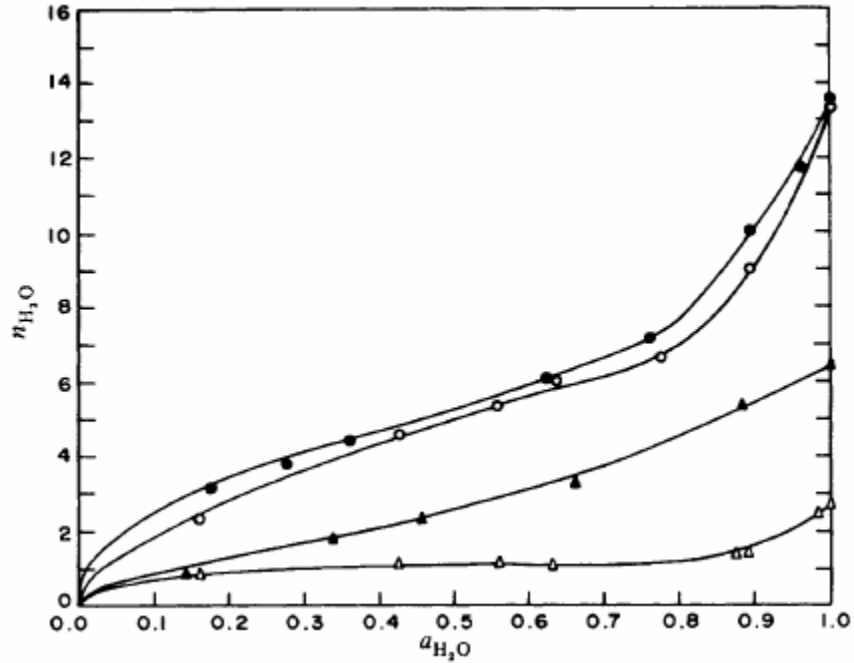
where D is the diffusion coefficient for each respective state of water (tb = tightly bound, lb = loosely bound, and f = free water), t is the diffusive time of water, and λ is the decay of time of the proton associated with each type of water.

Zawodzinski and et al. have been able to determine the diffusion coefficient for Nafion 117. It was found that as the amount of water increases the diffusion coefficient increases as well. For example, a water content of 2 H₂O/SO₃H yields a $D = 0.6 \pm 0.06 \times 10^{-6} \text{ cm}^2/\text{s}$ in comparison to a 14 H₂O/SO₃H, $D = 5.8 \pm 0.21 \times 10^{-6} \text{ cm}^2/\text{s}$. This corresponds to the following adsorption curve, Figure 2-17.



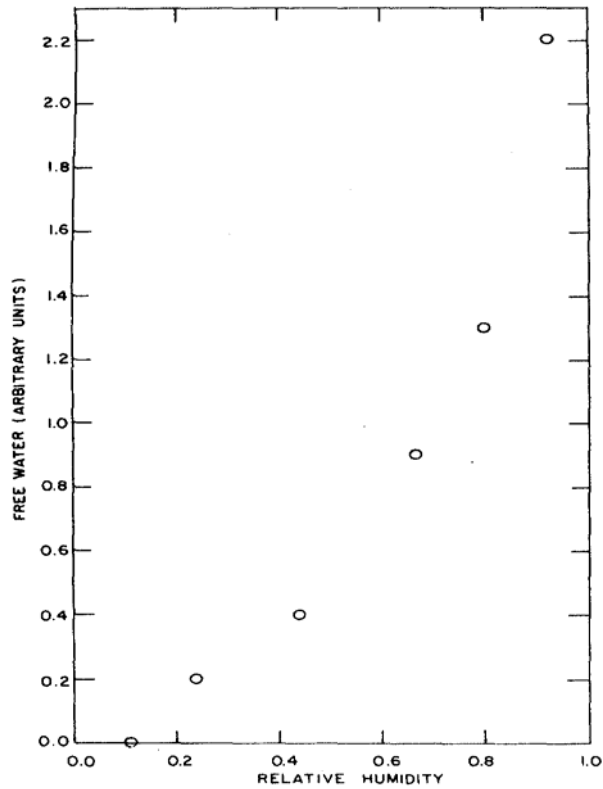
³⁷Figure 2-17: Water Sorption curve for Nafion 117 at T = 30 °C.

These were similar results that Pushpa et al., Figure 2-18,³⁴ received for the acid form of Nafion at 25 °C. A relatively small change in water content was observed for water activities ranging from 0.15 to 0.75. At water activities above 0.75, a steeper or faster increase in water content was seen. Water activity is the vapor pressure of water divided by that of pure water at a certain temperature and is a measure of the energy of water in a system. Pure distilled water has an activity of water.



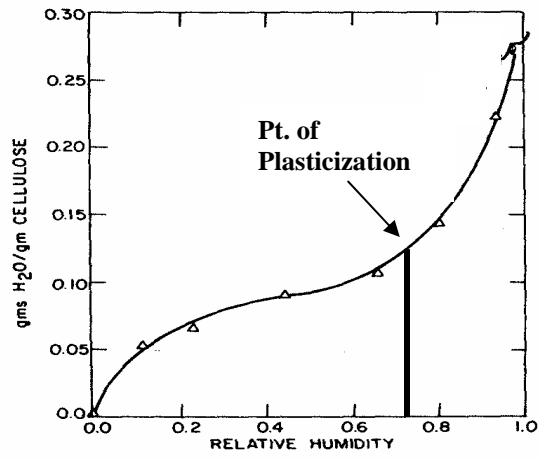
³⁵Figure 2-18: Water sorption curves for ● H^+ ; ○ Li^+ ; ▲ $N(CH_3)_4^+$; △ Cs^+ ionic forms of Nafion 117 at 25 °C.

This significant increase in water content is correlated to the rapid increase in the amount of free water in the system. This was observed by Froix and Nelson³⁴ in a cellulose system in 1975. It was found that free water is present in small quantities even at low moisture content, but there is a point of plasticization with water where the cellulose segments are impacted with additional modes of motion.



³⁴Figure 2-19: Relative humidity effect on amount of free water in cellulose.

Swelling occurs, but is limited by crystalline domains and eventually causing the system to reach maximum mobility. Figure 2-19 shows the effect relative humidity has on the sorption of water in a cellulose system. At approximately 0.7 RH, a transition occurs from a relative constant sorption to a more water sorbing system. This point is called the point of plasticization as shown in Figure 2-20.



³⁴Figure 2-20: Sorption curve for cellulose.

2.9 References

- [1] J. Larminie and A. Dicks, Fuel cell systems explained, Wiley, Chichester, 2003.
- [2] M. Zalbowitz and S. Thomas, Fuel Cells: Green Power, Department of Energy, (1999)
- [3] J. Mcbreen, Voltammetric Studies of Electrodes in Contact with Ionomeric Membranes, J. Electrochem. Soc., 132 (1985) 1112.
- [4] E. J. Taylor, E. B. Anderson and N. R. K. Vilambi, Preparation of High-Platinum-Utilization Gas-Diffusion Electrodes for Proton-Exchange-Membrane Fuel-Cells, J. Electrochem. Soc., 139 (1992) L45.
- [5] Z. Poltarzewski, P. Staiti, V. Alderucci, W. Wiczorek and N. Giordano, Nafion Distribution in Gas-Diffusion Electrodes for Solid-Polymer-Electrolyte-Fuel-Cell Applications, J. Electrochem. Soc., 139 (1992) 761.
- [6] K. Petrov, K. Xiao, E. R. Gonzalez, S. Srinivasan, A. J. Appleby and O. J. Murphy, An Advanced Proton-Exchange Membrane Electrolyzer with an Improved 3-Dimensional Reaction Zone, Int. J. Hydrogen Energy, 18 (1993) 907.
- [7] E. A. Ticianelli, C. R. Derouin, A. Redondo and S. Srinivasan, Methods to Advance Technology of Proton-Exchange Membrane Fuel-Cells, J. Electrochem. Soc., 135 (1988) 2209.
- [8] S. J. Lee, S. Mukerjee, J. McBreen, Y. W. Rho, Y. T. Kho and T. H. Lee, Effects of Nafion impregnation on performances of PEMFC electrodes, Electrochimica Acta, 43 (1998) 3693.
- [9] M. S. Wilson and S. Gottesfeld, Thin-Film Catalyst Layers for Polymer Electrolyte Fuel-Cell Electrodes, J. Appl. Electrochem., 22 (1992) 1.
- [10] A. H. Tullo, Fuel cells rally, Chemical & Engineering News, 83 (2005) 18.
- [11] S. Banerjee and D. E. Curtin, Nafion (R) perfluorinated membranes in fuel cells, J. Fluorine Chem., 125 (2004) 1211.
- [12] L. M. Robeson, Correlation of Separation Factor Versus Permeability for Polymeric Membranes, J. Membr. Sci., 62 (1991) 165.
- [13] M. Ueda, H. Toyota, T. Ouchi, J. I. Sugiyama, K. Yonetake, T. Masuko and T. Teramoto, Synthesis and Characterization of Aromatic Poly(Ether Sulfone)S Containing Pendant Sodium-Sulfonate Groups, J. Polym. Sci. A: Polym. Chem., 31 (1993) 853.
- [14] W. L. Harrison, F. Wang, J. B. Mecham, V. A. Bhanu, M. Hill, Y. S. Kim and J. E. McGrath, Influence of the bisphenol structure on the direct synthesis of sulfonated poly(arylene ether) copolymers. I, J. Polym. Sci. A: Polym. Chem., 41 (2003) 2264.
- [15] F. Wang, M. Hickner, Y. S. Kim, T. A. Zawodzinski and J. E. McGrath, Direct polymerization of sulfonated poly(arylene ether sulfone) random (statistical) copolymers: candidates for new proton exchange membranes, J. Membr. Sci., 197 (2002) 231.
- [16] F. Wang, M. Hickner, Q. Ji, W. Harrison, J. Mecham, T. A. Zawodzinski and J. E. McGrath, Synthesis of highly sulfonated poly(arylene ether sulfone) random (statistical) copolymers via direct polymerization, Macromol. Symp, 175 (2001) 387.
- [17] Y. S. Kim, F. Wang, M. Hickner, T. A. Zawodzinski and J. E. McGrath, Fabrication and characterization of heteropolyacid (H3PW12O40)/directly polymerized sulfonated poly(arylene ether sulfone) copolymer composite membranes for higher temperature fuel cell applications, J. Membr. Sci., 212 (2003) 263.
- [18] Y. S. Kim, F. Wang, M. Hickner, S. McCartney, Y. T. Hong, W. Harrison, T. A. Zawodzinski and J. E. McGrath, Effect of acidification treatment and morphological stability of sulfonated poly(arylene ether sulfone) copolymer proton-exchange membranes for fuel-cell use above 100 degrees C, J. Polym. Sci. B: Polym. Phys., 41 (2003) 2816.

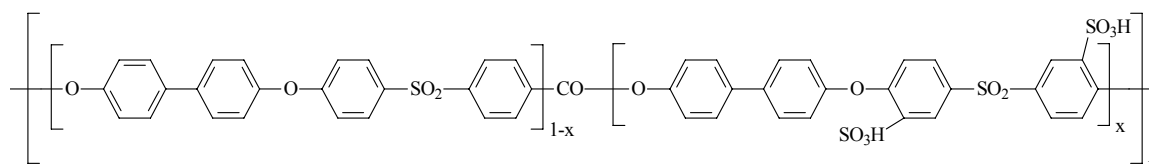
- [19] Y. S. Kim, L. M. Dong, M. A. Hickner, T. E. Glass, V. Webb and J. E. McGrath, State of water in disulfonated poly(arylene ether sulfone) copolymers and a perfluorosulfonic acid copolymer (nafion) and its effect on physical and electrochemical properties, *Macromolecules*, 36 (2003) 6281.
- [20] C. H. Fujimoto, M. A. Hickner, C. J. Cornelius and D. A. Loy, Ionomeric poly(phenylene) prepared by diels-alder polymerization: Synthesis and physical properties of a novel polyelectrolyte, *Macromolecules*, 38 (2005) 5010.
- [21] K. Nakamura, T. Hatakeyama and H. Hatakeyama, Relationship between hydrogen bonding and bound water in polyhydroxystyrene derivatives, *Polymer*, 24 (1983) 871.
- [22] T. Graham, *Philos. Magazine*, 32 (1866) 401.
- [23] V. T. Stannett and J. Crank, *J. Diffusion in Polymers*, Academic Press, (1968)
- [24] K. Ghosal and B. D. Freeman, *Gas Separation Using Polymer Membranes: An Overview*, *Polymers for Advanced Technologies*, 5 (1994) 673.
- [25] L. Zhang, C. S. Ma and S. Mukerjee, Oxygen permeation studies on alternative proton exchange membranes designed for elevated temperature operation, *Electrochimica Acta*, 48 (2003) 1845.
- [26] C. C. Hu, C. S. Chang, R. C. Ruaan and J. Y. Lai, Effect of free volume and sorption on membrane gas transport, *J. Membr. Sci.*, 226 (2003) 51.
- [27] S. Brunauer, *The adsorption of gases and vapors*, Princeton University Press, Princeton, 1943.
- [28] S. J. Gregg and K. S. W. Sing, *Adsorption, surface area, and porosity*, Academic Press, London, New York, 1967.
- [29] T. D. Naylor. Permeation Properties. In *Comprehensive polymer science : the synthesis, characterization, reactions & applications of polymers*; 1st ed.; G. Allen, J. C. Bevington, Eds.; Pergamon Press: Oxford, England ; New York, 1989; Vol. 2; pp 643.
- [30] W. R. Vieth, J. M. Howell and J. H. Hsieh, Dual Sorption Theory, *J. Membr. Sci.*, 1 (1976) 177.
- [31] W. J. Koros, A. H. Chan and D. R. Paul, Analysis of hydrocarbon gas sorption and transport in ethyl cellulose using the dual sorption/partial immobilization models, *J. Membr. Sci.*, 3 (1978) 117.
- [32] D. R. Paul and D. R. Kemp, The Diffusive Time Lag in Polymer Membranes Containing Adsorptive Fillers, *J. Polym. Sci.: Polym. Symp.*, 41 (1973) 79.
- [33] C. E. Rogers and D. Machin. In *Encyclopedia of Polymer Science and Technology*; H. F. Mark, N. Gaylord, Eds.; Interscience: New York, 1970; Vol. 12; pp 684.
- [34] M. F. Froix and R. Nelson, Interaction of Water with Cellulose from Nuclear Magnetic-Resonance Relaxation-Times, *Macromolecules*, 8 (1975) 726.
- [35] K. K. Pushpa, D. Nandan and R. M. Iyer, Thermodynamics of Water Sorption by Perfluorosulfonate (Nafion-117) and Polystyrene-Divinylbenzene Sulfonate (Dowex 50W) Ion-Exchange Resins at 298 +/- 1-K, *J Chem Soc Farad T 1*, 84 (1988) 2047.
- [36] J. E. Carles and A. M. Scallan, The Determination fo the Amount of Bound Water Within Cellulosic Gels by NMR Spectroscopy, *J Appl Polym Sci*, 17 (1973) 1855.
- [37] T. A. Zawodzinski, M. Neeman, L. O. Sillerud and S. Gottesfeld, Determination of Water Diffusion-Coefficients in Perfluorosulfonate Ionomeric Membranes, *Journal of Physical Chemistry*, 95 (1991) 6040.

[38] A. Roy, M. Hickner, T. Glass and J. McGrath. “State of Water for Proton Conducting Membranes – Influencing transport properties”; Advances in Materials for Proton Exchange Membrane Fuel Cell Systems, 2005, AsilomarCA.

3.1 Introduction

Proton exchange membrane fuel cells (PEMFCs) are alternative energy devices capable of producing high current densities, which make these systems viable for a wide range of portable and mobile applications such as automobile, computers, and generators¹ However the current state of the art membrane, Nafion[®] (Trademark of Dupont), offers several limitations. Nafion[®] has high methanol crossover, high price of manufacturing, and a limited upper operating temperature of approximately 80 °C before a decrease in performance occurs. Liquid water is produced as a by-product in PEMFCs and the water content inside the fuel cell is critical in ensuring optimal gas transport, proton conductivity, and performance. Mass transport issues need to be considered when water molecules are formed and distributed throughout the membrane. Proton conductivity of the electrolyte is higher when the membrane is fully saturated. However, there is an optimal water content threshold above which the fuel cell ceases to operate efficiently.² There are three ways that water molecules are transported and distributed in the membrane: osmotic drag, back-diffusion of water from the cathode to the anode, and the diffusion of water from the anode through the fuel stream.³

Because of the limitations of Nafion such as low operating temperatures and membrane swelling due to large water sorption, other polymer-based systems such as polyketones⁴⁻⁶ polyimides⁷⁻⁹ and polysulfones¹⁰⁻¹² have been investigated. In particular, disulfonated poly(arylene ether sulfone) (BPSH), Structure 3-1, has shown comparable property relationship to that of Nafion.^{10,13,14}



Structure 3-1

The proton conductivity and water transport in BPSH has been shown to depend on the hydration level¹⁵. The hydration level is attributed to the solvation of the acid group and the amount of water bound to the acid group and the amount of water in the bulk within a pore. We expect that likewise, the O₂ permeability will be sensitive to the state in which the water is present in the system. Therefore, the purpose of this work is to examine the gas transport mechanism in the BPSH membrane and to compare it to that observed in Nafion 112. The gas transport study consists of two parts. In the first part H₂ and O₂ permeability through BPSH-35 membranes and the Nafion 112 membrane are measured utilizing a constant volume apparatus¹⁶. In the second part O₂ gas sorption measurements are performed as a function of relative humidity (RH) and temperature.

3.2 Experimental

3.2.1 Materials

The synthesis of the disulfonated poly(arylene ether sulfone) membrane was carried out according to well documented procedures.^{10,17-19} Modified procedure allowed wholly aromatic, highly sulfonated poly(arylene ether sulfone) copolymers via direct polymerization to be produced. The BPSH polymer had 35% disulfonation and samples with two different molecular weights, 25K and 80K g mol⁻¹, were prepared.

3.2.2 Membrane Preparation

Approximately 0.5 grams BPS (salt form) with 12 mL DMAc was added into a 120 mL glass jar with lid containing a magnetic stirrer. The solution was allowed to stir for 8 hrs. The solution was then filtered using a 0.45 μm Teflon syringe filter and cast onto a 4.5" x 4.5" glass plate. The solvent was evaporated and the membrane dried using a UV lamp for 24 hrs. The membrane was then placed in a vacuum oven and the temperature was ramped to 100 °C for at least 8 hours. The film was removed and acidified for approximately 2 hours in a 0.5 M boiling sulfuric acid bath (T = 80 °C) followed by a boiling deionized water bath (T = 80 °C) for an additional 2 hours.²⁰

3.2.3 Gas Permeation Characterization

The H₂ and O₂ gas permeabilities of the disulfonated poly(arylene ether sulfone) copolymer and Nafion 112 were determined using a constant volume permeation apparatus¹⁶. A 2.5 " circular sample was cut from each membrane sheet and used in the permeation measurement. Gases were used as received from Air Products and possessed a purity of 99.99%. The feed pressure and temperature were kept constant at close to 1 atm and 35 °C, respectively, for all experiments. Each gas was run through a membrane three times and the average results and the standard deviations were recorded. Permeabilities are reported in units of Barrer (1 Barrer = 1×10⁻¹⁰ cm³·(STP) ·cm/(cm²·sec·cmHg)).

3.2.4 Gas Sorption Characterization

Sorption studies were performed by the gravimetric system (IGA-002, Hiden Isochema, UK). All chambers and tubing were degassed by applying vacuum ($P \leq 10^{-4}$ mbar). The gas used was oxygen with 99.99 % purity and purified further by attaching a molecular sieve to the gravimetric system. Relative humidity was introduced into the gravimetric two-gas system. One feed was a dry gas stream and the other gas feed was piped through a stainless steel deionized water bath. The water bath had an upper temperature limit of 80°C. These two streams mixed at the exit of the water bath. A change in the percentage of total flow through the wet stream and temperature dictated the relative humidity. For each sample temperature, the vapor pressure of water was determined by the IGA software, which utilizes the appropriate Antoine's equation. Equation 3-1 was used to determine the percentage of the wet stream flow necessary for a desired relative humidity

$$\% \text{ Wet Flow} = RH \frac{P_{\text{sample}}(T)}{P_{\text{vaporgen}}(T)} \quad \text{Eq. 3-1}$$

where % Wet Flow = percentage of total flow containing water vapor

$P_{\text{sample}}(T)$ = vapor pressure of water in the sample holder in millibar

$P_{\text{vaporgen}}(T)$ = vapor pressure of water in the vapor generator (i.e.-water bath) in millibar

RH = desired relative humidity (%)

3.3 Results

Table 3-1 compares the ion exchange capacity, water uptake as a weight percentage, and proton conductivity of poly(arylene ether sulfone) to that of Nafion 112.²¹ The BPSH-35 samples have a higher ion exchange capacity reflected by higher sulfonation content, which leads to a higher water uptake.

Table 3-1: Membrane water dependence for BPSH-35 series and Nafion 112

* Sample	IEC ^a (mequiv g ⁻¹)	Water Uptake ^b (%)	Proton Conductivity ^c (S cm ⁻¹)
BPSH-35 (25 K)	1.50	41	0.075
BPSH-35 (80K)	1.50	36	0.077
Nafion 112	0.91	19	0.11

^a IEC = (1000/MW_{repeatunit}) X degree of sulfonation X 2(-SO₃H)

$$\text{Water Uptake} = \frac{W_{wet} - W_{dry}}{W_{dry}} \times 100\%$$

^c Impedance Spectroscopy in liquid water at 30 °C

* Reproduced from reference 22.

Table 3-2 shows that BPSH-35 maintains a larger water uptake over Nafion 112 over the desired temperature range of 25 to 75 °C. The proton conductivity in the BPSH-35 samples is slightly lower but is still competitive with that of Nafion 112. The characteristic parameters of the two BPSH-35 samples are the same for both molecular weights.

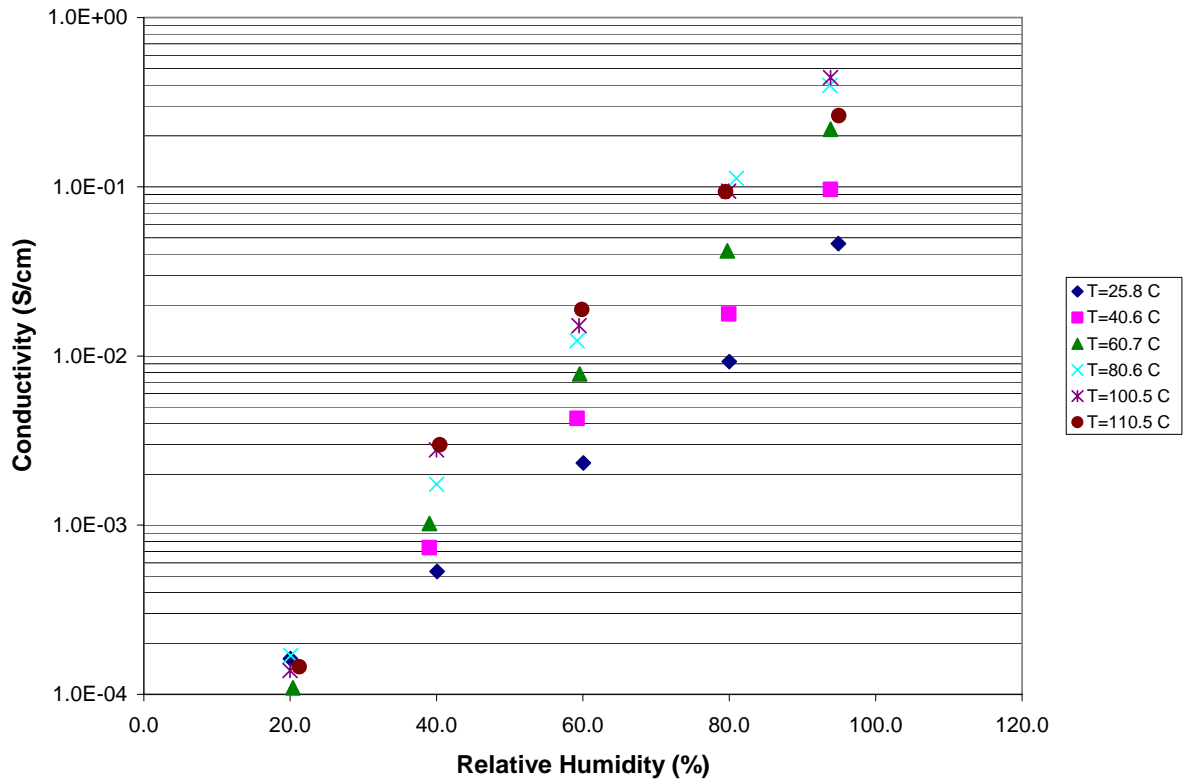
Table 3-2: % Water Uptake for Nafion 112 and BPSH-35 over a temperature range of 25-75 °C.

	25 °C	40 °C	60 °C	75 °C
Nafion 112	16	16	17	19
BPSH-35	33	34	40	46

- Films were submerged in deionized water at the desired temperature. The films were submerged till full hydration was achieved.

Figure 3-1 shows the proton conductivity of BPSH-35 and Nafion 117 as a function of relative humidity. As the temperature is increased, the proton conductivity increases until approximately 80 °C for both systems. Above 80 °C, the conductivity remains relatively constant. Nafion has a more uniform, constant proton conductivity over the given RH range. The conductivity of BPSH-35 membrane is more dependent on the state of water compared to Nafion.²²⁻²⁴ The differences are due to the material: hydrocarbon versus fluorinated polymer, glass transition temperatures, and process of sulfonation. This properties effect the state of water in each system. At relative humidities below 80 %, the proton conductivity is lower than that compared to Nafion. Above 80% RH, the proton conductivity becomes comparable to Nafion. This is because the onset of loosely bound and free water is introduced into the BPSH system. The ratio of loosely bound and free water to the total water content (tightly bound + loosely bound + free water = total water) in the system has been shown to be an indicator of how water is transported in the membrane.¹⁵ For higher ratios of loosely bound/free water to total water content, the larger the transport of water in the membrane. This helps further support the reduction in gas permeability of the BPSH compared to Nafion because Nafion has a larger presence of loosely bound and free water in the membrane.

a)



b)

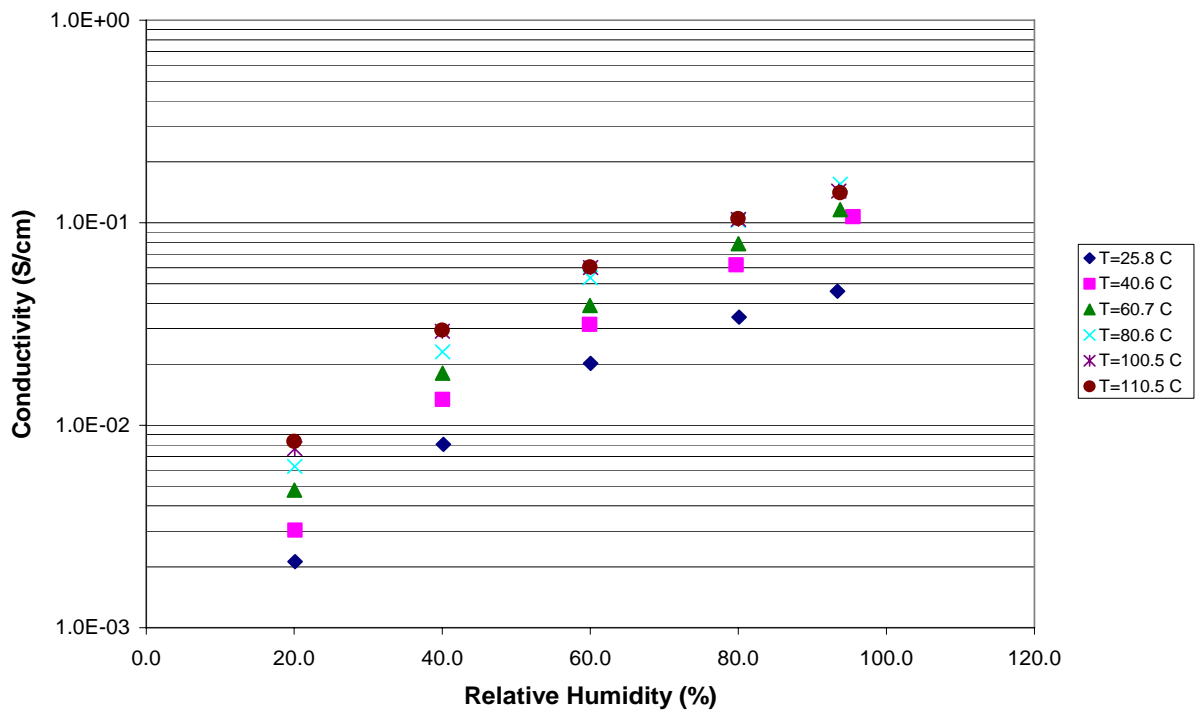


Figure 3-1: Proton Conductivity measurements for (a) BPSH-35 and (b) Nafion 117.

3.3.1 Gas Permeability Measurements

The samples (H^+ form) were soaked in deionized water, removed from water and any excess water was blotted from the surface. These samples were immediately inserted into the permeation cell. The change in swelling of the membranes during the time-frame of the measurement was not significant to effect the permeability measurements. Furthermore, the samples had sulfonation levels low enough so as not to exceed the water percolation threshold. Membranes having lower gas permeability than that of Nafion 112 are desirable, because more O_2 gas can react at the cathode. The results in Table 3-3 (a), indicate a reduction in H_2 and O_2 gas permeability for both BPSH-35 samples compared to that of Nafion 112. Molecular weight has a negligible effect on the permeability in the BPSH-35 samples. The decrease in H_2 and O_2 gas permeability is most likely a result of the higher glass transition temperature of BPSH-35, $T_g = 150^\circ C$, when compared to Nafion 112 with a $T_g=150^\circ C$. The lower chain flexibility in the case of -35 slows down gas diffusion even in the presence of water.²⁵ Table 3-3 (b) compares the O_2 solubility in the BPSH-35 and Nafion 112 systems as measured by the time-lag method²⁶ in units of $cc@STP/cc\cdot atm$ and also converted to % O_2 mass uptake to permit comparison with equilibrium sorption measurements. Clearly, the O_2 sorption is much higher in BPSH-35 than the Nafion.

Table 3-3 (a): Gas permeability in Barrers for the respective polyelectrolyte membranes under fully hydrated conditions.

	Hydrogen (Barrers)	Oxygen (Barrers)
BPSH-35 25K	3.06 ± 0.14	0.19 ± 0.00
BPSH-35 80K	3.86 ± 0.26	0.21 ± 0.00
Nafion 112	8.14 ± 0.10	1.23 ± 0.04

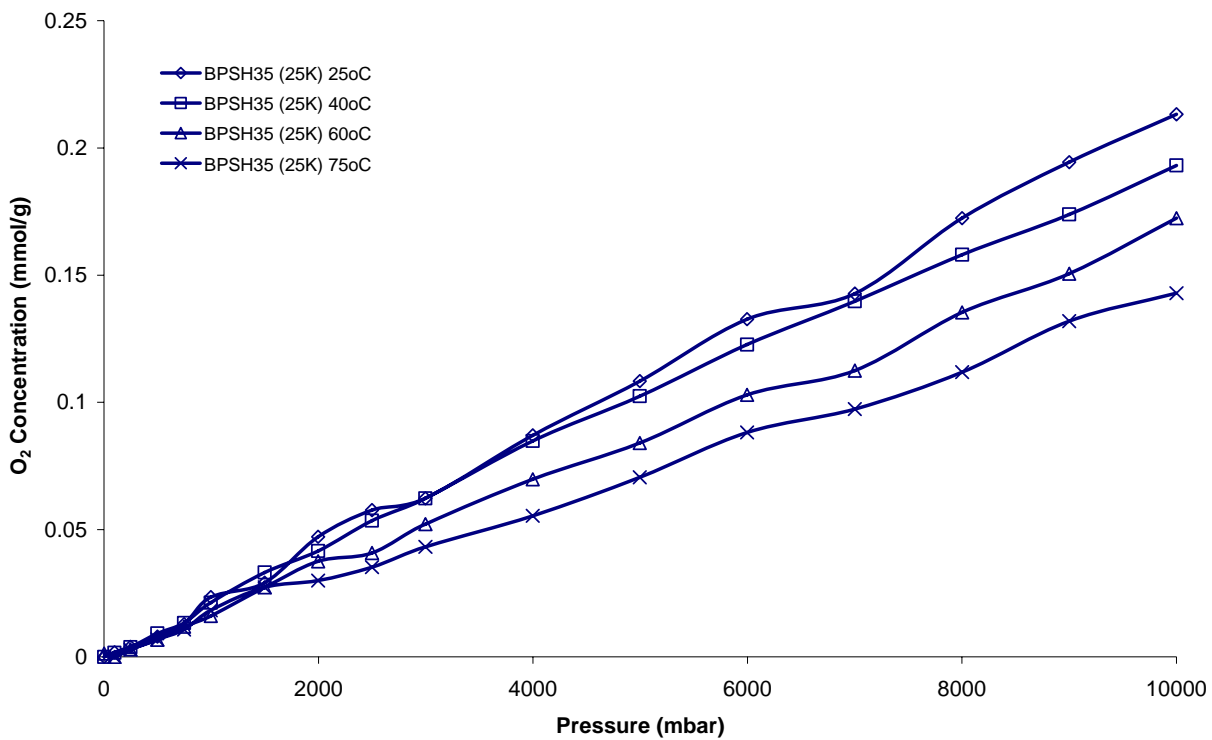
Table 3-3 (b): Pure oxygen solubility in BPSH-35 and Nafion under fully hydrated conditions

	O ₂ Solubility (cc@STP/cc-atm)	% O ₂ Mass Uptake
BPSH-35 25K	0.29	0.024
BPSH-35 80K	0.27	0.022
Nafion 112	0.06	0.005

3.3.2 Gas Sorption Measurements

Gas Sorption measurements using Nafion 112 and BPSH-35 membranes were carried out as a function of pressure (0 to 10 bar), temperature (25 to 75 °C) and relative humidity (0 to 80% RH). Figure 3-2 displays the O₂ pressure isotherms for (a) BPSH-35 and (b) Nafion 112 samples under dry conditions.

a)



b)

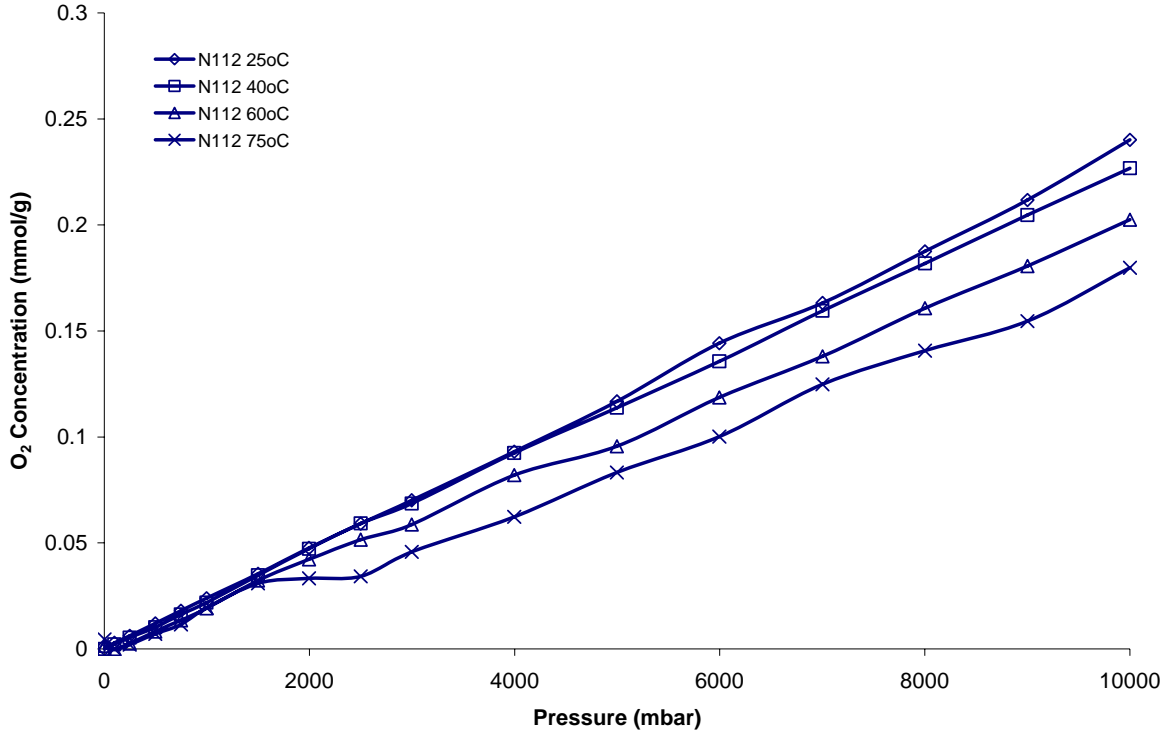


Figure 3-2: Pressure O₂ Sorption isotherms for (a) BPSH-35 (25K) and (b) Nafion 112 over a temperature range of 25-75 °C.

When no moisture is present in the system, the sorption of O₂ in BPSH-35 (25K) and in Nafion 112 membranes exhibit Henry's Law type behavior. Therefore, the enthalpy of solution can be calculated by linearly fitting the variation of solubility, S, vs. temperature, T. The solubility can be related to temperature by a van't Hoff relationship expressed in Equation 3-2:²⁷

$$S = S_o \exp\left(\frac{-\Delta H_s}{RT}\right) \quad \text{Eq. 3-2}$$

where S_o is a constant, R is the ideal gas constant, T is temperature, and ΔH_s is the partial molar enthalpy of sorption. ΔH_s has two contributions as expressed by Equation 3-3:^{28,29}

$$\Delta H_s = \Delta H_{cond} + \Delta H_{mix} \quad \text{Eq. 3-3}$$

where ΔH_{cond} is the change in enthalpy associated with a penetrant going from the gas state to a condensed state and ΔH_{mix} is the enthalpy change associated with creating a gap for the a gas molecule to dissolve in the membrane. In the case of small molecules with low molecular weight and low critical temperatures, ΔH_{cond} is small causing the ΔH_{mix} term to dominate ΔH_s . When weak interactions between the polymer and gas occur, ΔH_{mix} is positive causing an increase in solubility with an increase in temperature.²⁹ In our case, however, the solubility decreases with temperature. Table 4 displays the results of the analysis, showing negative ΔH_s values. In the case of BPSH-35, the absolute value of ΔH_s decreases with increasing pressure, while that of Nafion 112 stays nearly constant. This suggests the presence of molecular interactions, most likely between the oxygen molecules and the sulfonic acid groups in the BPSH-35 polymer membranes.³⁰ These interactions decrease with increasing O_2 pressure as the environment into which the O_2 dissolves includes more oxygen clusters. Furthermore, as the temperature increases, these interactions are disrupted and the solubility drops.

Table 3-4: Enthalpy results for the BPSH-35 (25K) and Nafion 112 membranes at 0% relative humidity.

	8000 (mbar)	9000 (mbar)	10,000 (mbar)
BPSH-35 (25K)			
ΔH_S (kJ/mol)	-7.30	-6.61	-6.58
S_o	0.01	0.01	0.01
Nafion 112			
ΔH_S (kJ/mol)	-4.96	-5.36	-4.94
S_o	0.03	0.03	0.03

As indicated earlier there is always a need for water to be present inside a fuel cell in order to facilitate the transport of ions. Likewise, the transport of O_2 will depend on the presence of water and the state it is in. Therefore, experiments were carried out to determine the percent O_2 mass uptake as a function of temperature and relative humidity at a pressure of 1 atm. The

introduction of relative humidity has shown to dramatically change the O₂ sorption behavior in both Nafion and BPSH-35. Relative humidity is defined as the extent of water saturation in an air-water vapor mixture. When expressing the results, it is probably not useful to correlate the results as a function of relative humidity. This is because at each temperature and relative humidity, the moisture content is not necessarily the same. Therefore, to be more accurate, the results are reported as a function of the water's vapor pressure at the respective temperature. Equation 3-4 defines the relationship between the relative humidity and water vapor pressure.

$$yP_{\text{vapor},H_2O} = \frac{xP^{\text{SAT}}(T)}{100} \quad \text{Eq. 3-4}$$

where,

yP_{vapor,H_2O} = vapor pressure of water [=] mbars

x = relative humidity in %

$P^{\text{SAT}}(T)$ = saturation pressure of water in mbar

The saturation pressure of water occurs at the following pressures: 31.8 (25 °C), 73.8 (40 °C), 199 (60 °C), and 384.8 (75 °C) mbar according to the Antoine's Equation³¹ Figures 3-3 through 3-5 display the mass uptake of wet O₂ for all membranes at 1 atm total pressure as a function of vapor pressure of H₂O for the various polymer systems.

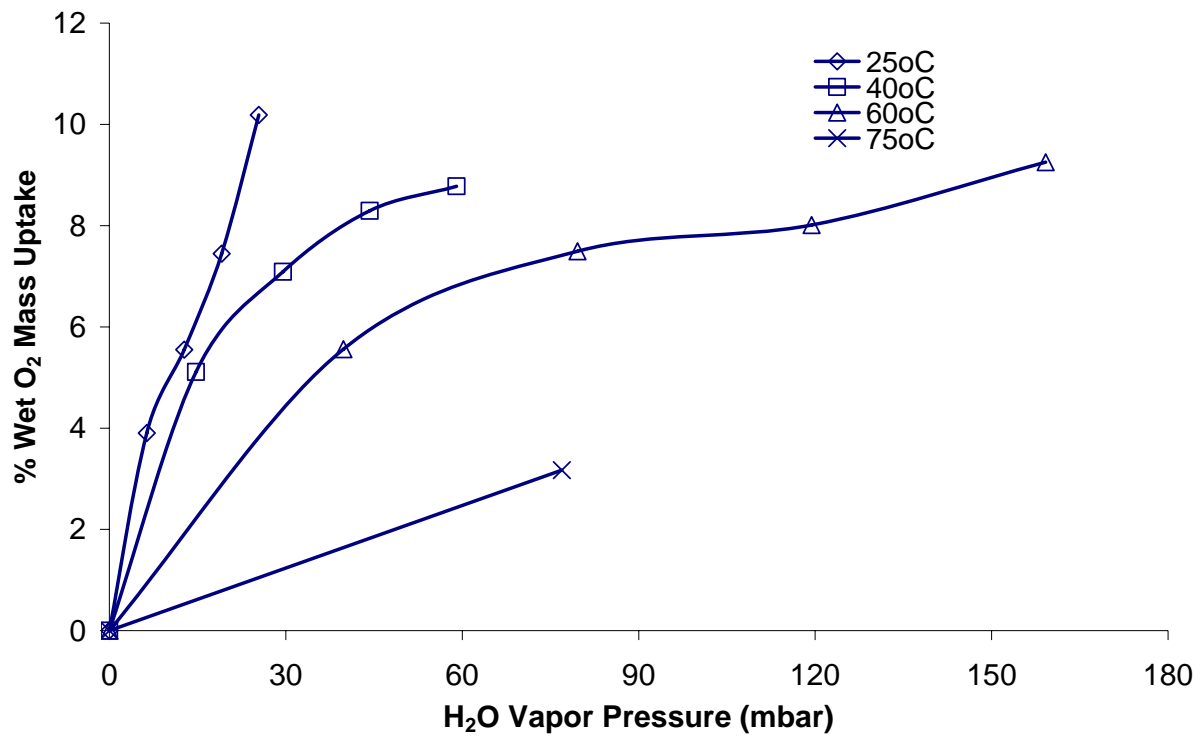


Figure 3-3: O₂ Sorption isotherm for Nafion 112.

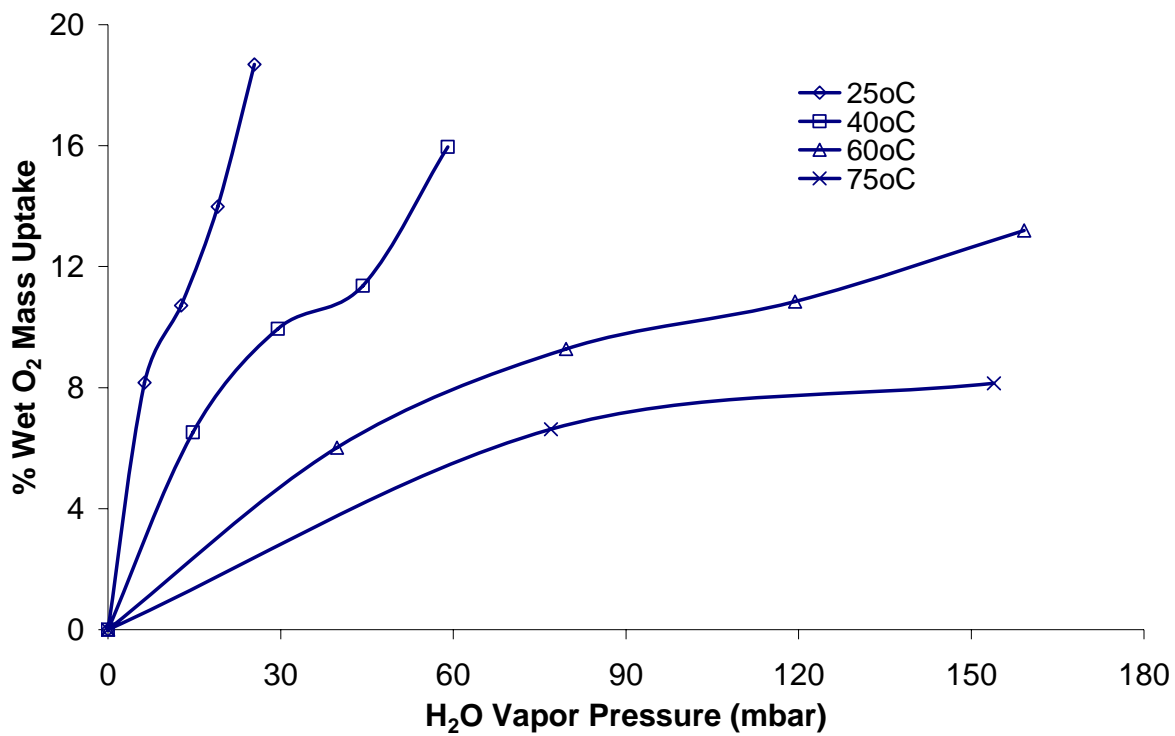


Figure 3-4: O₂ Sorption isotherm for BPSH-35 25K.

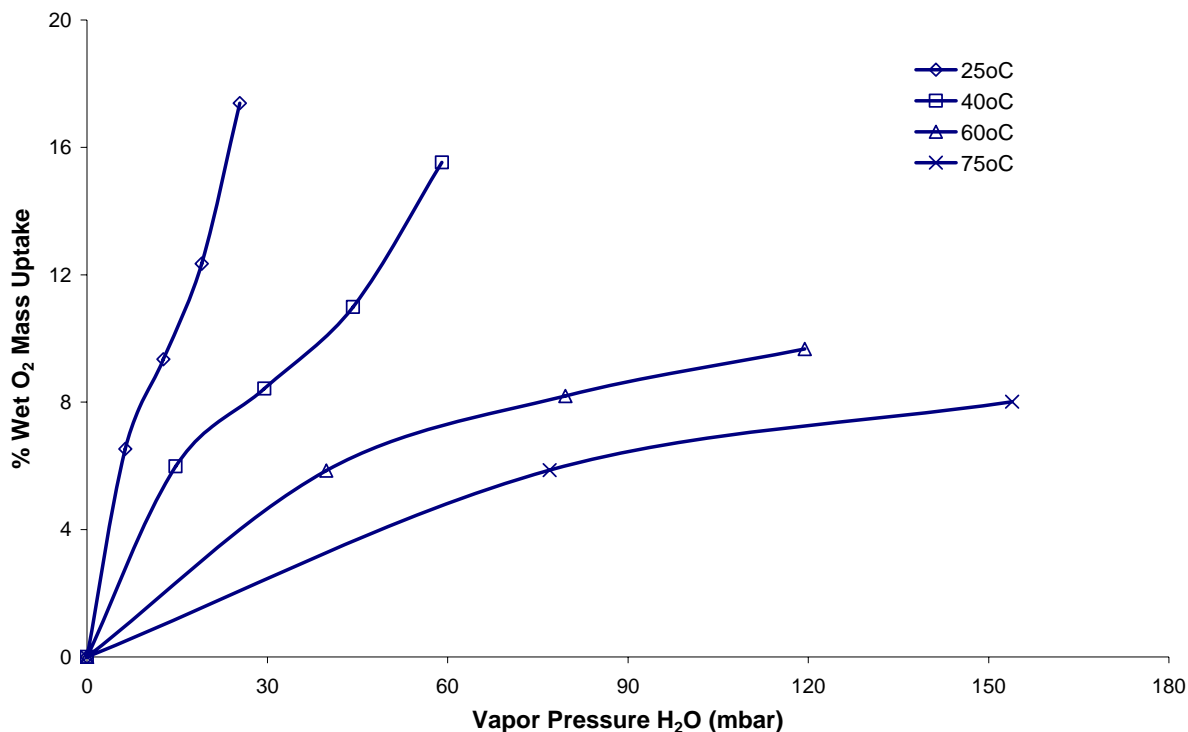


Figure 3-5: O₂ Sorption isotherm for BPSH-35 80K.

In all cases, the wet O₂ percent mass uptake increases with increasing vapor pressure. The rate of increase in the wet O₂ % mass uptake with H₂O vapor pressure is higher at low temperatures. At low temperatures there is also the appearance of Type IV sorption, also called the Brunnauer, Emmett and Teller (BET) sorption²⁹ Type IV sorption is the sum of Type II (Langmuir) and Type III (Flory-Huggins) sorptions, and is typical of water sorbing in a highly hydrophilic polymer. Therefore, as the temperature increases, the number of hydrogen bonding interactions between the sulfonic acid groups on the polymer and the free H₂O decrease and the sorption isotherms follow a dual sorption behavior.²³ When comparing Figures 3-3, 3-4 and 3-5, it is quite evident that the total mass uptake of wet O₂ in the BPSH-35 samples is much higher than that observed in Nafion. This is consistent with the higher water uptake observed in BPSH-35 over Nafion 112 shown in Table 3-2 as the temperature is increased from 25 to 75 °C. While it is difficult to resolve the contribution of O₂ and H₂O sorption to the overall percent mass

uptake because these sorptions are coupled, one can at least get a sense of their relative magnitude. The weight percent uptake of pure O₂ in a completely hydrated BPSH-35 sample at 1 atm is 0.0244 wt% as listed in Table 3-3 (b). This value is clearly much lower than the wt% uptake of wet O₂ recorded in Figures 3-3 and 3-4, which tends to be two orders of magnitude higher. Consequently, the sorption isotherms mostly reflect the sorption of water into the BPSH-35 system. However, comparing the sorption of pure O₂ into a dry BPSH-35 (0.025 mmol/g from Figure 3-2) vs. sorption of pure O₂ in a hydrated BPSH system (0.008 mmol/g or 2.44×10^{-4} - mg/mg from Table 3-3 (b)) and sorption of O₂ in pure water (7.2×10^{-4} mmol/g) at 1 atm and 25 °C are lower than the pure water uptake values found in Table 3-2.

3.4 Conclusions

The transport behavior of H₂ and O₂ gases in disulfonated poly(arylene ether sulfone) was compared to the transport behavior in Nafion. The presence of moisture dictated the sorption behavior. Under dry conditions, the sorption of O₂ in both BPSH-35 and Nafion followed Henry's law. In the presence of humidity and low temperatures, sorption followed Type IV behavior, suggesting the formation of hydrogen bonding between the sulfonic acid groups on the polymer backbone and the water, thus, swelling the polymer. The presence of water has also significantly increased the sorption of O₂ into the BPSH, much more so than in Nafion.

3.5 References

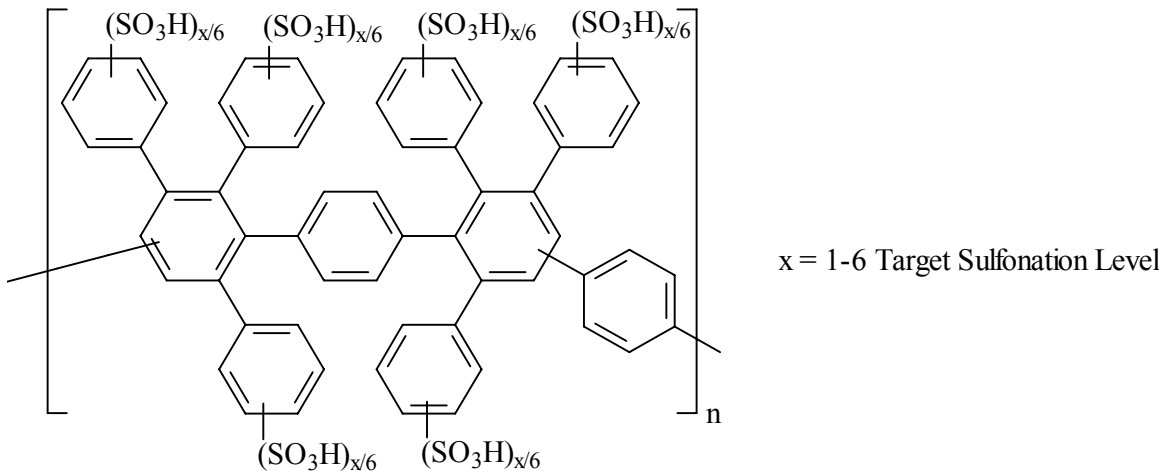
- [1] M. Zalbowitz and S. Thomas, Fuel Cells: Green Power, Department of Energy, (1999)
- [2] M. V. Williams, H. R. Kunz and J. M. Fenton, Operation of Nafion((R))-based PEM fuel cells with no external humidification: influence of operating conditions and gas diffusion layers, *J. Power Sources*, 135 (2004) 122.
- [3] J. Larminie and A. Dicks, Fuel cell systems explained, J. Wiley, Chichester, West Sussex, 2003.
- [4] S. L. Zhong, T. Z. Fu, Z. Y. Dou, C. J. Zhao and H. Na, Preparation and evaluation of a proton exchange membrane based on crosslinkable sulfonated poly(ether ether ketone)s, *J. Power Sources*, 162 (2006) 51.
- [5] X. F. Li, C. J. Zhao, H. Lu, Z. Wang and H. Na, Direct synthesis of sulfonated poly(ether ether ketone)s (SPEEKs) proton exchange membranes for fuel cell application, *Polymer*, 46 (2005) 5820.
- [6] S. M. J. Zaidi, S. D. Mikhailenko, G. P. Robertson, M. D. Guiver and S. Kaliaguine, Proton conducting composite membranes from polyether ether ketone and heteropolyacids for fuel cell applications, *J. Membr. Sci.*, 173 (2000) 17.
- [7] Y. Li, R. Jin, Z. Wang, Z. Cui, W. Xing and L. Gao, Synthesis and Properties of Novel Sulfonated Polyimides Containing Binaphthyl as Proton-Exchange Membranes for Fuel Cells, *J. Polym. Sci. A: Polym. Chem.*, 45 (2007) 222.
- [8] B. R. Einsla, Y. T. Hong, Y. S. Kim, F. Wang, N. Gunduz and J. E. McGrath, Sulfonated naphthalene dianhydride based polyimide copolymers for proton-exchange-membrane fuel cells. I. Monomer and copolymer synthesis, *J. Polym. Sci. A: Polym. Chem.*, 42 (2004) 862.
- [9] C. Genies, R. Mercier, B. Sillion, N. Cornet, G. Gebel and M. Pineri, Soluble sulfonated naphthalenic polyimides as materials for proton exchange membranes, *Polymer*, 42 (2001) 359.
- [10] F. Wang, M. Hickner, Y. S. Kim, T. A. Zawodzinski and J. E. McGrath, Direct polymerization of sulfonated poly(arylene ether sulfone) random (statistical) copolymers: candidates for new proton exchange membranes, *J. Membr. Sci.*, 197 (2002) 231.
- [11] R. Nolte, K. Ledjeff, M. Bauer and R. Mulhaupt, Partially Sulfonated Poly(Arylene Ether Sulfone) - a Versatile Proton Conducting Membrane Material for Modern Energy-Conversion Technologies, *J. Membr. Sci.*, 83 (1993) 211.
- [12] C. Iojoiu, M. Marechal, F. Chabert and J. Y. Sanchez, Mastering sulfonation of aromatic polysulfones: Crucial for membranes for fuel cell application, *Fuel Cells*, 5 (2005) 344.
- [13] Y. S. Kim, L. M. Dong, M. A. Hickner, B. S. Pivovar and J. E. McGrath, Processing induced morphological development in hydrated sulfonated poly(arylene ether sulfone) copolymer membranes, *Polymer*, 44 (2003) 5729.
- [14] Y. S. Kim, M. A. Hickner, L. M. Dong, B. S. Pivovar and J. E. McGrath, Sulfonated poly(arylene ether sulfone) copolymer proton exchange membranes: composition and morphology effects on the methanol permeability, *J. Membr. Sci.*, 243 (2004) 317.
- [15] Y. S. Kim, L. M. Dong, M. A. Hickner, T. E. Glass, V. Webb and J. E. McGrath, State of water in disulfonated poly(arylene ether sulfone) copolymers and a perfluorosulfonic acid copolymer (nafion) and its effect on physical and electrochemical properties, *Macromolecules*, 36 (2003) 6281.
- [16] T. Pechar, Fabrication and Characterization of Polyimide-based Mixed Matrix Membranes for Gas Separations. Virginia Polytechnic Institute and State University, 2004.

- [17] W. L. Harrison, F. Wang, J. B. Mecham, V. A. Bhanu, M. Hill, Y. S. Kim and J. E. McGrath, Influence of the bisphenol structure on the direct synthesis of sulfonated poly(arylene ether) copolymers. I, *J. Polym. Sci. A: Polym. Chem.*, 41 (2003) 2264.
- [18] F. Wang, M. Hickner, Q. Ji, W. Harrison, J. Mecham, T. A. Zawodzinski and J. E. McGrath, Synthesis of highly sulfonated poly(arylene ether sulfone) random (statistical) copolymers via direct polymerization, *Macromol. Symp.*, 175 (2001) 387.
- [19] Y. S. Kim, F. Wang, M. Hickner, T. A. Zawodzinski and J. E. McGrath, Fabrication and characterization of heteropolyacid (H3PW12O40)/directly polymerized sulfonated poly(arylene ether sulfone) copolymer composite membranes for higher temperature fuel cell applications, *J. Membr. Sci.*, 212 (2003) 263.
- [20] Y. S. Kim, F. Wang, M. Hickner, S. McCartney, Y. T. Hong, W. Harrison, T. A. Zawodzinski and J. E. McGrath, Effect of acidification treatment and morphological stability of sulfonated poly(arylene ether sulfone) copolymer proton-exchange membranes for fuel-cell use above 100 degrees C, *J. Polym. Sci. B: Polym. Phys.*, 41 (2003) 2816.
- [21] Y. X. Li, F. Wang, J. Yang, D. Liu, A. Roy, S. Case, J. Lesko and J. E. McGrath, Synthesis and characterization of controlled molecular weight disulfonated poly(arylene ether sulfone) copolymers and their applications to proton exchange membranes, *Polymer*, 47 (2006) 4210.
- [22] N. L. Garland and J. P. Kopasz, The United States Department of Energy's high temperature, low relative humidity membrane program, *J. Power Sources*, 172 (2007) 94.
- [23] T. L. Kalapos, B. Decker, H. A. Every, H. Ghassemi and T. A. Z. Jr., Thermal Studies of the state of water in proton conducting fuel cell membranes, *J. Power Sources*, 172 (2007) 14.
- [24] D. B. Spry, A. Goun, K. Glusac, D. E. Moilanen and M. D. Fayer, Proton transport and the water environment in nafion fuel cell membranes and AOT reverse micelles, *J. Am. Chem. Soc.*, 129 (2007) 8122.
- [25] C. M. Laot, E. Marand, B. Schmittman and R. Zia, Effects of Cooling Rate and Physical Aging on the Gas Transport Properties of Polycarbonate, *Macromolecules*, 36 (2003) 8673.
- [26] J. Crank, *The Mathematics of Diffusion*, Oxford Press; London, (1990)
- [27] L. M. Robeson, W. F. Burgoyne, M. Langsam, A. C. Savoca and C. F. Tien, High-Performance Polymers for Membrane Separation, *Polymer*, 35 (1994) 4970.
- [28] B. D. Freeman. In *Comprehensive Polymer Science*; S. L. Aggarwal, S. Russo, Eds.; Pergamon Press: Oxford, 1992.
- [29] T. D. Naylor. Permeation Properties. In *Comprehensive polymer science : the synthesis, characterization, reactions & applications of polymers*; 1st ed.; G. Allen, J. C. Bevington, Eds.; Pergamon Press: Oxford, England ; New York, 1989; Vol. 2; pp 643.
- [30] K. Tanaka, M. N. Islam, M. Kido, H. Kita and K. Okamoto, Gas permeation and separation properties of sulfonated polyimide membranes, *Polymer*, 47 (2006) 4370.
- [31] J. M. Smith, H. C. V. Ness and M. M. Abbott, *Introduction to Chemical Engineering Thermodynamics*, McGraw Hill, New York, NY, 2001.

4.1 Introduction

As has been stated in earlier chapters, there are many research efforts aimed at developing new proton exchange membranes to replace Nafion as the commercially available membrane. The alternative membrane should have high ionic conductivity, thermal stability for operation above 100 °C, chemical stability due to the presence of strong acids used as a proton conductor and oxidation, good barrier properties, and good processability. To reach this goal, researchers have sulfonated existing thermoplastics such as polyketones¹⁻³ and polysulfones⁴⁻⁶, which allow for an increase in thermal stability and lower processing costs. However, these materials have lower ionic conductivities at the same ion exchange capacity of Nafion and are more exposed to acid-catalyzed or oxidative degradation.

A group at Sandia National Laboratories in Albuquerque, New Mexico decided to utilize a purely aromatic polymer, poly(phenylene), which will improve the thermochemical stability, chemical stability, and barrier properties compared to Nafion. High molecular weights are needed for polymer chain entanglements to occur and form physically robust films. The ability to obtain physically robust films is an important characteristic for a proton exchange membrane due to the harsh fuel cell environment. This section will be devoted to the post sulfonated Diels-Alder poly(phenylene) (SDAPP), Structure 4-1, which has shown comparable ionic conductivities, good processability, and thermally and chemical stability as compared to Nafion.⁷



Structure 4-1

As has been stated earlier, the proton conductivity and water transport has been shown to depend on the hydration level.⁸⁻¹¹ The hydration level is attributed to the solvation of the acid group and the amount of water bound to the acid group and the amount of water in the bulk within a pore. Once again we expect the O_2 permeability will be sensitive to the state of the water present in the system for SDAPP series. Therefore, the purpose of this work is to examine the gas transport mechanism in the SDAPP membrane and to compare it to that observed in Nafion 112. The gas transport study consists of two parts. In the first part, H_2 and O_2 permeability is measured for the SDAPP membranes containing an ion exchange capacity of 1.6 (SDAPP 1.6) and 2.2 (SDAPP 2.2) mequiv cm^{-1} and Nafion 112, utilizing a constant volume apparatus.¹² In the second part O_2 gas sorption measurements are performed in the non-humidified and humidified state over a temperature range of 25 to 75 °C at a constant pressure of 1 bar.

4.2 Experimental

4.2.1 Materials

The synthesis of the Diels-Alder polyphenylene (SDAPP0) has been documented in ref. 7. The polymer repeat unit is formed by the Diels-Alder condensation reaction of 1,4-bis(2,4,5-triphenylcyclopentadienone)-benzene with diethnylbenzene. This reaction will allow for a wide range of functionalities and configurations allowing the poly(phenylene) to be modified to achieve optimal properties desired for PEM's. For sulfonation, the SDAPP0 (not sulfonated) solution is mixed dropwise with chlorosulfonic acid diluted with chloroform. The resulting precipitate is converted to the salt form by adding 0.5M NaOH and allowed to react at room temperature for 12 h.

4.2.2 Membrane Preparation

Membrane formation is outline in more detailed in reference 7. The sodium salt form of SDAPP is dissolved in DMAc and filtered through a 2 μm glass microfiber syringe filter. The solution is cast onto a glass plate in an oven under N_2 at 90 $^\circ\text{C}$. After approximately 20 h, the film was removed from the glass plate and immersed into a deionized water bath at 100 $^\circ\text{C}$ for 1 h to remove any excess DMAc. The film is then converted to proton form by immersing the film into a 0.5 M H_2SO_4 at 100 $^\circ\text{C}$ for 1 h. This film is then rinsed thoroughly with deionized water and then submerged in a deionized water bath at 100 $^\circ\text{C}$ for 1 h to remove any residual acid.

4.2.3 Gas Permeation Characterization

The H_2 and O_2 gas permeabilities of the disulfonated poly(arylene ether sulfone) copolymer and Nafion 112 were determined using a constant volume permeation apparatus¹² A 2.5 " circular sample was cut from each membrane sheet and used in the permeation measurement. The films were masked with aluminum tape and sealed with epoxy to prevent leaks.¹³ Gases were used as received from Air Products and possessed a purity of 99.99%. The feed pressure and temperature were kept constant at close to 1 atm and 35 $^\circ\text{C}$, respectively, for all experiments. Each gas was run through a membrane three times and the average results and the standard

deviations were recorded. Permeabilities are reported in units of Barrer ($1 \text{ Barrer} = 1 \times 10^{-10} \text{ cm}^3 \cdot (\text{STP}) \cdot \text{cm} / (\text{cm}^2 \cdot \text{sec} \cdot \text{cmHg})$).

4.2.4 Gas Sorption Characterization

Sorption studies were performed by the gravimetric system (IGA-002, Hiden Isochema, UK). All chambers and tubing were degassed by applying vacuum ($P \leq 10^{-4} \text{ mbar}$). The gas used was oxygen with 99.99 % purity and purified further by attaching a molecular sieve to the gravimetric system. Relative humidity was introduced into the gravimetric system using a two-gas feed system. One feed was a dry gas stream and the other gas feed was piped through a stainless steel deionized water bath. The water bath had an upper temperature limit of 80°C . These two streams mixed at the exit of the water bath. A change in the percentage of total flow through the wet stream and temperature dictated the relative humidity. For each sample temperature, the vapor pressure of water was determined by the IGA software, which utilizes the appropriate Antoine's equation. Equation 4-1 was used to determine the percentage of the wet stream flow necessary for a desired relative humidity.

$$\% \text{ Wet Flow} = RH \frac{P_{\text{sample}}(T)}{P_{\text{vaporgen}}(T)} \quad \text{Eq. 4-1}$$

where % Wet Flow = percentage of total flow containing water vapor

$P_{\text{sample}}(T)$ = vapor pressure of water in the sample holder in millibar

$P_{\text{vaporgen}}(T)$ = vapor pressure of water in the vapor generator (i.e.-water bath) in millibar

RH = desired relative humidity (%)

4.3 Results

Table 4-1 compares the ion exchange capacity, water uptake as a weight percentage, and proton conductivity of SDAPP series to that of Nafion 112. The SDAPP samples have a larger ion exchange capacity than Nafion, i.e.- higher sulfonation content, which leads to the increase in the water uptake. The proton conductivity in the SDAPP 1.6 sample is lower but is still competitive with that of Nafion 112. The SDAPP 2.2 has a higher proton conductivity than Nafion 112 due to the presence of more sulfonic acid groups.

Table 4-1: Membrane water dependence for SDAPP 1.6, SDAPP 2.2, and Nafion 112.

	IEC (mequiv g ⁻¹)	Water Uptake (%)	Proton Conductivity (S cm ⁻¹)
SDAPP 1.6	1.6	56	0.074
SDAPP 2.2	2.2	137	0.123
Nafion 112	0.91	19	0.11

4.3.1 Gas Permeability Measurements

The samples were soaked in deionized water, removed and any excess water was blotted from the surface. These samples were immediately inserted into the permeation cell. The change in swelling of the membranes during the time-frame of the measurement was not significant to effect the permeability measurements. Membranes having lower gas permeability than that of Nafion 112 are desirable because more O₂ gas can react at the cathode. The results in Table 4-2 (a), indicate a similar H₂ gas permeability for SDAPP 2.2 as compared to Nafion 112, but a reduction for O₂. The bulky, pendant benzene groups allow hydrogen to permeate through the membrane at a rate similar to that of Nafion. However, the pendant benzene groups have π - π interactions with each other causes a hindrance and a reduction in O₂ permeability. Also, the free volume available to aid hydrogen is not large enough to allow oxygen to pass through at a similar rate to Nafion. The H₂ and O₂ permeability for SDAPP 1.6 is higher than expected and

could be the result of sample preparation. The SDAPP 1.6 sample used for gas permeability measurements was prepared in Dr. Don Baird's Group using a film coater and the SDAPP 2.2 sample was prepared by solvent casting involving the above mentioned procedure.

Table 4-2 (b) compares the O₂ solubility in the SDAPP and Nafion 112 systems as measured by the time-lag method¹⁴ in units of cc@STP/cc·atm and also converted to % O₂ mass uptake, to permit comparison with equilibrium sorption measurements. Clearly, the O₂ sorption is much higher in SDAPP 2.2 than with the Nafion.

Table 4-2 (a): Gas permeability in Barrers for the respective polyelectrolyte membranes under fully hydrated conditions.

	Hydrogen (Barrers)	Oxygen (Barrers)
SDAPP 1.6 (Baird's Group)	49.31 ± 2.04	6.83 ± 0.20
SDAPP 2.2 (Cornelius Group)	8.63 ± 0.76	0.57 ± 0.04
Nafion 112	8.14 ± 0.10	1.23 ± 0.04

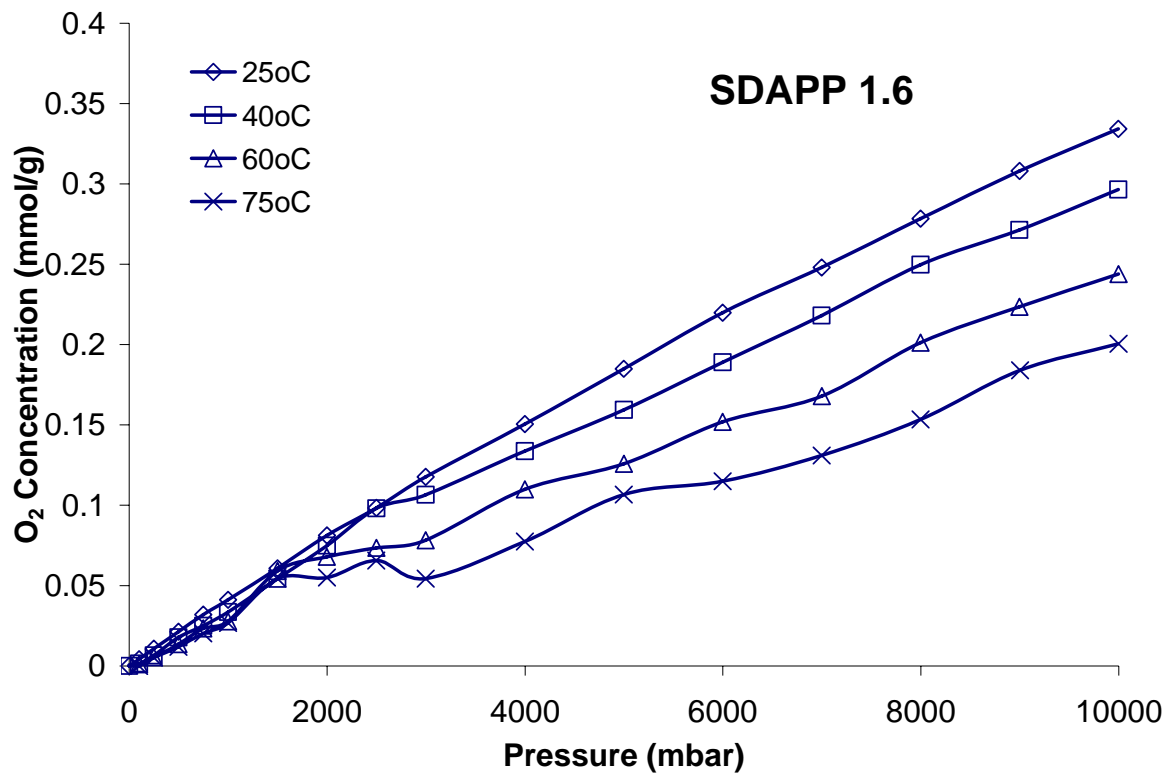
Table 4-2 (b): Pure oxygen solubility in SDAPP series and Nafion under fully hydrated conditions

	O ₂ Solubility (cc@STP/cc·atm)	% O ₂ Mass Uptake
SDAPP 1.6	0.55	0.065
SDAPP 2.2	0.39	0.04
Nafion 112	0.06	0.005

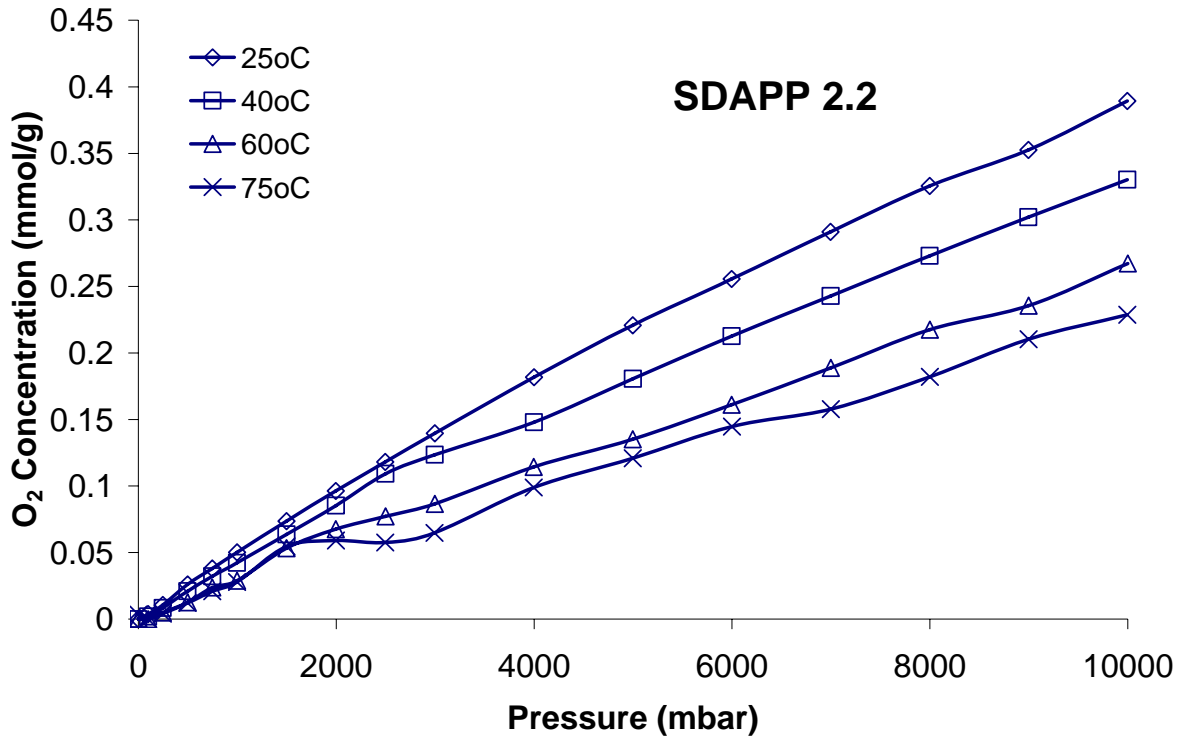
4.3.2 Gas Sorption Measurements

Gas Sorption measurements were carried out as a function of pressure (0 to 10 bar), temperature (25 to 75 °C) and relative humidity (0 to 80% RH) for Nafion 112 and the SDAPP membranes. Figure 4-1 displays the O₂ pressure isotherms for (a) SDAPP 1.6, (b) SDAPP 2.2 and (c) Nafion 112 samples under dry conditions.

a)



b)



c)

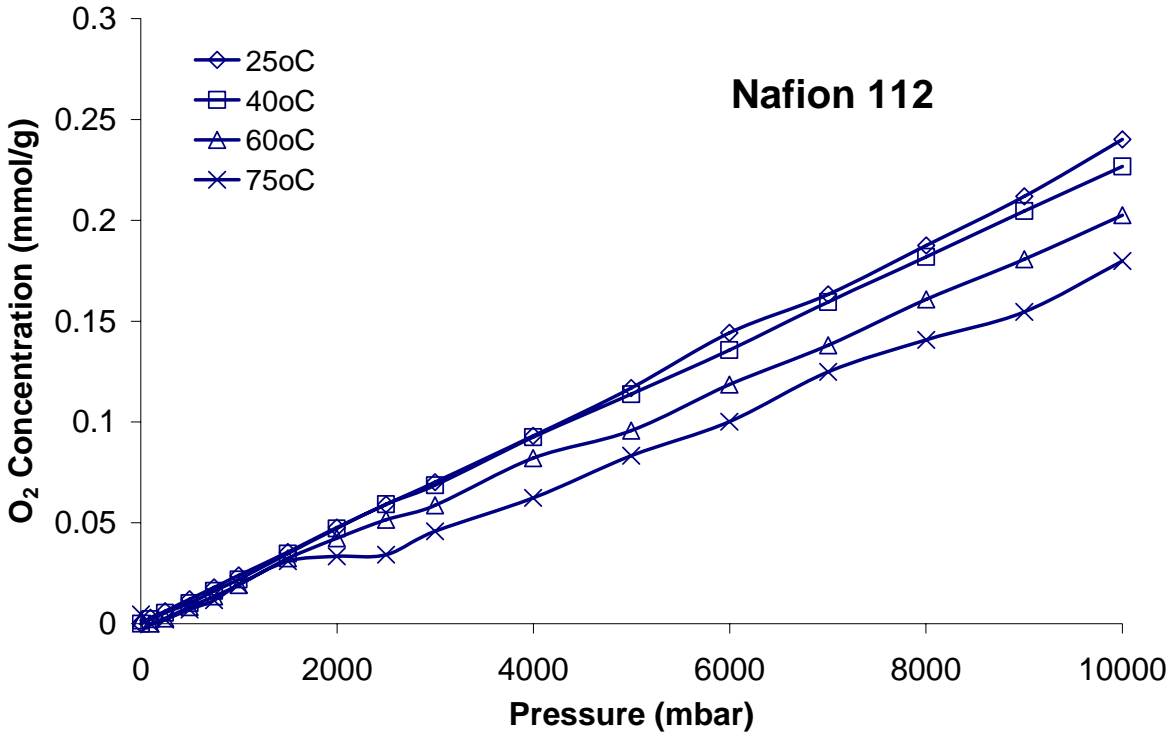


Figure 4-1: Non-Humidified pressure O₂ Sorption isotherms for (a) SDAPP 1.6 (b) SDAPP 2.2 and (c) Nafion 112 over a temperature range of 25-75 °C.

The O₂ sorption in SDAPP 1.6, SDAPP 2.2, and Nafion 112 exhibited Henry's Law type behavior, which will allow for the enthalpy of solution to be calculated by linearly fitting the variation of solubility, S, vs. temperature, T. At 75 °C, there is a change in the sorption behavior. The resulting change could be related to the sulfonic acid groups in the SDAPP material (H⁺ form) participating in the rearrangement of the ionic domains at 75 °C. This could be confirmed by DMTA studies. The solubility can be related to temperature by a van't Hoff relationship expressed in Equation 4-2:¹⁵

$$S = S_o \exp\left(\frac{-\Delta H_s}{RT}\right) \quad \text{Eq. 4-2}$$

where S_o is a constant, R is the ideal gas constant, T is temperature, and ΔH_s is the partial molar enthalpy of sorption. ΔH_s has two contributions as expressed by Equation 4-3:^{16,17}

$$\Delta H_s = \Delta H_{cond} + \Delta H_{mix} \quad \text{Eq. 4-3}$$

where ΔH_{cond} is the change in enthalpy associated with a penetrant going from the gas state to a condensed state and ΔH_{mix} is the enthalpy change associated with creating a gap for the a gas molecule to dissolve in the membrane. In the case of small molecules with low molecular weight and low critical temperatures, ΔH_{cond} is small causing the ΔH_{mix} term to dominate ΔH_s . When weak interactions between the polymer and gas occur, ΔH_{mix} is positive causing an increase in solubility with an increase in temperature.¹⁷ In the case of the SDAPP series, the solubility decreases with temperature. Table 4-3 displays the results showing negative ΔH_s values. . The SDAPP membranes contain stronger O_2 - HSO_3 interactions because of a higher ion exchange capacity and more negative ΔH_s values as compared to Nafion.¹⁸ The absolute value of ΔH_s increases with increasing pressure, which suggests the presence of molecular interactions, most likely between the oxygen molecules and the sulfonic acid groups in the polymer membranes.¹⁹ These interactions decrease with increasing O_2 pressure as the environment into which the O_2 dissolves includes more oxygen clusters. Furthermore, as the temperature increases, these interactions are disrupted and the solubility drops.

Table 4-3: Enthalpy results for the SDAPP 1.6, SDAPP 2.2, and Nafion 112 membranes at 0% relative humidity.

	8000 (mbar)	9000 (mbar)	10,000 (mbar)
SDAPP 1.6			
ΔH_s (kJ/mol)	-10.0	-8.8	-8.7
S_o	0.01	0.01	0.01
SDAPP 2.2			
ΔH_s (kJ/mol)	-10.0	-9.2	-9.2
S_o	0.01	0.01	0.01
Nafion 112			
ΔH_s (kJ/mol)	-4.96	-5.36	-4.94
S_o	0.03	0.03	0.03

As earlier indicated, there is always a need for water to be present inside a fuel cell in order to facilitate the transport of ions. Similarly, the transport of O₂ also depends on the presence of water and the state it is in. Therefore, experiments were carried out to determine the percent O₂ mass uptake as a function of temperature and relative humidity at a pressure of 1 atm. The introduction of relative humidity has shown to dramatically change the O₂ sorption behavior in Nafion 112, SDAPP 1.6, and SDAPP 2.2. Relative humidity is defined as the extent of water saturation in an air-water vapor mixture. Relative humidity is not the most useful way to report the results as due to the mix feed system of oxygen and water. The moisture content at each temperature and relative humidity has a strong dependence on the structural architecture of the membrane being tested and the water uptake. Therefore, to be more accurate and to try to separate out the effect of O₂ gas and moisture (water), the results are reported as a function of the water's vapor pressure at the respective temperature. Equation 4-4 defines the relationship between the relative humidity and water vapor pressure.

$$yP_{\text{vapor},H_2O} = \frac{xP^{\text{SAT}}(T)}{100} \quad \text{Eq. 4-4}$$

where,

yP_{vapor,H_2O} = vapor pressure of water [=] mbars

x = relative humidity in %

$P^{\text{SAT}}(T)$ = saturation pressure of water

The saturation pressure of water occurs at the following pressures: 31.8 (25 °C), 73.8 (40 °C), 199 (60 °C), and 384.8 (75 °C) mbar according to the Antoine's Equation²⁰ Figures 4-2 through 4-4 display the mass uptake of O₂ for all membranes at 1 atm total pressure as a function of vapor pressure of H₂O.

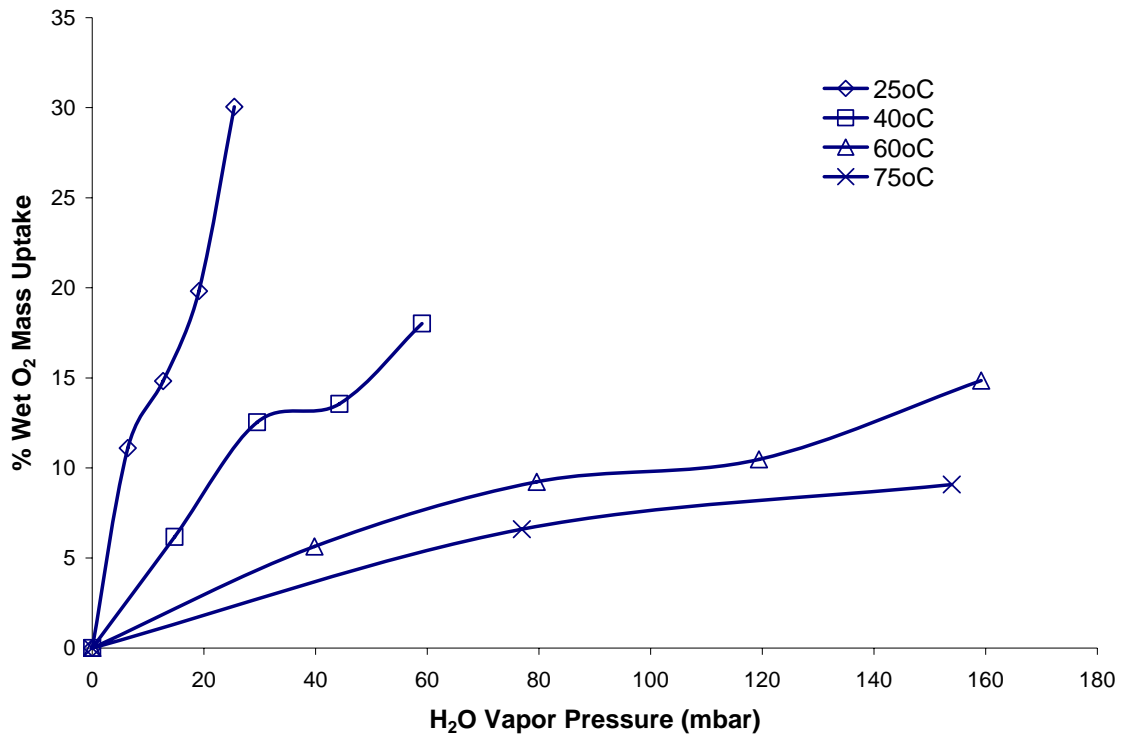


Figure 4-2: O₂ Sorption isotherm for SDAPP 1.6.

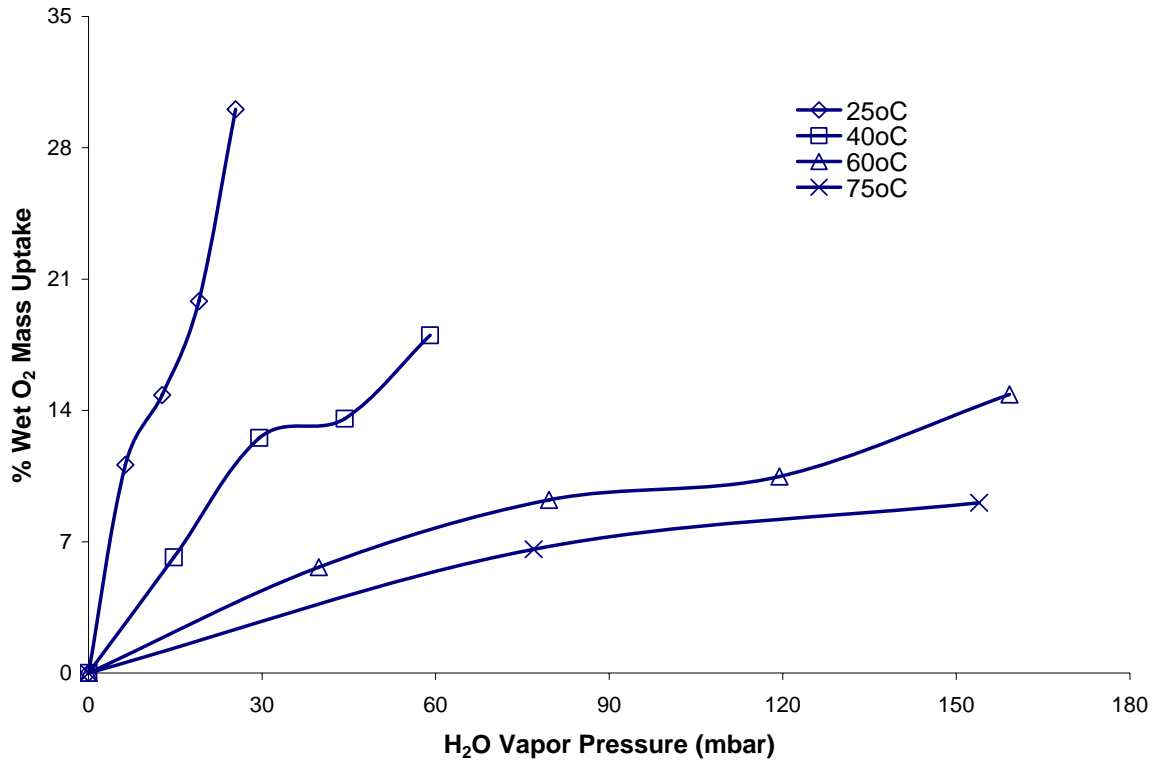


Figure 4-3: O₂ Sorption isotherm for SDAPP 2.2.

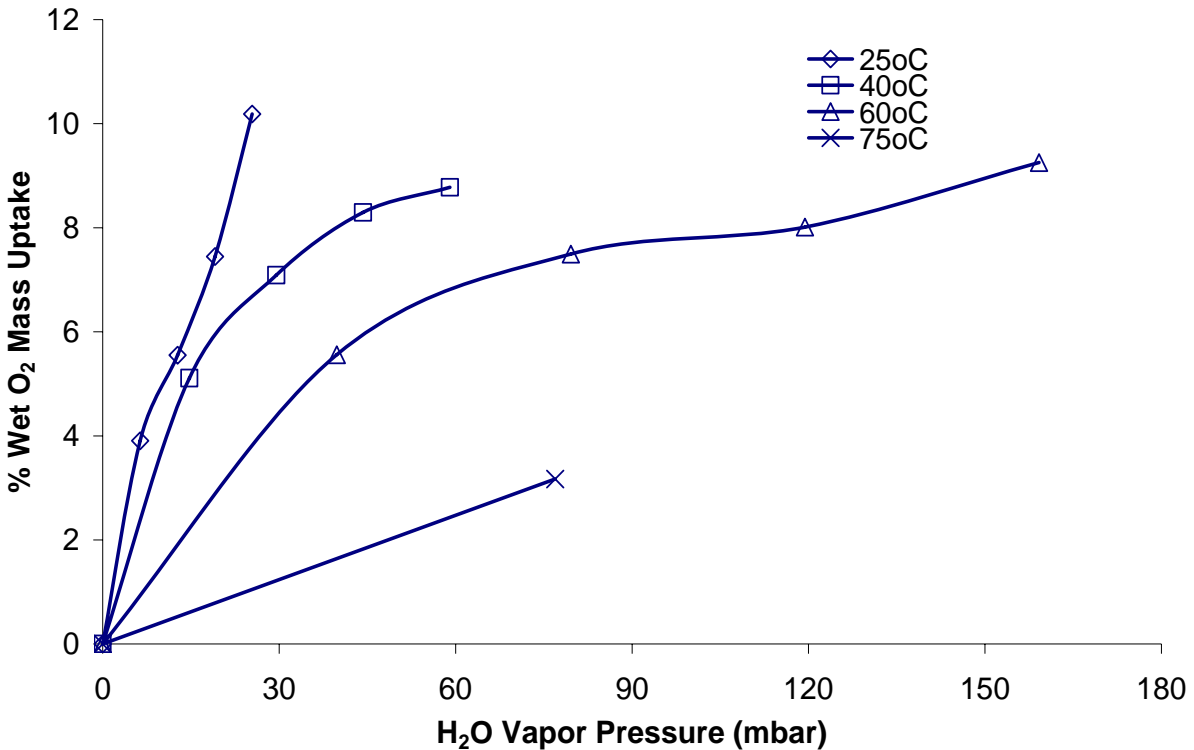


Figure 4-4: O₂ Sorption isotherm for Nafion 112.

In all cases, the percent wet O₂ mass uptake increases with increasing vapor pressure. The rate of increase in the H₂O vapor pressure is higher at low temperatures. At low temperatures there is also the appearance of Type IV sorption, also called the Brunnauer, Emmett and Teller (BET) sorption¹⁷. Type IV sorption is the sum of Type II (Langmuir) and Type III (Flory-Huggins) sorptions, and is typical of water sorbing in a highly hydrophilic polymer. The initial sorption increase (low H₂O vapor pressure) is the water hydrating the sulfonic acid groups. Once saturation of the membrane occurs, swelling takes place at higher H₂O vapor pressures (high RH) and causes the sorption to increase as well as the free volume.²¹ The increase in free volume will help aid proton transport. Since O₂ and H₂O sorptions are coupled in these experiments, it is difficult to separate the role each has in the sorption. However, comparing the solubility of O₂ in the polymer, water, and the polymer/water will allow some insight. The solubility of pure O₂ in the dehydrated SDAPP 2.2 is 0.05 mmol/g or 0.16 % O₂ uptake from Figure 4-1a. The solubility of O₂ in water is 7.2×10^{-4} mmol/g. Solubility of O₂-water in polymer is 0.013

mmol/g or a percent O₂ uptake of 0.042%. These O₂ mass uptake values found at 1 atm and 25 °C are significantly lower than the pure water uptake values found in Table 4-1. Therefore, the sorption isotherms primarily reflect sorption behavior of water in the polymer and not of the oxygen.

As the temperature increases, the percent wet O₂ mass uptake decreases. A review by Moore and Mauritz suggested that water would condense on the membrane surface with more difficulty at higher temperatures and would lower the sorption.²² Also, the vapor phase sorption is more complex than liquid sorption process for the membrane. When comparing Figures 4-2, 4-3, and 4-4, it is quite evident that the total mass uptake of wet O₂ in the SDAPP samples is much higher than that observed in Nafion. The presence of water facilitates sorption of O₂ into the polymer system. This effect seems to be greater in the SDAPP material than in the Nafion.

4.4 Conclusions

The transport behavior of H₂ and O₂ gases in a Diels Alder synthesized poly(phenylene) was compared to the transport behavior in Nafion. The presence of moisture dictated the sorption behavior. Under dry conditions, the sorption of O₂ in both SDAPP and Nafion membranes showed Henry's law behavior. In the presence of humidity and low temperatures, the sorption isotherms followed Type IV behavior. This suggests the formation of hydrogen bonding between the sulfonic acid groups on branches of the membrane and the water, thus, the appearance of swelling. The presence of water in the SDAPP membrane caused a larger O₂ sorption than in the Nafion 112 membrane.

4.5 References

- [1] S. M. J. Zaidi, S. D. Mikhailenko, G. P. Robertson, M. D. Guiver and S. Kaliaguine, Proton conducting composite membranes from polyether ether ketone and heteropolyacids for fuel cell applications, *J. Membr. Sci.*, 173 (2000) 17.
- [2] D. J. Jones and J. Roziere, Recent advances in the functionalisation of polybenzimidazole and polyetherketone for fuel cell applications, *J. Membr. Sci.*, 185 (2001) 41.
- [3] X. F. Li, C. J. Zhao, H. Lu, Z. Wang and H. Na, Direct synthesis of sulfonated poly(ether ether ketone)s (SPEEKs) proton exchange membranes for fuel cell application, *Polymer*, 46 (2005) 5820.
- [4] R. Nolte, K. Ledjeff, M. Bauer and R. Mulhaupt, Partially Sulfonated Poly(Arylene Ether Sulfone) - a Versatile Proton Conducting Membrane Material for Modern Energy-Conversion Technologies, *J. Membr. Sci.*, 83 (1993) 211.
- [5] F. Wang, M. Hickner, Y. S. Kim, T. A. Zawodzinski and J. E. McGrath, Direct polymerization of sulfonated poly(arylene ether sulfone) random (statistical) copolymers: candidates for new proton exchange membranes, *J. Membr. Sci.*, 197 (2002) 231.
- [6] C. Iojoiu, M. Marechal, F. Chabert and J. Y. Sanchez, Mastering sulfonation of aromatic polysulfones: Crucial for membranes for fuel cell application, *Fuel Cells*, 5 (2005) 344.
- [7] C. H. Fujimoto, M. A. Hickner, C. J. Cornelius and D. A. Loy, Ionomeric poly(phenylene) prepared by diels-alder polymerization: Synthesis and physical properties of a novel polyelectrolyte, *Macromolecules*, 38 (2005) 5010.
- [8] Y. S. Kim, L. M. Dong, M. A. Hickner, T. E. Glass, V. Webb and J. E. McGrath, State of water in disulfonated poly(arylene ether sulfone) copolymers and a perfluorosulfonic acid copolymer (nafion) and its effect on physical and electrochemical properties, *Macromolecules*, 36 (2003) 6281.
- [9] T. L. Kalapos, B. Decker, H. A. Every, H. Ghassemi and T. A. Z. Jr., Thermal Studies of the state of water in proton conducting fuel cell membranes, *J. Power Sources*, 172 (2007) 14.
- [10] D. B. Spry, A. Goun, K. Glusac, D. E. Moilanen and M. D. Fayer, Proton transport and the water environment in nafion fuel cell membranes and AOT reverse micelles, *J. Am. Chem. Soc.*, 129 (2007) 8122.
- [11] N. L. Garland and J. P. Kopasz, The United States Department of Energy's high temperature, low relative humidity membrane program, *J. Power Sources*, 172 (2007) 94.
- [12] T. Pechar, Fabrication and Characterization of Polyimide-based Mixed Matrix Membranes for Gas Separations. Virginia Polytechnic Institute and State University, 2004.
- [13] T. T. Moore, S. Damle, P. J. Williams and W. J. Koros, Characterization of low permeability gas separation membranes and barrier materials; design and operation considerations, *J. Membr. Sci.*, 245 (2004) 227.
- [14] J. Crank, *The Mathematics of Diffusion*, Oxford Press; London, (1990)
- [15] L. M. Robeson, W. F. Burgoyne, M. Langsam, A. C. Savoca and C. F. Tien, High-Performance Polymers for Membrane Separation, *Polymer*, 35 (1994) 4970.
- [16] B. D. Freeman. In *Comprehensive Polymer Science*; S. L. Aggarwal, S. Russo, Eds.; Pergamon Press: Oxford, 1992.
- [17] T. D. Naylor. Permeation Properties. In *Comprehensive polymer science : the synthesis, characterization, reactions & applications of polymers*; 1st ed.; G. Allen, J. C. Bevington, Eds.; Pergamon Press: Oxford, England ; New York, 1989; Vol. 2; pp 643.

- [18] K. Tanaka, M. N. Islam, M. Kido, H. Kita and K. Okamoto, Gas permeation and separation properties of sulfonated polyimide membranes, *Polymer*, 47 (2006) 4370.
- [19] C. W. J. JR, A. Roy, J. McGrath and E. Marand, Determination of the Effect of Temperature and Humidity on the O₂ Sorption in Sulfonated Poly(arylene ether sulfone) membranes, *J. Membr. Sci.*, Accepted (2007) Accepted.
- [20] J. M. Smith, H. C. V. Ness and M. M. Abbott, *Introduction to Chemical Engineering Thermodynamics*, McGraw Hill, New York, NY, 2001.
- [21] J. T. Hinatsu, M. Mizuhata and H. Takenaka, Water-Uptake of Perfluorosulfonic Acid Membranes from Liquid Water and Water-Vapor, *J. Electrochem. Soc.*, 141 (1994) 1493.
- [22] K. A. Mauritz and R. B. Moore, State of understanding of Nafion, *Chemical Reviews*, 104 (2004) 4535.

5.1 Introduction

A proton exchange membrane fuel cell (PEMFC) includes a PEM membrane sandwiched between two catalyst layers.¹ The membrane and two catalyst layers form the membrane electrode assembly. Advancements in the design of the catalyst layer in the fuel cell are essential both from the viewpoint of quality and cost reduction. A series of electrochemical reactions take place in the catalyst layers. Hydrogen is oxidized at the anode, while the oxygen is reduced at the cathode. Catalyst layers are present at both the anode and cathode with the oxygen reaction being the limiting reaction at the cathode. The catalyst layer helps facilitate the transport of ions, electrons, reactants, and products throughout the fuel cell and provides a large catalyst surface area needed for the half reactions to occur.²

There are four different phases that make-up the catalyst layer: ionomer phase, platinum phase, carbon phase, and voids/pores. The catalyst layer typically has low catalyst loading around 0.4 mg Pt/cm² and an ionomer loading close 1.9 mg/cm² for a H₂/Air fuel cell.³ At the cathode, the ionomer phase allows for the transport of oxygen gas and the H⁺ ion from the membrane to the reaction sites in the catalyst layer. The ionomer content ranges from 5 to 20 wt% depending on the application. The carbon phase provides a support for the platinum particles and helps with the transport of electrons to the platinum reaction site. The platinum phase acts as the reaction site where O₂ gas, H⁺ protons, and electrons react to form water. The optimal platinum content ranges from 20 to 40 wt% supported on carbon. Voids or pores aid in the movement of oxygen and with the removal of water within the catalyst layer. Figure 5-1 provides a simple structure of the catalyst layer.

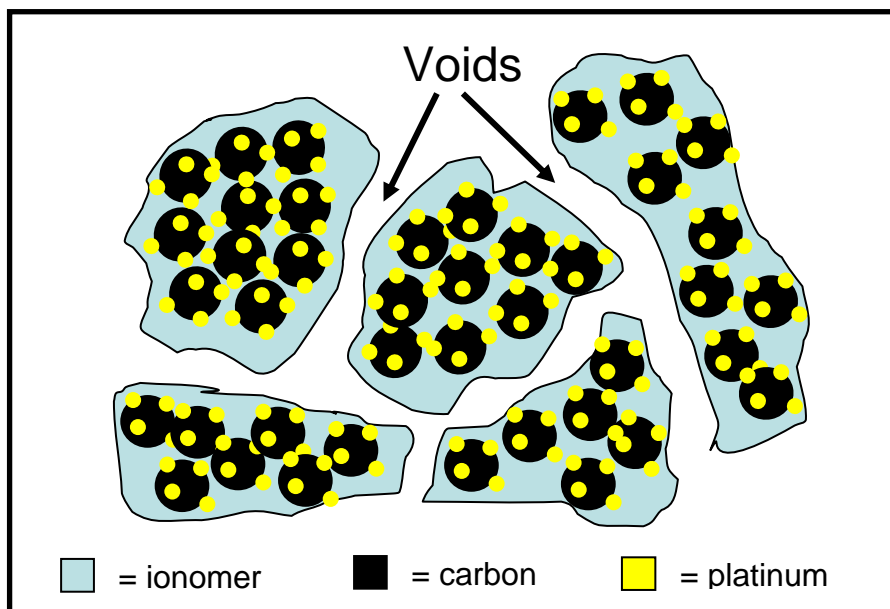


Figure 5-1: Simple structure make-up of the catalyst layer of a PEMFC.

Ideally, the catalyst layer should be thin and have low mass transport resistances, high platinum surface area, and high electrical and ionic conductivities. The thickness of the catalyst layer determines the rate of oxygen transport through the layer to utilize the platinum. The layer should be thin to allow access to all of the platinum and to reduce the paths that the electrons, protons, and reactant gases travel. Only the platinum that comes in contact with the membrane and reactant gases are active, other platinum particles are inactive. The move from unsupported catalyst to supported catalyst along with the use of ionomer caused similar performances to be achieved at low low platinum loadings.⁴⁻⁶ The carbon support allowed the mass transport to be reduced and allow more accessibility to the reaction sites and aid in the removal of water. Lower platinum loadings allowed for more surface area to be active, good dispersion within the catalyst layer matrix, and reduce cost.^{7,8}

The fuel cell performance is dependent partially on the relative humidity (RH) and temperature of the system.⁹ The presence of water affects the transport of gas and water molecules, ions, and electrons. This chapter is devoted to explaining the O₂ gas sorption on different catalyst powders ranging from 20 wt% Pt-C to 80 wt% Pt-C, as well as unsupported platinum black in the non-humidified and humidified state for a temperature range of 25 to 75 °C. The non-humidified sorption is performed using gravimetric equilibrium sorption as a function of pressure. In the humidified state, the O₂ sorption is determined over a relative

humidity range of 20 to 80% RH. From O₂ sorption measurements, the type of sorption can be determined. The sorption in the platinum, for the non-humidified state, is expected to follow straight Knudsen diffusion as is the case in porous solid media. However, in the presence of water, the sorption behavior of O₂ will depend on the O₂ interaction with water as well as the porosity of the carbon.

5.2 Experimental

5.2.1 Materials

The catalyst powders used are the High Power (HP) Platinum on Vulcan XC-72R series, which were purchased from PEMEAS Fuel Cell Technologies (an E-Tek Division). The amount of platinum varied from 20 wt% to 80 wt% platinum supported on carbon black. The HP unsupported platinum black powder was also purchased from PEMEAS Fuel Cell Technologies.

5.2.2 MEA Preparation

Electrodes are added to the membrane forming membrane electrode assemblies (MEAs) using a variety of different techniques such as hot-pressing, inking, or airbrushing. The membranes electrode assemblies discussed in this chapter were prepared using the “decal” or hotpressing method.^{10,11} This method involves inking the electrode onto Teflon blanks for transfer onto the membrane. The “ink” solution consisted mainly of 5 wt% Nafion ionomer solution, 40 wt% Pt-C, and deionized water. The decals are hotpressed onto the surface at 210 °C and 3000 psig.¹²

5.2.3 Gas Permeation Characterization

The H₂ and O₂ gas permeabilities of the disulfonated poly(arylene ether sulfone) and Nafion 112 MEA were determined using a constant volume permeation apparatus.¹³ Utilizing the 5 cm² electrode area, the MEAs were masked with aluminum tape and sealed with epoxy to prevent leaks.¹⁴ Gases were used as received from Air Products and possessed a purity of 99.99%. The feed pressure and temperature were kept constant at close to 1 atm and 35 °C, respectively, for all experiments. Each gas was run through a MEA three times and the average results and the standard deviations were recorded. Permeabilities are reported in units of Barrer (1 Barrer = $1 \times 10^{-10} \text{ cm}^3 \cdot (\text{STP}) \cdot \text{cm} / (\text{cm}^2 \cdot \text{sec} \cdot \text{cmHg})$).

5.2.4 Gas Sorption Characterization

Sorption studies were performed using the gravimetric system (IGA-002, Hiden Isochema, UK). All chambers and tubing were degassed by applying vacuum ($P \leq 10^{-4}$ mbar). The gas used was oxygen with 99.99 % purity and purified further by attaching a molecular sieve to the gravimetric system. Relative humidity was introduced into the gravimetric system utilizing two gas feeds. One feed was a dry gas stream and the other gas feed was piped through a stainless steel deionized water bath. The water bath had an upper temperature limit of 80°C. These two streams mixed at the exit of the water bath. A change in the percentage of total flow through the wet stream and temperature dictated the relative humidity. For each sample temperature, the vapor pressure of water was determined by the IGA software, which utilized the appropriate Antoine's equation. Equation 3-1 was used to determine the percentage of the wet stream flow necessary for a desired relative humidity.

$$\% \text{ Wet Flow} = RH \frac{P_{\text{sample}}(T)}{P_{\text{vaporgen}}(T)} \quad \text{Eq. 3-1}$$

where % Wet Flow = percentage of total flow containing water vapor

$P_{\text{sample}}(T)$ = vapor pressure of water in the sample holder in millibar

$P_{\text{vaporgen}}(T)$ = vapor pressure of water in the vapor generator (i.e.-water bath) in millibar

RH = desired relative humidity (%)

5.3 Results

5.3.1 Catalyst Powders

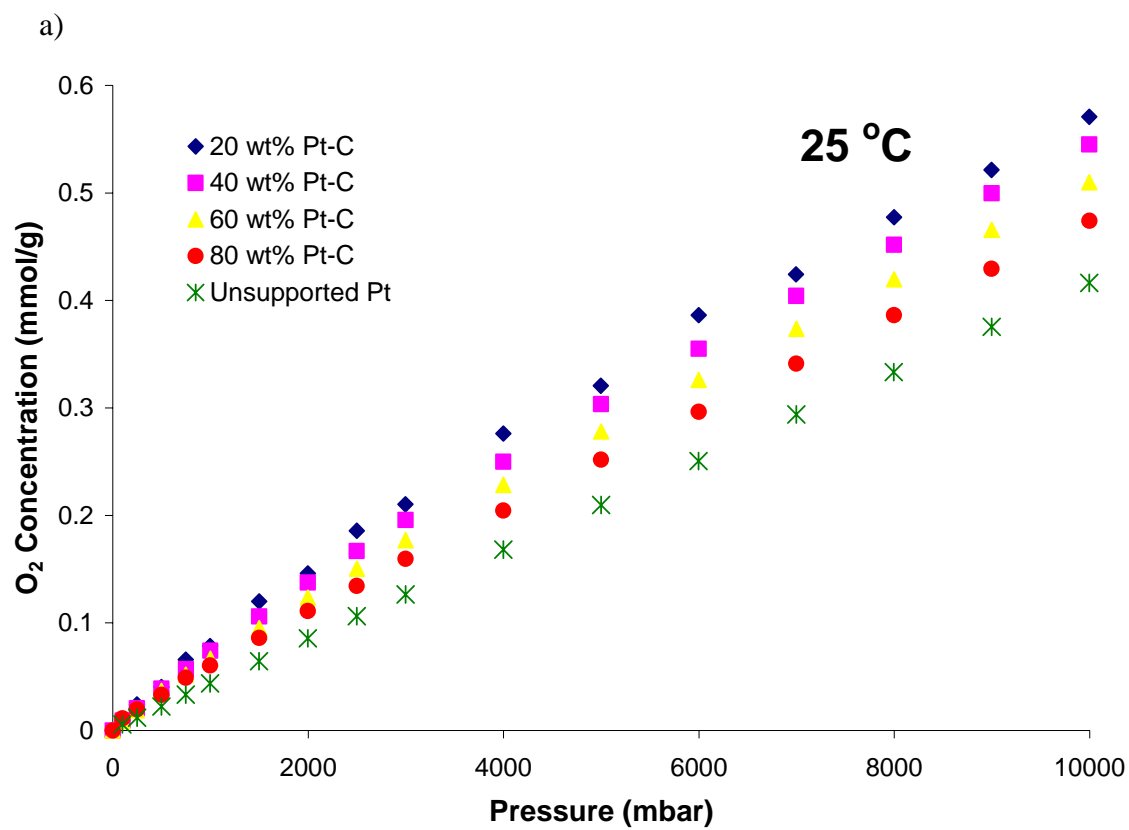
Table 5-1 gives the Pt crystallite particle size and the catalyst metal surface area for the various Pt-C powders.

Table 5-1: Particle Size and surface areas for various Pt-C powders and unsupported Pt black.

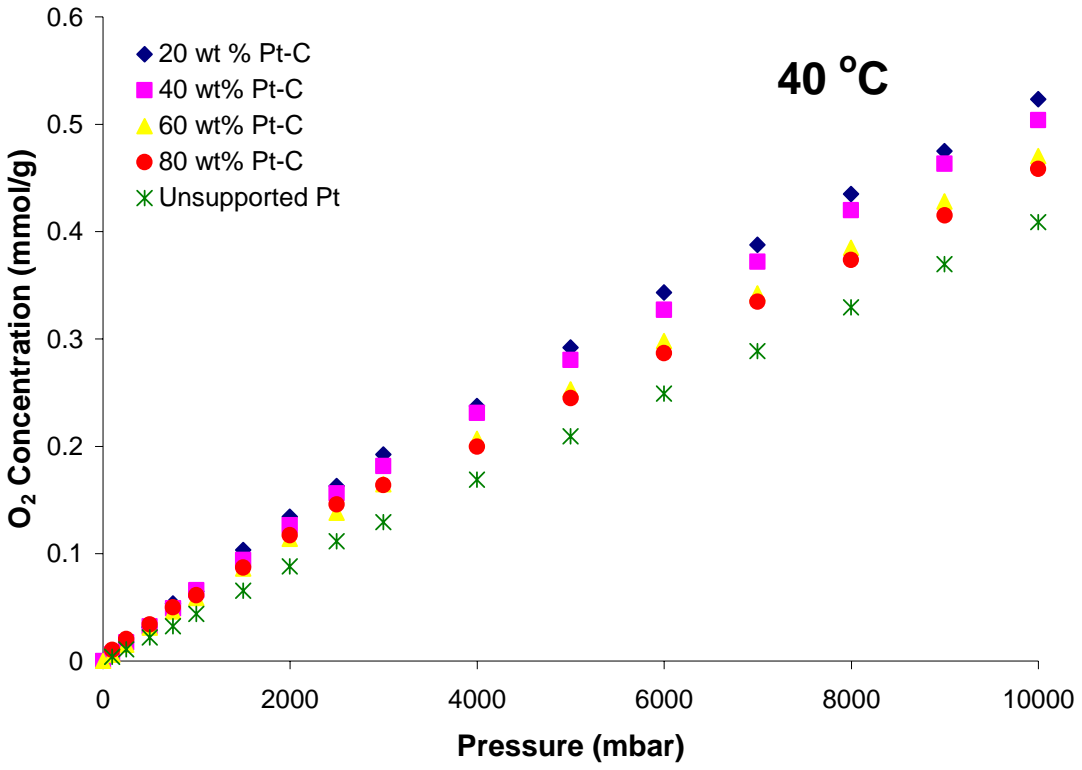
wt % Pt on Carbon	XRD Pt Crystallite Size, nm	Surface Area $\text{m}^2 \text{g}^{-1} \text{Pt}$
20	2.2	128
40	2.9	100
60	3.7	76
80	4.9	57
Unsupported Pt Black	5.5	34

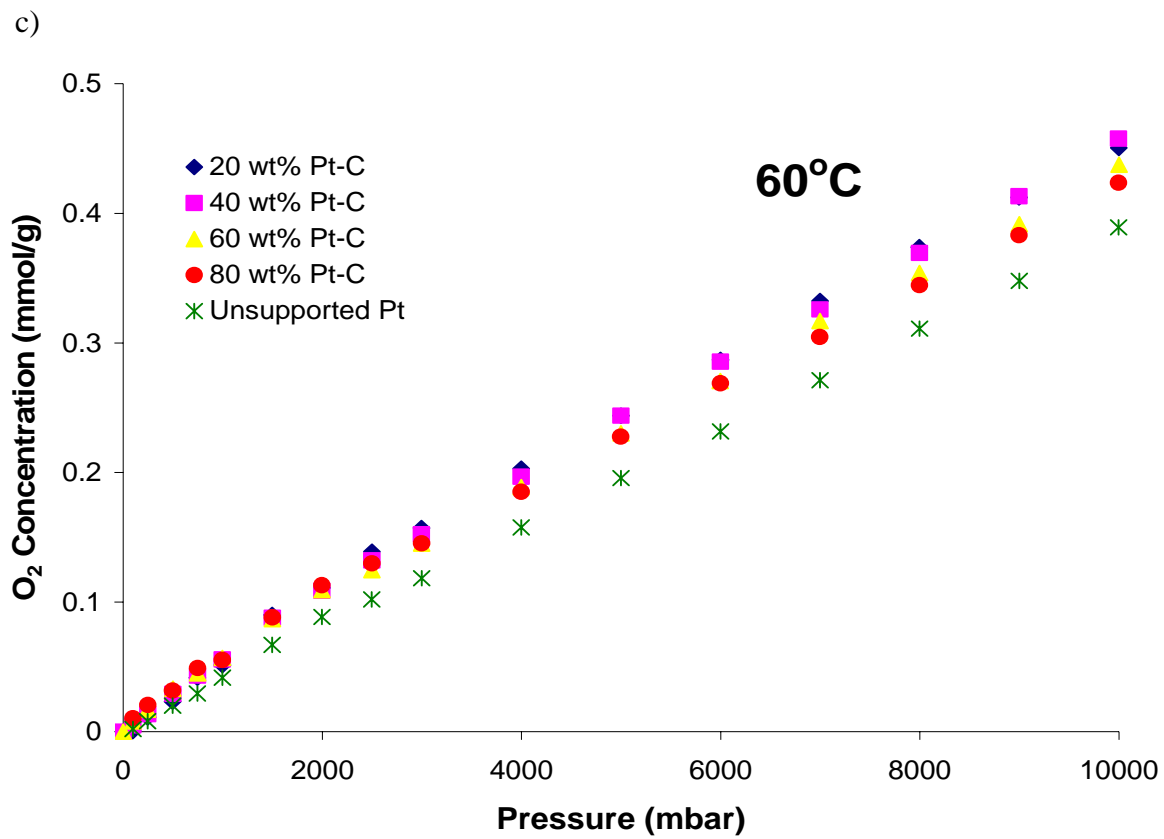
* Data taken from E-Tek website: <http://www.etek-inc.com/custom/index.php>

O₂ Gas Sorption measurements were carried out as a function of pressure (0 to 10 bar), temperature (25 to 75 °C) and relative humidity (0 to 80% RH) for the various Pt-C powders. Figure 5-2 displays the O₂ pressure isotherms for platinum catalyst ranging from 20 to 80 wt% Pt-C and unsupported platinum black.



b)





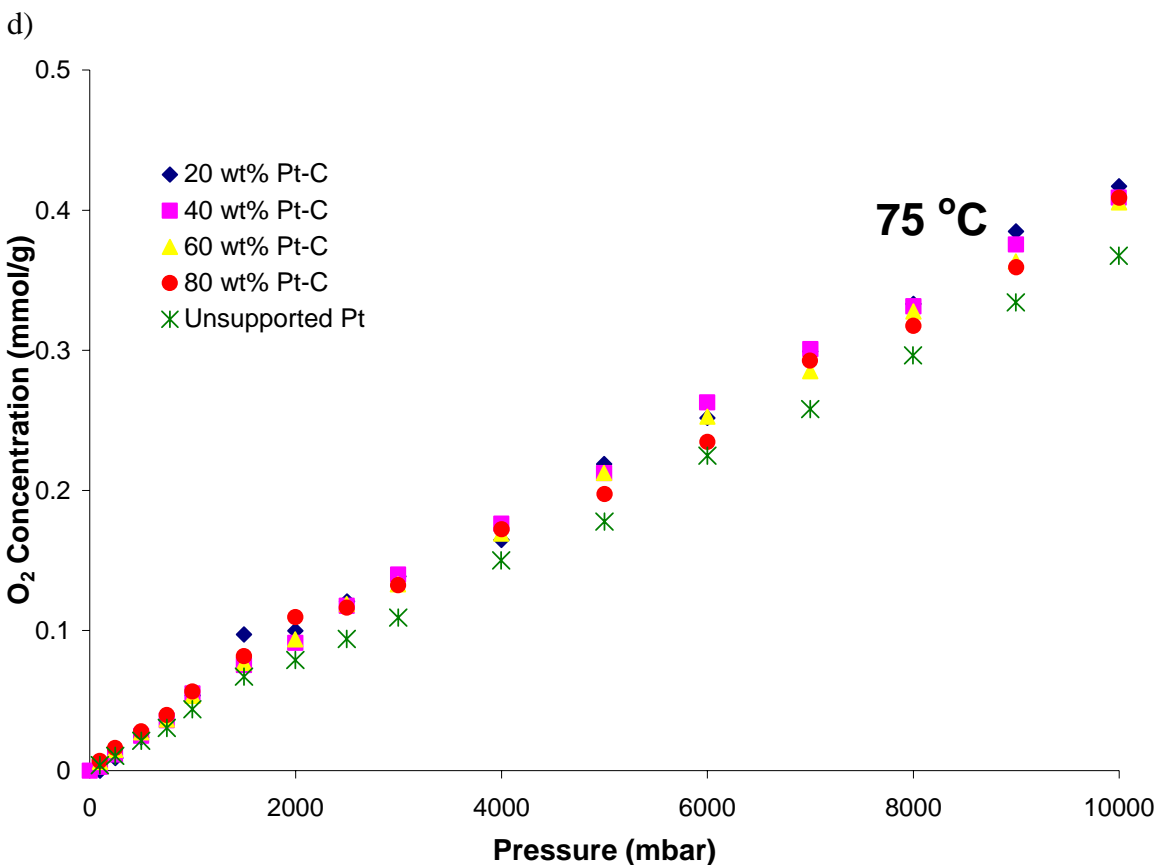


Figure 5-2: O_2 sorption isotherms for various Pt-C powders as a function of pressure and temperature in the non-humidified state over a temperature range of 25-75 °C.

The O_2 concentration follows a linear profile with increasing pressure. Based on the XRD data provided in Table 5-1, and the sorption data, it is interesting to note that the O_2 sorption increases as the amount of platinum decreases and the fraction of carbon support increases. At 25 °C, 20 wt% Pt-C exhibited the largest O_2 sorption followed by 40 wt% > 60 wt% > 80 wt% > unsupported Pt. The lower amount of platinum means that the mesoporous volume associated with the carbon is greater, allowing higher oxygen uptake. As the temperature is increased, the overall O_2 sorption decreases and the isotherms collapse onto one profile, suggesting that sorption is independent of Pt content.

There is always a need for water to be present inside a fuel cell in order to facilitate the transport of ions. Similarly, the transport of O_2 also depends on the presence of water and the state it is.^{15,16} Therefore, experiments were carried out to determine the percent wet O_2 mass uptake as a function of temperature and relative humidity at a pressure of 1 atm. These are the same experiments that were conducted for the proton exchange membranes discussed in the

earlier chapters. The introduction of relative humidity has shown to dramatically change the O₂ sorption behavior in PEMs. Relative humidity is defined as the extent of water saturation in an air-water vapor mixture and is related to water pressure via Equation 5-4.

$$yP_{\text{vapor},H_2O} = \frac{xP^{\text{SAT}}(T)}{100} \quad \text{Eq. 5-4}$$

where,

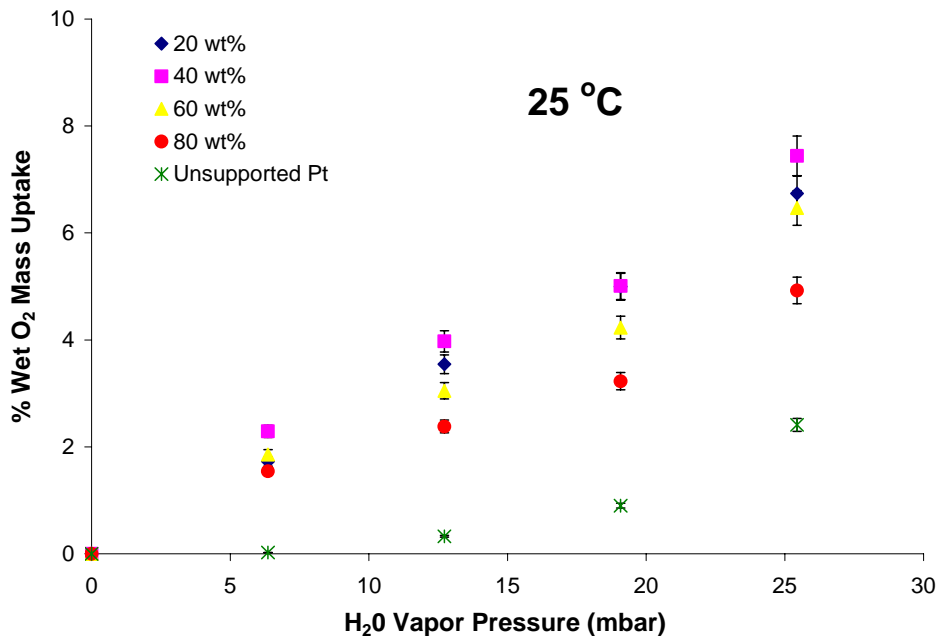
yP_{vapor,H_2O} = vapor pressure of water [=] mbars

x = relative humidity in %

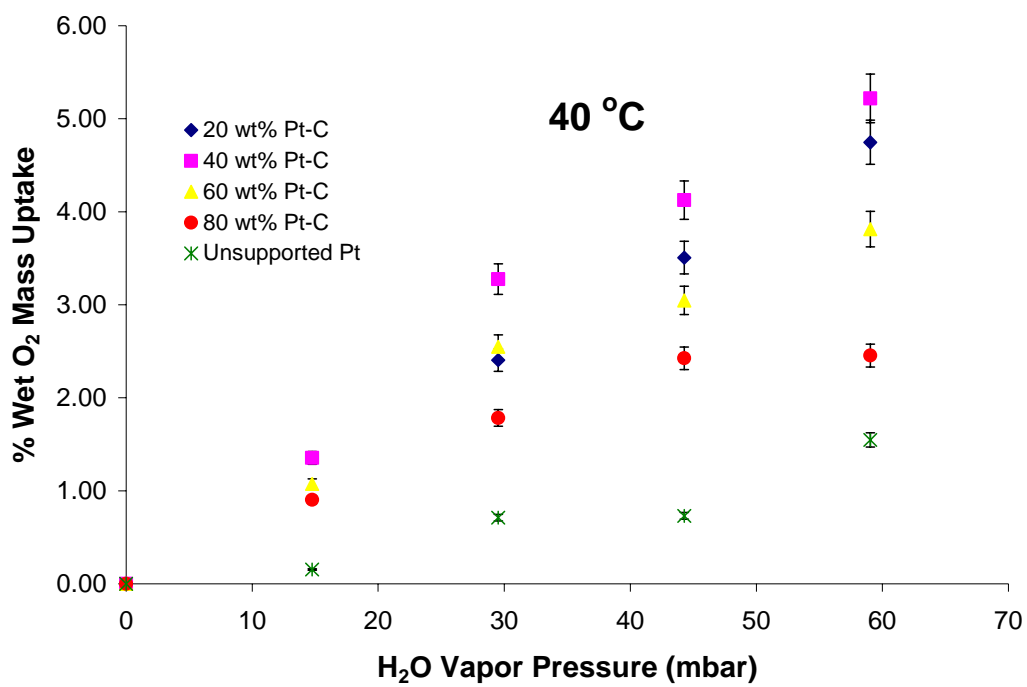
$P^{\text{SAT}}(T)$ = saturation pressure of water

The saturation pressure of water occurs at the following pressures: 31.8 (25 °C), 73.8 (40 °C), 199 (60 °C), and 384.8 (75 °C) mbar according to the Antoine's Equation^{17,18} Figure 5-3 display the mass uptake of O₂ for the various Pt-C catalysts and unsupported Pt black at 1 atm total pressure as a function of vapor pressure of H₂O.

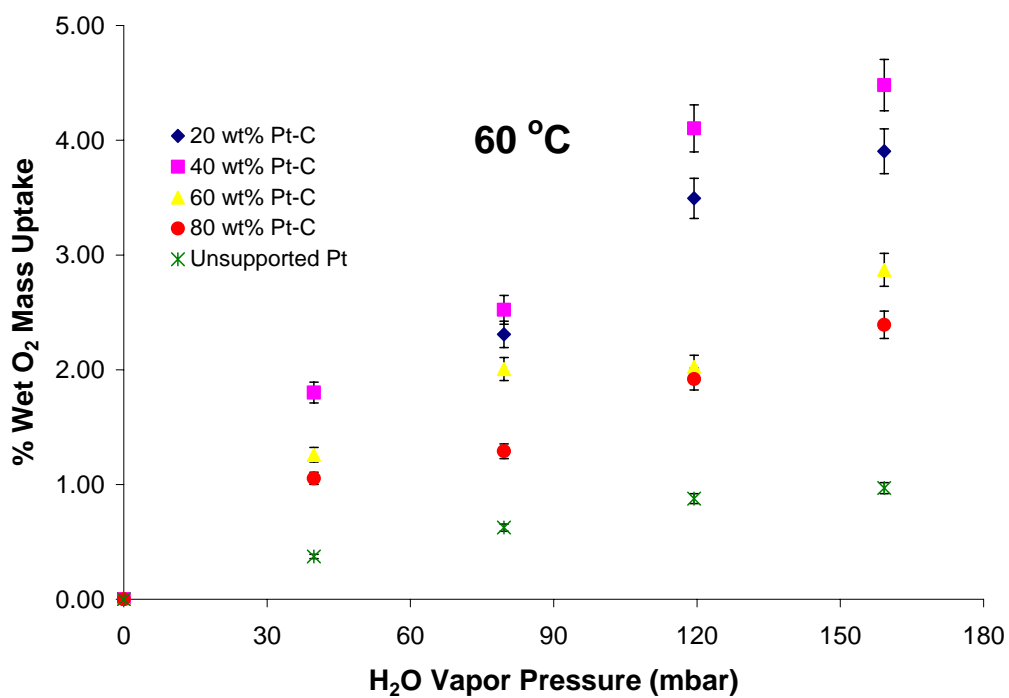
a)



b)



c)



d)

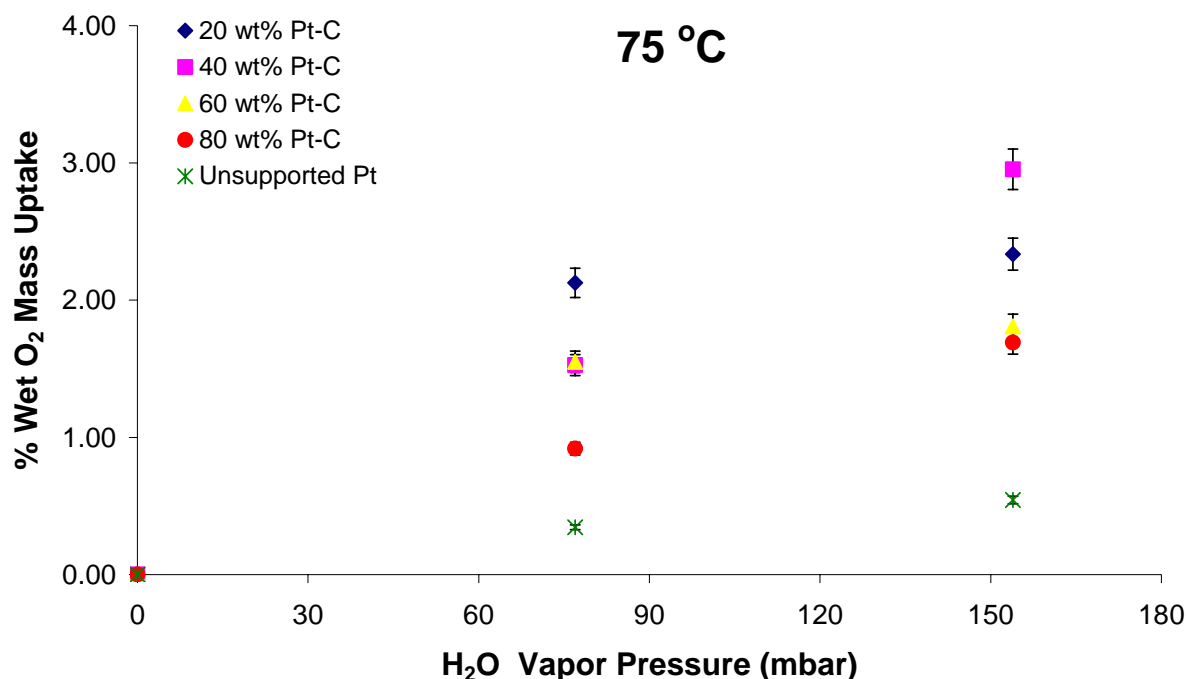


Figure 5-3: % Wet O₂ mass uptake as a function of temperature and vapor pressure of water for various Pt-C catalyst powders in the humidified state.

In all cases, the wet O₂ percent mass uptake increases with increasing vapor pressure. The rate of increase of the O₂ percent mass uptake with H₂O vapor pressure is higher at low temperatures. At low temperatures there is also the appearance of Type IV sorption (not as distinct as in the membranes), also called the Brunnauer, Emmett and Teller (BET) sorption¹⁹ Type IV sorption is the sum of Type II (Langmuir) and Type III (Flory-Huggins) sorptions. When comparing Figure 5-3 a through d, it is quite evident that the total mass uptake of O₂ in the 40 wt % Pt-C is the highest than that of any other Pt-C system and the unsupported Pt black. This reflects an optimal composition of the catalyst dispersion and available surface area of the platinum with the porosity of carbon with which the water/O₂ has to interact.

This behavior is similar to the “volcano effect” described by Boudart and Mariadoassou.²⁰ Figure 5-4, indicates that as the weight percent of platinum increases, the particle size (*d*) increases (see Table 5.1). At the same time, the number of exposed platinum atoms dispersed in

the matrix decreases. This causes a “volcano effect,” where the surface area of the catalyst has a maximum only at one particle size. In our case, the sorption of O_2 in the presence of water reaches a maximum at 40 wt% Pt-C, which corresponds to maximum porosity of the carbon.

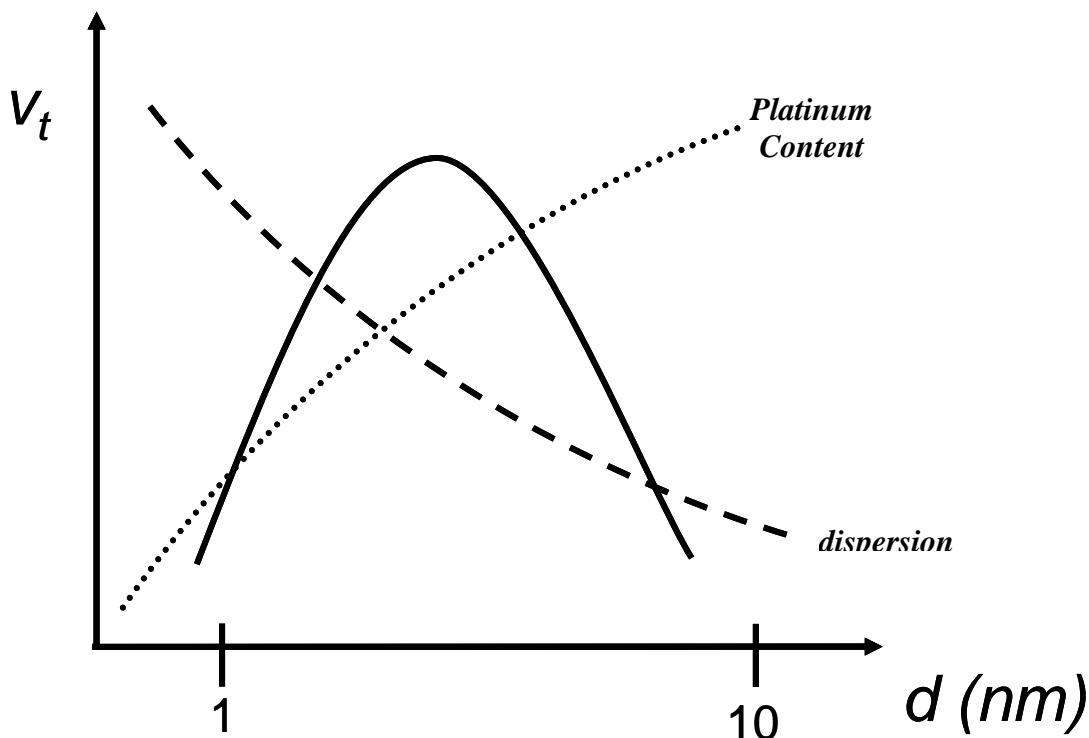


Figure 5-4: Simple schematic of turnover frequency as a function of particle size.

5.3.2 Membrane Electrode Assembly Characterization

So far, the O_2 sorption behavior in both the non-humidified and humidified state has been shown for various proton exchange membranes and catalyst powders. Both of these materials are used to make membrane electrode assemblies. Ultimately in a fuel cell, the MEA is the operational “battery,” which consists of catalyst layer at the anode, the membrane, and a catalyst layer at the cathode, Figure 5-5.

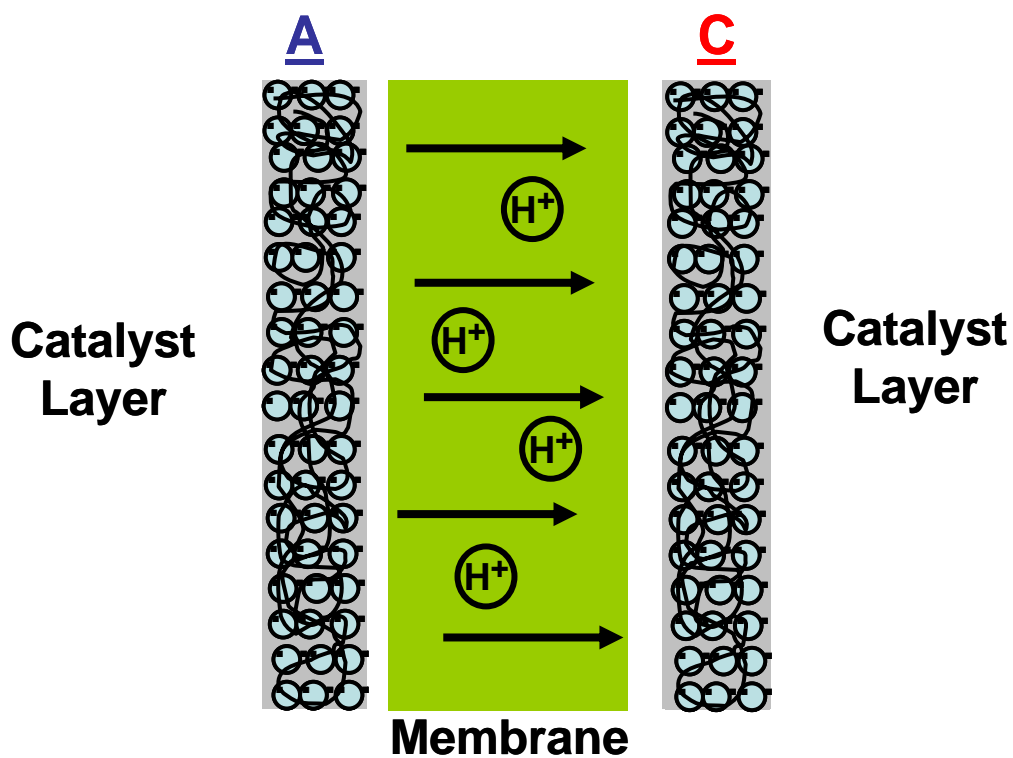


Figure 5-5: Membrane electrode assembly schematic.

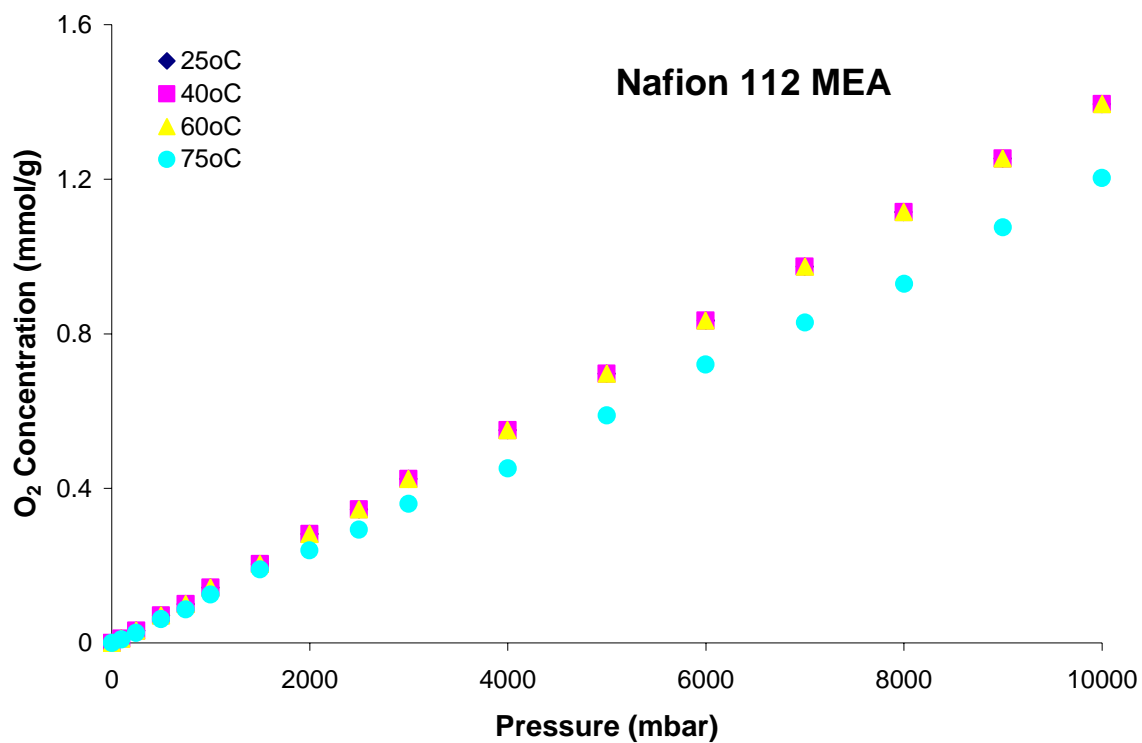
Therefore, this section is designated to investigate the O_2 sorption in the non-humidified and humidified state of the MEAs. Table 5-2 shows the H_2 and O_2 gas permeability values for two BPSH-35 MEAs and a Nafion 112 MEA. The BPSH-35 and Nafion 112 MEA systems demonstrate higher gas permeabilities when compared to the neat membrane series discussed in Chapter 3. The increase in permeability is related to the porosity of Pt-C catalyst, which allows the gas molecules to have a more direct transport path and to pass faster through the membrane.

Table 5-2: Permeability values for various MEAs hot pressed at 210 °C and 40 wt% Pt-C.

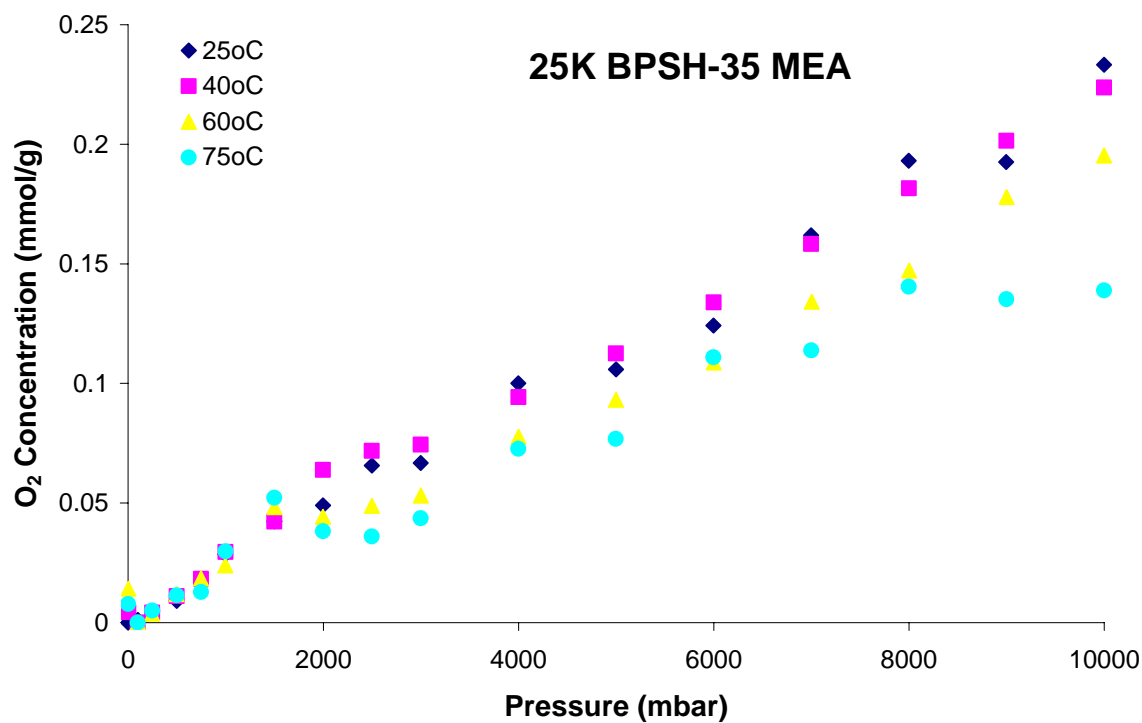
	Hydrogen (Barrers)	Oxygen (Barrers)
BPSH-35 25K	13.99 ± 0.71	10.93 ± 1.87
BPSH-35 80K	7.60 ± 0.09	0.98 ± 0.26
Nafion 112	138.0 ± 1.84	83.0 ± 1.57

Once again, O₂ gas sorption measurements were carried out as a function of pressure (0 to 10 bar), temperature (25 to 75 °C) and relative humidity (0 to 80% RH) for the BPSH-35 and Nafion 112 MEA systems.

a)



b)



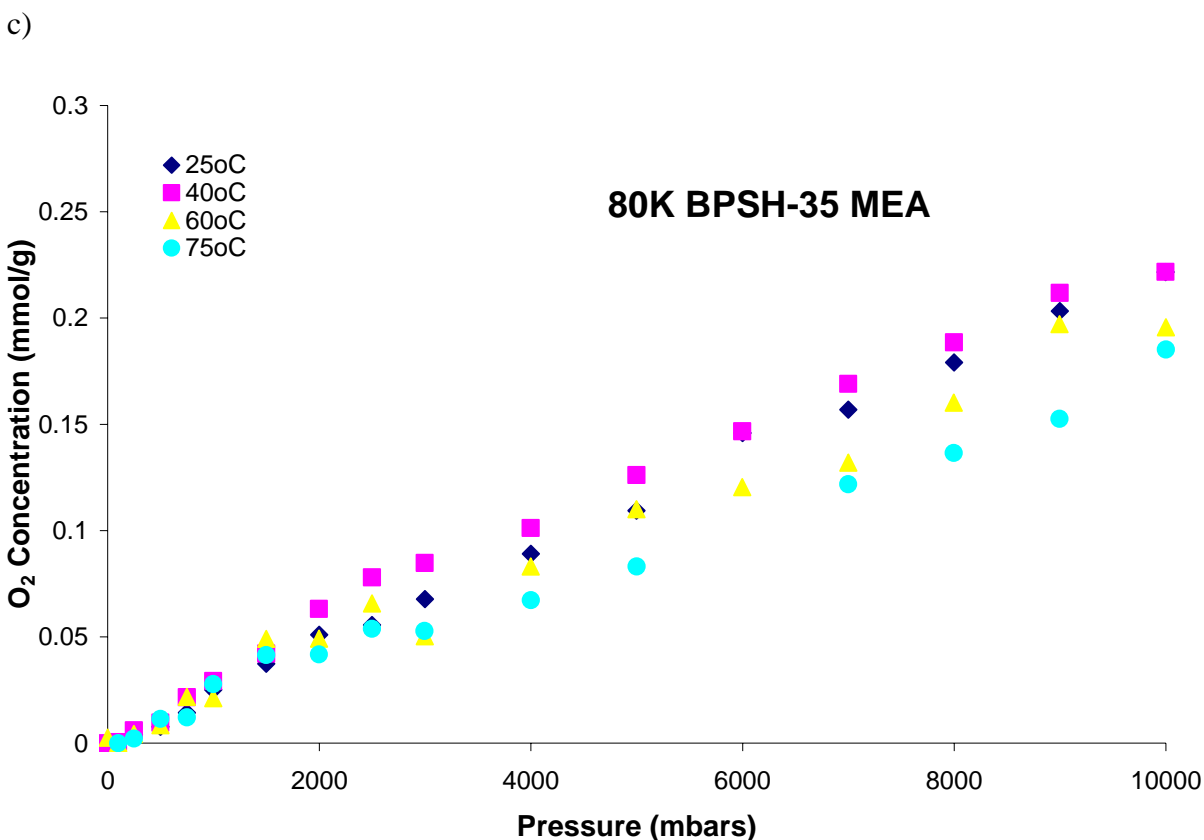
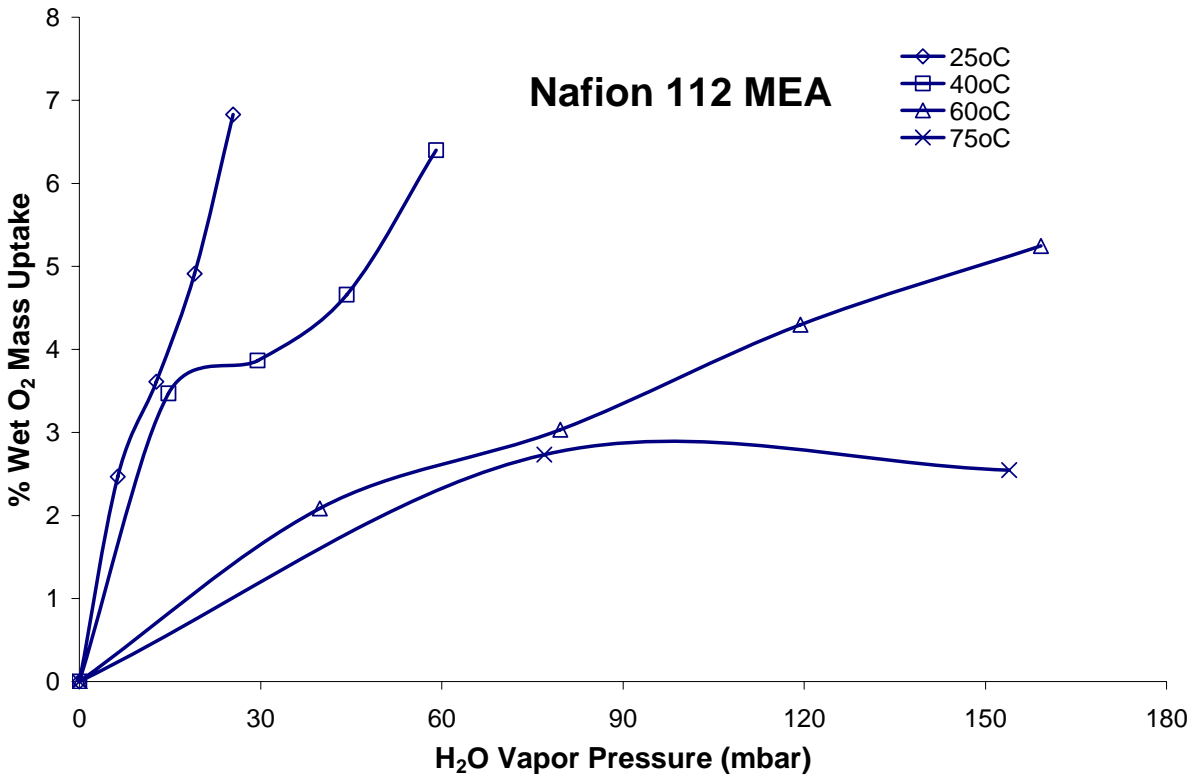


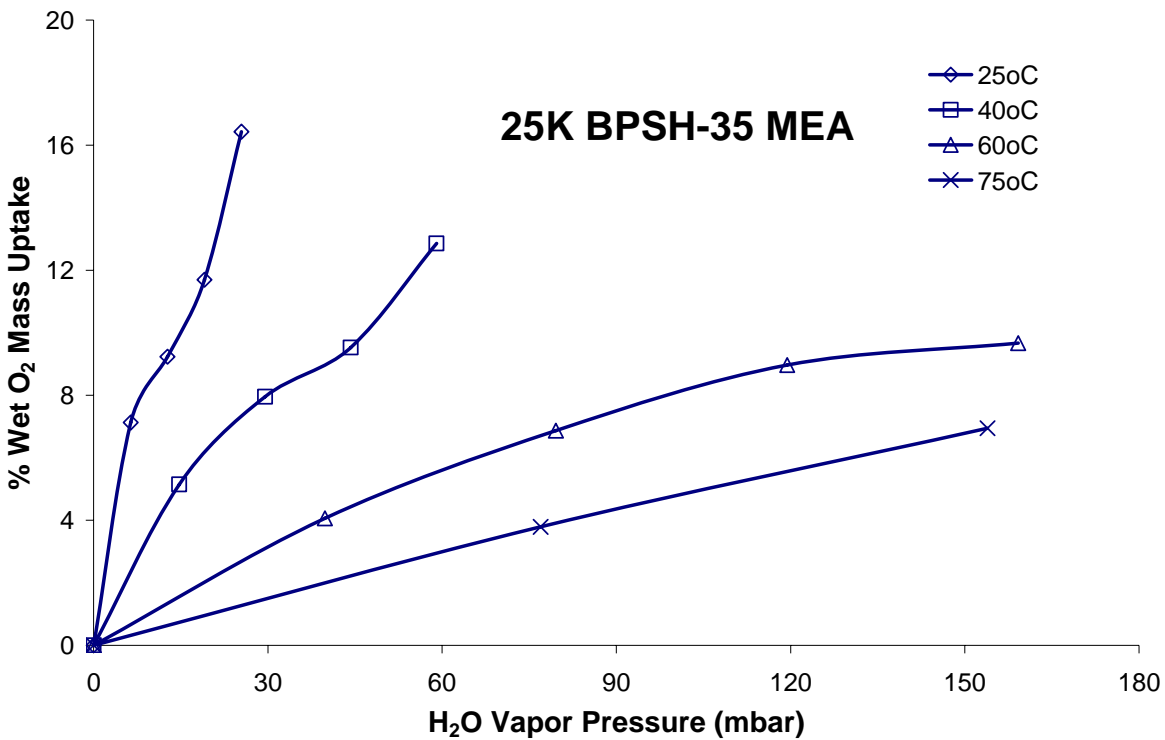
Figure 5-6: O₂ sorption isotherm for MEAs hotpressed at 210 °C in the non-humidified state: (a) Nafion 112, (b) BPSH-35 (25K), (c) BPSH-35 (80K).

The O₂ sorption in the Nafion 112, BPSH-35 25K, and BPSH-35 80K MEAs exhibited Henry's Law type behavior shown in Figure 5-6. In comparison to the pure polymer systems, the MEA's have lower sorption capacity. Figure 5-7 shows the O₂ sorption in the presence of moisture. The O₂ sorption behavior is a more distinct Type IV sorption as found in the earlier work involving the proton exchange membranes. The transport of O₂ depends on the presence of water and the state it is in. Therefore, experiments were carried out to determine the percent O₂ mass uptake as a function of temperature and relative humidity at a pressure of 1 atm.

a)



b)



c)

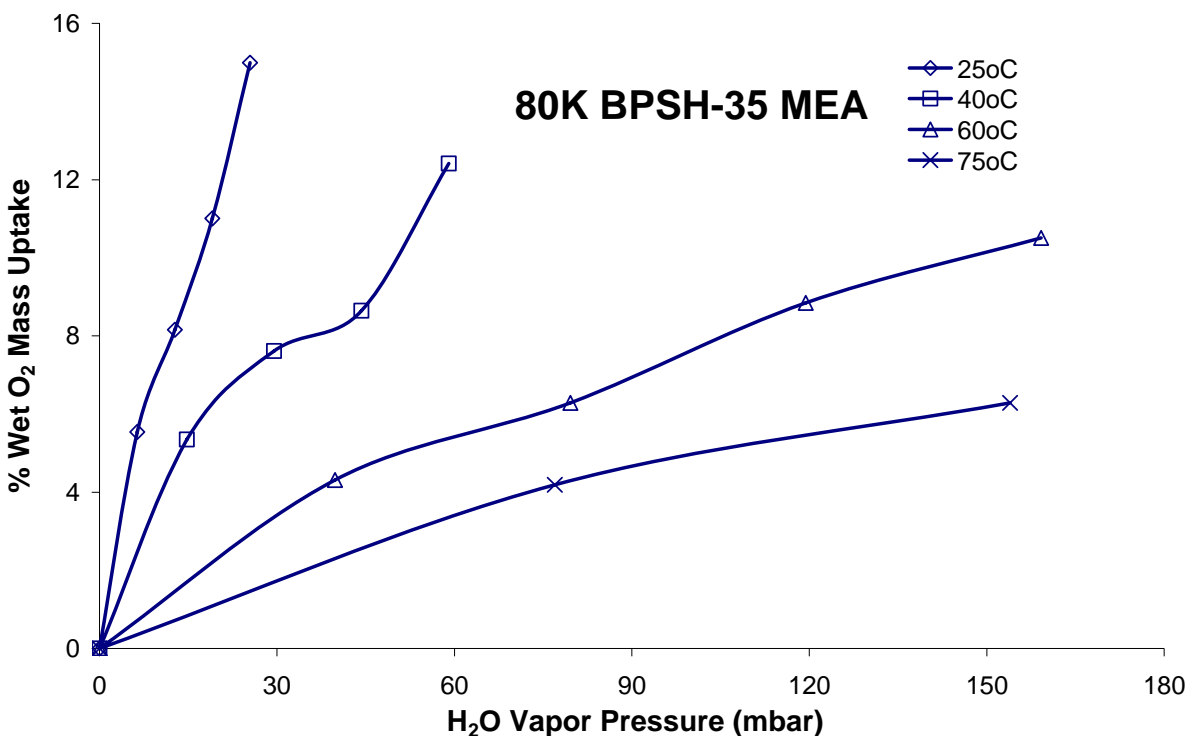


Figure 5-7: O₂ sorption isotherm for MEAs hotpressed at 210 °C for the humidified state: (a) Nafion 112, (b) BPSH-35 (25K), (c) BPSH-35 (80K).

The BPSH-35 series have higher wet O₂ mass uptake than Nafion due to higher exchange capacity. The O₂ sorption is lower in the MEA than in the pure polymer membrane due to the low O₂ sorption in Pt and Nafion ionomer when compared to the pure polymer. The electrode also provides a more tortuous pathway to the membrane, which is where the majority of sorption is happening because of the porosity of the carbon and the lower % wet O₂ mass uptake in 40 wt % Pt-C, Figure 5-3, compared to the neat polymer, Figures 3-3 to 3-5.

5.4 Conclusions

The O₂ sorption behavior was compared in both the non-humidified and humidified state for various platinum supported on a carbon catalyst powders and an unsupported platinum black powder. Under dry conditions, the catalysts followed Knudsen's diffusion behavior for porous solids, which increased with increasing carbon content. In the presence of moisture, the catalysts followed Type IV sorption behavior, but the sorption behavior was not as distinct as in the neat membranes because of the lower sorption capacity of Pt-C in comparison to the polymer system.

The same methods were utilized for the membrane electrode assemblies. The H₂ and O₂ gas permeabilities were measured for a BPSH-35 (25 and 80K membrane) and Nafion 112 MEA containing 40 wt% Pt-C. The presence of a porous catalyst induced higher gas permeabilities in the MEAs than in the neat polymer membranes. For O₂ sorption, the presence of moisture once again dictated the sorption behavior. Type IV sorption occurred as a result of the formation of hydrogen bonding between the polymer and H₂O clusters. Most likely, the sorption is taking place in the polymer of the MEA because the polymer has a larger sorption capacity and is hydrophilic.

5.5 References

- [1] E. G. T. S. Inc., Fuel Cell Handbook, U.S. Department of Energy, Office of Fossil Energy, National Energy Technology Laboratory, 2004.
- [2] J. B. Russell, Investigation of the Effect of Catalyst Layer Composition on the Performance of PEM Fuel Cells. Virginia Polytechnic Institute and State University, 2003.
- [3] S. J. Lee, S. Mukerjee, J. McBreen, Y. W. Rho, Y. T. Kho and T. H. Lee, Effects of Nafion impregnation on performances of PEMFC electrodes, *Electrochimica Acta*, 43 (1998) 3693.
- [4] E. J. Taylor, E. B. Anderson and N. R. K. Vilambi, Preparation of High-Platinum-Utilization Gas-Diffusion Electrodes for Proton-Exchange-Membrane Fuel-Cells, *J. Electrochem. Soc.*, 139 (1992) L45.
- [5] K. Petrov, K. Xiao, E. R. Gonzalez, S. Srinivasan, A. J. Appleby and O. J. Murphy, An Advanced Proton-Exchange Membrane Electrolyzer with an Improved 3-Dimensional Reaction Zone, *Int. J. Hydrogen Energy*, 18 (1993) 907.
- [6] J. MCBreen, Voltammetric Studies of Electrodes in Contact with Ionomeric Membranes, *J. Electrochem. Soc.*, 132 (1985) 1112.
- [7] E. A. Ticianelli, C. R. Derouin, A. Redondo and S. Srinivasan, Methods to Advance Technology of Proton-Exchange Membrane Fuel-Cells, *J. Electrochem. Soc.*, 135 (1988) 2209.
- [8] Z. Poltarzewski, P. Staiti, V. Alderucci, W. Wiecek and N. Giordano, Nafion Distribution in Gas-Diffusion Electrodes for Solid-Polymer-Electrolyte-Fuel-Cell Applications, *J. Electrochem. Soc.*, 139 (1992) 761.
- [9] J. Larminie and A. Dicks, Fuel cell systems explained, J. Wiley, Chichester, West Sussex, 2003.
- [10] M. S. Wilson and S. Gottesfeld, Thin-Film Catalyst Layers for Polymer Electrolyte Fuel-Cell Electrodes, *J. Appl. Electrochem.*, 22 (1992) 1.
- [11] M. A. Hickner, Transport and Structure in Fuel Cell Proton Exchange Membranes. Virginia Polytechnic Institute and State University, 2003.
- [12] M. S. Wilson, J. A. Valerio and S. Gottesfeld, Low Platinum Loading Electrodes for Polymer Electrolyte Fuel-Cells Fabricated Using Thermoplastic Ionomers, *Electrochimica Acta*, 40 (1995) 355.
- [13] T. Pechar, Fabrication and Characterization of Polyimide-based Mixed Matrix Membranes for Gas Separations. Virginia Polytechnic Institute and State University, 2004.
- [14] T. T. Moore, S. Damle, P. J. Williams and W. J. Koros, Characterization of low permeability gas separation membranes and barrier materials; design and operation considerations, *J. Membr. Sci.*, 245 (2004) 227.
- [15] Y. S. Kim, L. M. Dong, M. A. Hickner, T. E. Glass, V. Webb and J. E. McGrath, State of water in disulfonated poly(arylene ether sulfone) copolymers and a perfluorosulfonic acid copolymer (nafion) and its effect on physical and electrochemical properties, *Macromolecules*, 36 (2003) 6281.
- [16] C. W. J. JR, A. Roy, J. McGrath and E. Marand, Determination of the Effect of Temperature and Humidity on the O₂ Sorption in Sulfonated Poly(arylene ether sulfone) membranes, *J. Membr. Sci.*, Accepted (2007) Accepted.
- [17] J. M. Smith, H. C. V. Ness and M. M. Abbott, Introduction to Chemical Engineering Thermodynamics, McGraw Hill, New York, NY, 2001.
- [18] J. M. Prausnitz, R. N. Lichtenthaler and E. G. d. Azevedo, Molecular thermodynamics of fluid-phase equilibria, Prentice-Hall PTR, Upper Saddle River, N.J., 1999.

[19] T. D. Naylor. Permeation Properties. In *Comprehensive polymer science : the synthesis, characterization, reactions & applications of polymers*; 1st ed.; G. Allen, J. C. Bevington, Eds.; Pergamon Press: Oxford, England ; New York, 1989; Vol. 2; pp 643.

[20] M. Boudart and G. Djâega-Mariadassou, *Kinetics of heterogeneous catalytic reactions*, Princeton University Press, Princeton, N.J., 1984.

The overall objective of this work is to gain an understanding of the gas transport in various proton exchange membranes used for fuel cell applications. The membranes used were a disulfonated poly(arylene ether sulfone) (BPSH), post sulfonated diels alder poly(phenylene) (SDAPP), and poly(perfluoro sulfonic acid) (Nafion 112).

The first chapter was a comparison of BPSH with 35 % disulfonation in the polymer's backbone with Nafion 112. The H₂ and O₂ gas permeability of the BPSH-35 was lower than the permeability of Nafion 112 because of the higher T_g of BPSH-35. The BPSH-35 segments are more rigid and inflexible compared to the Nafion 112 chemical structure, netting a reduction in gas permeability. The O₂ sorption in the non-humidified state displayed Henry's law type behavior. However, in the presence of moisture, the type of sorption changes to Type IV sorption, which is typical for highly hydrophilic polymers. The percent wet O₂ mass uptake in BPSH-35 was higher than that of Nafion 112 due to a higher ion exchange capacity, i.e.-water uptake. This type of sorption suggests hydrogen bonding between the sulfonic acid groups contained in the backbone of the polymer and the water.

The next chapter compares SDAPP with an IEC = 1.6 and 2.2 mequiv g⁻¹ with Nafion 112. The H₂ gas permeability in the SDAPP 2.2 samples was similar to Nafion because of bulky, pendant benzene side groups. However, the O₂ permeability is lower for the SDAPP because the free volume from the side groups are not large enough for oxygen to permeate through at a similar rate to Nafion. Also, the side groups contain π - π interactions with each other, to reduce the permeability. O₂ sorption in the non-humidified state displayed Henry's law behavior. Type IV sorption was observed in the presence of moisture and the percent wet O₂ mass uptake was higher in the SDAPP than Nafion 112. The percent wet O₂ mass uptake was also larger than that found in the BPSH series due to higher sulfonic acid content; thus, being consistent with the explanation that t hydrogen bonding exists between the sulfonic acid groups and water.

The last chapter discusses the same O₂ sorption technique in the non-humidified and humidified state, but instead of membranes, the focus is on catalysts powders and membrane electrode assemblies. The catalysts powders and MEAs exhibited Knudsen's diffusion of porous

solids and Henry's law behavior respectively in the non-humidified state. In the presence of moisture, 40 wt% Pt-C reached the highest % O₂ mass uptake compared to the other powders. The MEAs exhibited similar Type IV sorption that was found in the membranes.

Some recent work has been focused on examining the percent wet O₂ mass uptake as a function of proton conductivity over a relative humidity range of 20 to 80 % RH, shown in Figure 6-1. For Nafion 112, the percent wet O₂ mass uptake is relatively constant over a wide-range of proton conductivities and independent of temperature and total water content ($\lambda = \text{H}_2\text{O}/\text{SO}_3\text{H}$). However, BPSH-35 displays a different behavior. BPSH-35 is dependent on the water content and temperature because of morphological changes from a close to an open morphology. The open morphology promotes good proton transport. At low relative humidities, the proton conductivities and O₂ mass uptakes are low. As the amount of water present in the system is increased, there is a stronger dependence on the temperature. For example, at 60 °C, BPSH-35 has similar behavior to that of Nafion 112 because of similar, open morphology.

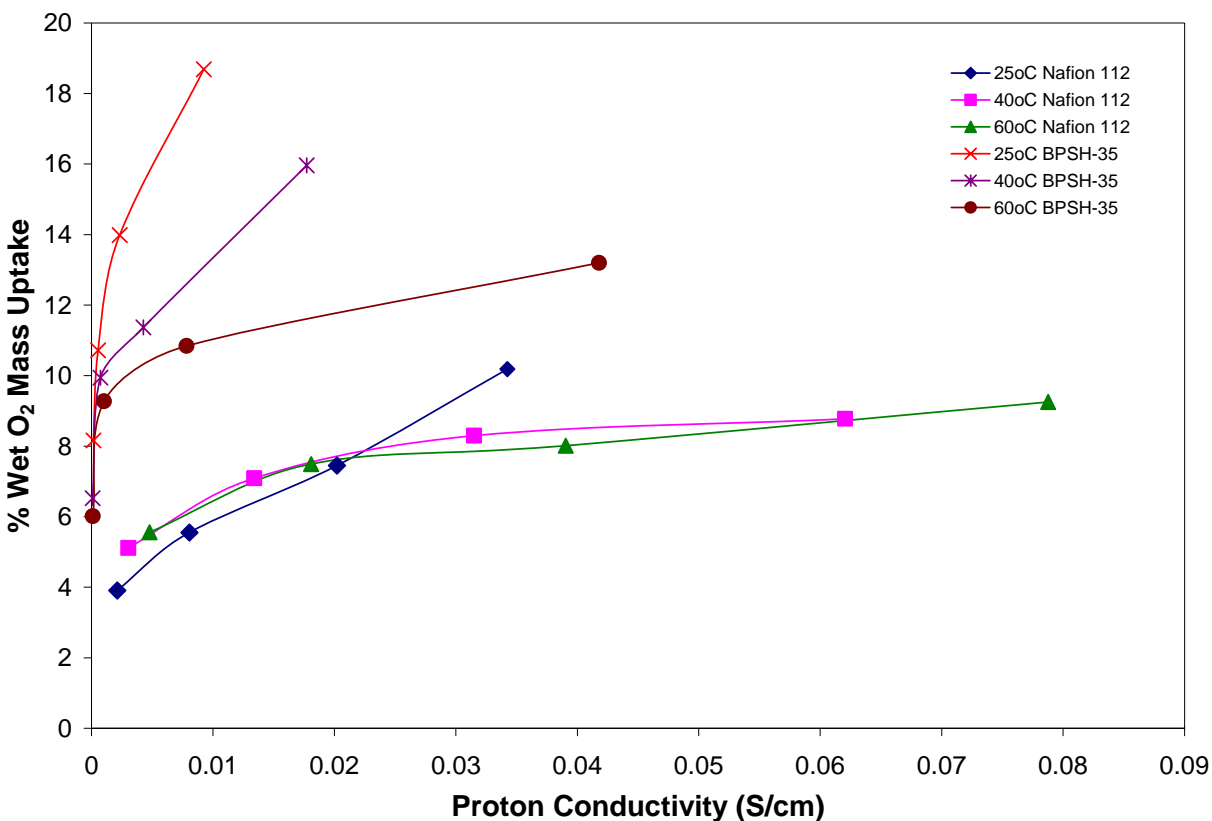
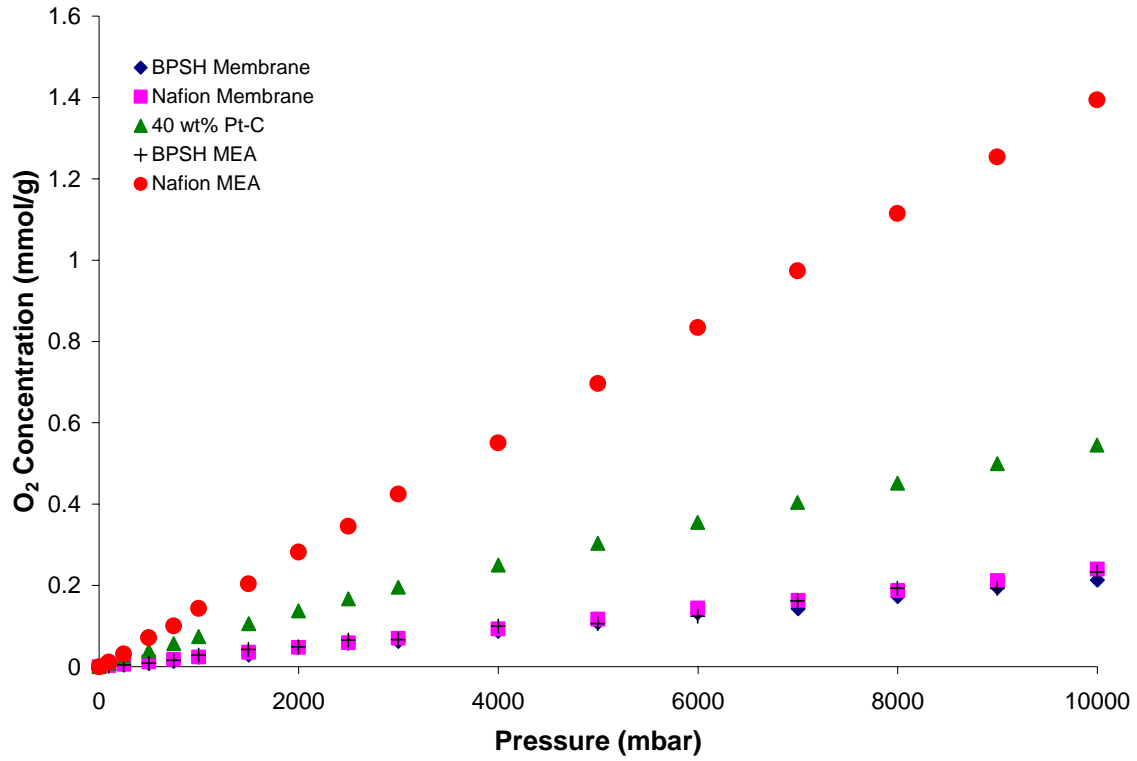


Figure 6-1: Isopiestic graph of % wet O₂ mass uptake as a function of proton conductivity for Nafion 112 and BPSH-35

Suggested future work in this area of research could be divided into two parts. The first is to continue the O₂ sorption experiments involving the membrane and the membrane electrode assemblies in the non-humidified and humidified state for variations of the proton exchange membranes including derivatives of the BPSH and SDAPP series such as fluorinated materials. This will allow us to answer such questions as: How does changing the structural architecture of the polymers change the O₂ sorption capacity (related to amount of IEC), Does Henry's Law and Type IV sorption hold for other proton exchange membranes in the non-humidified and humidified state, and if Type IV sorption holds in the humidified state, can we related high water uptake (IEC) to high O₂ mass uptake? To help explain the transport in the membrane, atomic force microscopy could be utilized for the dehydrated and hydrated state (liquid cell) to determine the impact water has on the morphology in proton exchange membrane. In the presence of water, will the membrane have a more open or close morphology? How does this correlate to gas permeability and gas sorption. There should be further work in developing the isopiestic curve. This curve will allow a better correlation between conductivity, percent O₂ mass uptake as a function of total water content ($\lambda = \text{H}_2\text{O}/\text{HSO}_3$). Indirectly, we will be able to relate other properties such as structure, T_g, water uptake, IEC, and states of water.

Secondly, these experiments will allow us to examine the O₂ sorption of each component that makes-up the membrane electrode assembly. For example, Figure 6-1, shows the effect of the membrane, catalyst, and membrane electrode assembly both in the non-humidified and humidified state. We can examine the catalyst layer make-up by changing the platinum loading as well as the ionomer concentration. The platinum loading would be less dependent on the O₂ sorption than the ionomer and membrane, the ionomer concentration would be an important factor. Experiments for this area include understanding the O₂ sorption in the humidified and non-humidified state for varying ionomer concentrations. Electrode make-up could include 25/75, 50/50, 75/25 wt% Pt-C to ionomer. Nafion ionomer solution (5 wt%) would be utilized, but possible BPSH and SDAPP ionomers could also be used. Ionomer loading could range from 0.5 to 5 mg Ionomers/cm² (based on typical Nafion loadings).

a)



b)

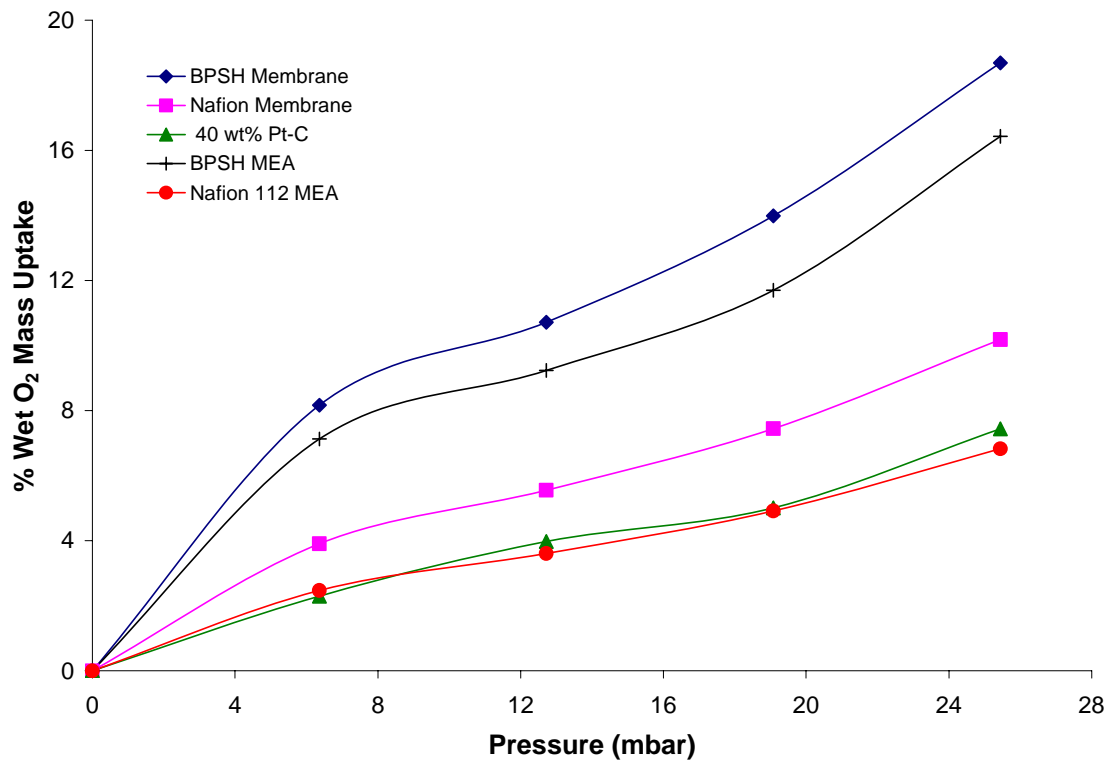


Figure 6-1: Compilation of the effect of O₂ sorption in the (a) non-humidified and (b) humidified state for Nafion 112, 25K BPSH-35, 40 wt% Pt-C, and the respective MEAs.

Vita

Charles William James Jr was born on January 18, 1980 in Columbia, South Carolina. He was raised in Hopkins, South Carolina, which is just outside of Columbia. He graduated from Lower Richland High School in 1998. During his time there, he was a member of the football, wrestling, track and field, and golf team. For college, he attended the University of South Carolina located in Columbia, South Carolina. He grew up a Gamecock fan and knew there was no other choice for college than USC. He decided to major in chemical engineering and graduated in 2002. He worked for Dr. John Van Zee in his fuel cell group as an undergraduate researcher. Also, Will worked for Roche Carolina, Inc. in Florence, South Carolina and Metalox, LLC in Charlotte, North Carolina as a summer intern. In Fall 2002, he enrolled in the Chemical Engineering program at Virginia Polytechnic Institute and State University in Blacksburg, VA. Furthermore, he joined the research group of Dr. Eva Marand to study the gas transport properties in proton exchange membranes used in fuel cell applications. During his time in graduate school, he was a summer intern in the Cornelius group at Sandia National Laboratories in Albuquerque, New Mexico and obtained a M.E. in chemical engineering in 2005. He will be defending his thesis in Fall 2007.